

Sheffield Hallam University

Laser ablation ICP spectrometry.

JANSEN, Andrew.

Available from the Sheffield Hallam University Research Archive (SHURA) at:

<http://shura.shu.ac.uk/19868/>

A Sheffield Hallam University thesis

This thesis is protected by copyright which belongs to the author.

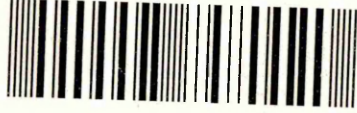
The content must not be changed in any way or sold commercially in any format or medium without the formal permission of the author.

When referring to this work, full bibliographic details including the author, title, awarding institution and date of the thesis must be given.

Please visit <http://shura.shu.ac.uk/19868/> and <http://shura.shu.ac.uk/information.html> for further details about copyright and re-use permissions.

CITY CAMPUS POND STREET
SHEFFIELD S1 1WB

101 585 591 1



BEN 387159

REFERENCE

ProQuest Number: 10697174

All rights reserved

INFORMATION TO ALL USERS

The quality of this reproduction is dependent upon the quality of the copy submitted.

In the unlikely event that the author did not send a complete manuscript and there are missing pages, these will be noted. Also, if material had to be removed, a note will indicate the deletion.



ProQuest 10697174

Published by ProQuest LLC (2017). Copyright of the Dissertation is held by the Author.

All rights reserved.

This work is protected against unauthorized copying under Title 17, United States Code
Microform Edition © ProQuest LLC.

ProQuest LLC.
789 East Eisenhower Parkway
P.O. Box 1346
Ann Arbor, MI 48106 – 1346

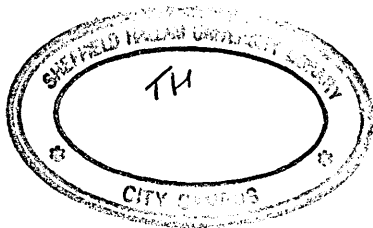
Laser Ablation ICP Spectrometry

Andrew Jansen

A thesis submitted in partial fulfilment of the requirements of
Sheffield Hallam University
for the degree of Doctor of Philosophy

July 1998

Collaborating Organisation: British Glass
Northumberland Road
Sheffield



ABSTRACT

Laser Ablation ICP Spectrometry

Andrew Jansen

This thesis reports investigations into laser ablation inductively coupled plasma emission spectrometry for rapid elemental analysis of a diverse range of samples: glasses, aqueous solutions, oils, coated steels and glasses, and biological samples.

Bulk analysis of glasses for major, minor and trace elements is reported. Results showed that element emission responses are dependent upon laser operating conditions. With optimised operating conditions of a Q switched laser operating at 60 J for 5 s ablation time with the laser defocused by 5 mm above the sample surface. The limits of detection are in the sub $\mu\text{g g}^{-1}$ level with precision ranging from 6.6 %RSD for a non volatile element such as boron to 23 %RSD for a volatile element silver.

Although the principal aim of using aqueous multielement solutions as novel calibration standards for quantitative analysis of other liquids was not achieved, optimised laser operating parameters needed for microsampling of aqueous solutions and analytical performance data were obtained. The optimum laser operating conditions for a 20 μl sample were found to be the same as for glasses and were as follows: a Q switched laser operating at 60 J for a 5 s ablation time with the laser defocused by 5 mm above the sample surface. Transport efficiencies of approximately 30 % can be achieved, compared to < 1% by pneumatic nebulisation. Also there was no differential loss of elements by laser ablation which may occur with electrothermal vapourisation. Limits of detection were found to be in the sub $\mu\text{g ml}^{-1}$ level. Precisions were typically between 6.6 and 12 %RSD. The main cause for lack of precision was spattering of the sample.

Microsampling of oils by laser ablation proved to be an effective and accurate technique for rapid determination of element concentration without the need for sample filtration or digestion. Precision proved to be better than for aqueous solutions, typically from 3 to 7 %RSD, because of a reduction in spattering. The same optimum laser operating conditions used for aqueous solutions were identical for oils.

This thesis reports the first experiments to fully utilise laser ablation as a routine method for quantitative measurement of coating depth for coated steels and glasses. It was found that the peak width at half the maximum height was proportional to the coating thickness (over a range of 1 to 10 μm). With optimised laser operating conditions a depth resolution of less than 1 μm was achieved. The optimum laser operating conditions were as follows: a Q switched laser ran continuously with a laser lamp energy of 60 J at 10 Hz pulse repetition rate.

Finally experiments show the great potential for the use of laser ablation as a microsampling technique for microtome tissue samples. Micro depth analysis of nickel distribution in skin shows that the technique could differentiate between two skin samples with different nickel concentrations. The use of gel multielement standards as a novel calibration technique for analysis of microtome tissue samples has also been demonstrated. Optimum laser operating condition were to use a moderate laser energy of 750 V with the laser defocused 5 mm above the sample surface.

Acknowledgements

I would like to extend thanks to Dr David Mowthorpe whose guidance and encouragement were invaluable, particularly during the last four months. I would also like to thank all the technicians with special mention to Mr Alan Cox. Finally a special thanks to all my friends and family.

Chapter one**Introduction**

| | | |
|-----|------------------------------------------------------------------------------|----|
| 1.1 | Trace element analysis | 2 |
| 1.2 | Development of inductively coupled plasma spectrometry | 7 |
| | 1.2.1 Historical | 8 |
| | 1.2.2 Plasma formation | 10 |
| | 1.2.3 Plasma temperatures | 12 |
| | 1.2.4 Plasma emission | 13 |
| | 1.2.5 Instrumentation | 14 |
| 1.3 | Solid sample introduction for inductively coupled plasma spectrometry | 18 |
| 1.4 | Basic characteristics of lasers | 25 |
| 1.5 | Role of lasers in trace element analysis | 29 |
| | 1.5.1 Laser microprobes | 29 |
| | 1.5.2 Laser ablation inductively coupled plasma atomic emission spectrometry | 33 |
| 1.6 | Laser interaction with materials | 39 |
| | 1.6.1 The ablation event | 39 |
| | 1.6.2 Influence of laser parameters | 42 |
| | 1.6.3 Influence of target properties | 46 |
| | 1.6.4 Laser interaction with liquids | 47 |
| 1.7 | Conclusions | 49 |
| 1.8 | Aims | 51 |

Chapter two**Experimental**

| | | |
|-----|------------------------------------------|----|
| 2.1 | Introduction | 54 |
| 2.2 | The laser | 55 |
| 2.3 | The ICP emission spectrometer | 56 |
| 2.4 | The laser ablation chambers | 59 |
| 2.5 | The laser ablation ICP mass spectrometer | 62 |
| 2.6 | Reagents, materials and procedures | 64 |

Chapter three**Glasses**

| | | |
|-----|-------------------------------|----|
| 3.1 | Introduction | 68 |
| 3.2 | Preliminary experiments | 70 |
| 3.3 | Effect of laser ablation time | 72 |
| 3.4 | Effect of laser focusing | 74 |
| 3.5 | Effect of laser energy | 76 |
| 3.6 | Calibration | 78 |
| 3.7 | Precision | 82 |
| 3.8 | Analysis of glasses | 84 |

Chapter four**Aqueous solutions**

| | | |
|-----|---------------------------------|-----|
| 4.1 | Introduction | 88 |
| 4.2 | Preliminary experiments | 89 |
| 4.3 | Calculation of analyte mobility | 92 |
| 4.4 | Effect of laser ablation time | 95 |
| 4.5 | Effect of laser energy | 97 |
| 4.6 | Effect of laser focusing | 101 |
| 4.7 | Effect of sample volume | 104 |
| 4.8 | Calibration | 106 |

| | | |
|-----|-----------|-----|
| 4.9 | Precision | 108 |
|-----|-----------|-----|

Chapter five

Oils

| | | |
|-----|-------------------------------|-----|
| 5.1 | Introduction | 112 |
| 5.2 | Preliminary experiments | 113 |
| 5.3 | Effect of laser ablation time | 116 |
| 5.4 | Calibration | 118 |
| 5.5 | Precision | 120 |
| 5.6 | Analysis of oils | 122 |

Chapter six

Thin coated materials

| | | |
|-----|----------------------------------------------------------------|-----|
| 6.1 | Introduction | 126 |
| 6.2 | Preliminary experiments | 127 |
| 6.3 | Depth profiling calibration | 135 |
| 6.4 | Zirconium nitride and titanium/zirconium nitride coated steels | 139 |
| 6.5 | Multilayered steels | 140 |
| 6.6 | Ultrathin coated steels | 143 |
| 6.7 | Tin oxide coated glass | 145 |

Chapter seven

Biological samples

| | | |
|-----|-------------------------------------------------------------|-----|
| 7.1 | Introduction | 149 |
| 7.2 | Gel multielement standards | 150 |
| 7.3 | Calibration | 152 |
| 7.4 | Analysis of microtome tissue samples | 153 |
| 7.5 | Determination of nickel distribution in skin tissue samples | 154 |

Chapter eight

Conclusions and future work

8.1 Conclusions and future work

158

References

1.1 Trace element analysis

Elemental analysis is undertaken for a wide range of analytical needs such as environmental, forensic, archaeological, and process control of manufactured materials. There are also a huge range of sample types: gases, waters, biological, metallurgical, geological, and organic samples; and then each sample may be present as a gas, liquid, or solid. The needs and wants of a particular analysis depend on what the sample is, the amount available and what state it is in, and on the number and concentration range of the elements that are to be determined. They will also depend on the of precision, accuracy, sensitivity and limits of detection required. There are a large number of analytical procedures and techniques which have been developed in response to the range of problems faced by the analytical scientist. The technique of choice depends on a knowledge of basic principles, analytical strengths and limitations and other factors such as cost.

While micro and elemental analysis (1,2) is concerned with the determination of major and minor constituents (10^{-2} %) in small samples (<10 mg), the aim of trace analysis (3-7) is to detect the elements that are at least 10^4 times less concentrated than the matrix elements, i.e. at the ppm level. Thus in microanalysis the small amount to be determined is dictated by the small amount of sample available, but in trace analysis by its very low concentration in the matrix.

The techniques used for trace element analysis may be characterised according to the concentrations they can handle. The absolute amounts of elements which can be determined by techniques presently at our disposal lie in the nanogram and upper picogram ranges, and in a few cases even lower. The extreme low limits of detection required are often raised by several orders of magnitude, by possible interference from high concentration of matrix. For this reason it is often necessary to separate the trace elements from the matrix or concentrate the trace elements.

Before the advent of instrumental analysis techniques (until perhaps 1920), the basis of trace elemental analysis was based on the measurement of mass and volume (gravimetric and volumetric analysis). As a consequence they have come to be known as *classical techniques*.

Some instrumental techniques are more sensitive than classical ones. With certain combinations of elements or compounds an instrumental technique may be more specific. With others, gravimetry and/or titrimetry may be less subject to interferences.

Table 1.1 lists many of the common techniques useful for analytical measurement. The first group of techniques involve the measurement of emitted radiation or the interaction of radiation with matter. The second group is concerned with the measurement of an electrical signal. The final group of techniques are the classical techniques of gravimetry and titrimetry. The limits of detection indicated are for easily determined elements, and are estimates under favourable conditions.

Table 1.1 Techniques used in trace elemental analysis

| Analytical techniques | Measured signal | Limit of detection/g |
|--------------------------------|-------------------------|----------------------|
| Atomic emission spectrometry | Emission of radiation | 10^{-10} |
| Fluorimetry | | 10^{-10} |
| X-Ray Fluorescence | | 10^{-9} |
| Atomic absorption spectrometry | Absorption of radiation | 10^{-13} |
| Spectrophotometry | | 10^{-9} |
| Potentiometry | Electrical potential | 10^{-10} |
| Polarography | Electrical current | 10^{-10} |
| Mass spectrometry | Mass to charge ratio | 10^{-16} |
| Gravimetry | Mass | 10^{-9} |
| Volumetry | Volume | 10^{-9} |

Analytical instruments can be viewed as a communication device between the system under study and the analytical scientist. Regardless of its complexity, an instrument is designed around five basic functions: (1) sample introduction, (2) signal generation, (3) transduction, (4) signal processing and (5) display.

Sample introduction is an extension of sample preparation. As a consequence the range of available sample introduction techniques depends on available and effective sample preparation procedures. In many cases sample introduction is dependant on the sample being in solution, although some devices allow gases as well as solids to be analysed directly.

Signal generation is produced by measurement of a range of signals as seen in **Table 1.1**. These signals may be due to the emission or absorption of radiation, the measurement of electrical potential or current, or the mass to charge ratio. Signals may be generated by atomisation and excitation of the sample in flames, plasmas, electrothermal heating, the use of electrical discharges, excitation with X rays and the interaction with laser energy.

Transduction is the conversion of the measured signal to an electrical voltage, current or resistance. For spectrometric measurements a photomultiplier device is used to convert light energy into an electrical signal. The signal processor converts the electrical signal in such a way as to make it more convenient to read.

Finally, the output readout or display on most modern instruments is based on the use of microprocessors, with the ability to convert analogue into digital information. It is the advent of computers which has up till now been the greatest revolution in analytical instrumentation. Which has made analysis cheaper, faster and has made data manipulation much easier and faster.

Atomic spectrometry is based upon absorption, fluorescence, or emission of electromagnetic radiation by atoms or ions. Three regions of the spectrum yield atomic information (the ultraviolet/visible and the X-ray). Electrons and ions may also be used as an excitation species. The table below (**Table 1.2**) categorises the various atomic spectrometric techniques on the basis of signal generation and the measured species. These techniques offer the advantages of high specificity, wide applicability, excellent sensitivity, speed, and convenience; they are amongst the most selective of all analytical techniques. Perhaps 70 elements can be determined with

sensitivities that fall in the parts per million range to parts per billion range. Many of these techniques are capable of direct analysis of solids as well as liquids.

Table 1.2 Comparison of some of the popular atomic spectroscopy techniques

| Technique | Excitation and/or sampling method | Measured signal | Sample types |
|-----------|-----------------------------------|-----------------|----------------|
| Flame AAS | Flame | Photons | Liquids/solids |

Key attributes: Low cost, and well developed. Suffers from chemical interferences, and is only able to perform single element analysis for each hollow cathode tube available. It also has a low dynamic linear range.

| | | | |
|-----------|-------|---------|---------|
| Flame AES | Flame | Photons | Liquids |
|-----------|-------|---------|---------|

Key attributes: Low cost, and well developed. Flame acts as an excitation source which leads to a multielement capability, using a turn table monochromator. Disadvantages include: Self absorption of analyte at higher concentration leading to non linear calibration curves, and the same chemical interferences as AAS.

| | | | |
|---------|----------------|---------|----------------|
| ETV AAS | Electrothermal | Photons | Liquids/solids |
|---------|----------------|---------|----------------|

Key attributes: Very high sensitivity, for small volume of sample (0.5-10 µl). However, it suffers from poor precision (5-10 %RSD) and from interferences due to matrix effects.

| | | | |
|---------|--------|---------|----------------------|
| ICP AES | Plasma | Photons | Liquids/gases solids |
|---------|--------|---------|----------------------|

Key attributes: Advantages include: few chemical interferences and matrix effects. Simultaneous multielement capability (up to 60 elements). High stability, low noise to background ratio source, good limits of detection (down to ppt levels), and a high dynamic linear range. Disadvantages include: low transport efficiency, using standard pneumatic nebulisation sample introduction techniques (1-3 %). High operating costs and the production of complex spectra leading to the possibility of spectral interferences from matrix elements.

| | | | |
|--------|--------|------|----------------------|
| ICP MS | Plasma | Ions | Liquids/gases solids |
|--------|--------|------|----------------------|

Key attributes: Advantages same as for ICP ES. This technique however, also offers greater sensitivity and isotopic information.

| | | | |
|----------------|--------|---------|--------|
| Ark /Spark AES | Plasma | Photons | Solids |
|----------------|--------|---------|--------|

Key attributes: Advantages include: quick and easy qualitative screening for direct bulk sampling of solids, with no need for sample preparation. Main disadvantages include: the need for matrix matched calibration standards, a need for the sample to be electrically conducting, and the production of complex spectra.

Table 1.2 Comparison of some popular atomic spectroscopy techniques - continued

| Technique | Excitation and/or sampling method | Measured signal | Sample types |
|-----------|-----------------------------------|-----------------|--------------|
| GDOS | Plasma | Photons | Solids |

Key attributes: Advantages include: a very high sensitivity (with a detection limit of 0.005-0.1 $\mu\text{g g}^{-1}$) and high precision. The technique offers depth profiling as well as bulk sampling. Disadvantages include: that the sample has to be electrically conducting, and the formation of complex spectra.

| | | | |
|-----|--------|--------|----------------|
| XRF | X rays | X rays | Solids/liquids |
|-----|--------|--------|----------------|

Key attributes: This technique is widely used, well characterised, and offers excellent precision for bulk sampling. Metal samples can be analysed directly but non conducting samples need to be prepared as lithium borate fusions. The technique offers moderate sensitivity.

| | | | |
|-----------|-------------------------------------------------------|---------|--------|
| LA ICP ES | Laser sub-sampling and secondary excitation in plasma | Photons | Solids |
|-----------|-------------------------------------------------------|---------|--------|

Key attributes: This technique offers high sensitivity, good mapping, and profiling. There is little or no need for sample preparation, no vacuum is needed, and virtually any sample type can be analysed. However, like most solid sampling techniques, quantitation is poor owing to the need for matrix matched calibration standards. Precision is poor owing to poor reproducibility of sampling yields.

| | | | |
|-----------|-------------------------------------------------------|------|--------|
| LA ICP MS | Laser sub-sampling and secondary excitation in plasma | Ions | Solids |
|-----------|-------------------------------------------------------|------|--------|

Key attributes: Similar to LA ICP ES but with the advantage of greater sensitivity and the ability to produce isotopic information. The main use is semiquantitative analysis.

Abbreviations used:

AAS Atomic absorption spectroscopy

AES Atomic emission spectroscopy

ETV Electrothermal vaporisation

ICP ES Inductively coupled plasma emission spectroscopy

ICP MS Inductively coupled plasma mass spectrometry

GDOS Glow discharge optical spectroscopy

XRF X ray fluorescence

LA ICP ES Laser ablation inductively coupled plasma emission spectrometry

LA ICP MS Laser ablation inductively coupled plasma mass spectrometry

Although instrumental analysis techniques offer numerous advantages, the main shortcoming of spectral techniques is the sample introduction system. Samples for trace element analysis are rarely in a form suitable for direct introduction into an analytical instrument. Generally they are treated to give aqueous solutions. Many solid materials, such as silicate containing materials are not easy to prepare for elemental analysis. In most cases preparation of such materials involves the use of fusion fluxes or complex acid digestion techniques followed by analysis. Many of these procedures are time consuming, and also very laborious requiring constant supervision during operation. It is therefore desirable to analyse materials directly without lengthy sample preparation procedures and all the disadvantages this entails. Many analytical techniques have been developed for direct solids analysis (see Table 1.2), each with its unique strengths and weaknesses.

Laser ablation has now been successfully used for a number of years. Two techniques can be employed either by measuring the emission signal directly as with laser microprobes or as a method of sample introduction by the laser into an atomic spectrometer. Developments are mostly concerned with its use with inductively coupled plasma spectrometry. Numerous possibilities have been recognised for laser ablation inductively coupled plasma spectrometry which is capable of analysing most sample types, is applicable to situ microsampling, and when coupled with a plasma spectrometer it offers the advantage of very fast multielement analysis. There is still, however, a lot of scope to advance the application of this technique for analysis of a range of sample types, and this is the central concern in this thesis.

1.2 Development of inductively coupled plasma spectrometry

During the 1960's inductively coupled plasmas (ICP) became alternative excitation sources for atomic spectrometry. Before this, atomic emission spectrometry was being superseded by atomic absorption spectrometry due to the increased sensitivity and accuracy offered by the latter. A flame is not a good excitation source due to its relatively low temperature which leads to chemical interference effects. Furthermore the relatively long optical path length leads to self absorption of

the emitted wavelengths by atoms in the cooler regions of the flame. Self absorption results in non linear calibration curves. However, atomic emission spectrometry offered one large advantage; namely the capability of simultaneous multielement analysis. Consequently, there was a push to find better excitation sources with thinner optical path lengths and increased temperatures. This lead directly to the development of the inductively coupled plasma.

Plasmas offer several benefits compared to flame techniques. Among their advantages is lower inter-element interference, which is a direct consequence of their higher temperatures. Second, good spectra can be obtained for most elements under a single set of excitation conditions; as a consequence, spectra for dozens of elements can be recorded simultaneously. This feature is of particular importance for multielement analysis of very small samples. Flame sources are less satisfactory in this regard because optimum conditions vary widely from element to element; high temperatures are needed for some elements and low temperatures for others. Another advantage of the more energetic sources is that they permit the determination of low concentrations of elements that tend to form refractory compounds. Finally, because of the thin optical pathways of plasma sources the determination of several decades of concentration is possible in contrast to one or two for flame emission sources.

1.2.1 Historical

Babat (8) is recognised as being the first to establish and sustain a plasma at atmospheric pressure by inductive heating. He used input powers of 30 to 50 kW and generated plasmas in closed systems. In 1962, Reed (9) developed a method whereby he could ignite and sustain a plasma at atmospheric pressure by induction heating within an open ended plasma torch through which gas flowed. Reeds interest was refractory crystal growth, and he did not speculate that inductively heated plasmas may be useful in spectroscopic studies. At about the same time Greenfield et al (10, 11) began investigating a toroidal plasma operating at high frequencies (36 MHz). They used relatively large torches for his argon-nitrogen (nitrogen cooled) ICP. They

postulated that their system offered higher sensitivity, fewer interferences, and better precision than lower powered all argon plasmas.

Also during this time Fassel et al (12) worked on an all argon plasma operating at a lower frequency (3.4 MHz), using a smaller diameter torch than Greenfield and a laminar gas flow system. With solution nebulisation technology already well established for flame AAS systems, it was natural that these research groups would consider the introduction of solutions into the plasma. Nebulisation of liquid samples is still the main sample introduction method today.

By 1969 Dickinson and Fassel (13) had reported how they had improved the detection limits of ICP spectrometry by two orders of magnitude better than had been achieved previously. By 1971, extensive research had established the viability of the plasma as a high power, high stability excitation source for atomic emission spectrometry. The potential of low power argon plasma as emission sources for simultaneous multielement analysis using compromised operating conditions was firmly established (14-17). Developments lead to exploitation of the exceptionally high sensitivity of ionic lines. Other advantages included, relative freedom from matrix interferences, detection limits in the microgram per litre range, a linear dynamic range of 4 to 6 orders of magnitude and a precision of 1-3 % RSD when using pneumatic nebulisation of solutions. Despite these great advantages, the introduction of samples into the plasma continues to be the limiting factor of analytical plasma spectrometry. The standard method of liquid sample introduction occurs by pneumatic nebulisation of sample, only 1-3 % (18) of the sample solution is injected into the plasma. With this in mind there would be great advantages in exploiting techniques that could be used for direct sampling of solids as well as liquids, not only improving transport efficiency of liquids but do away with the need for any sample pretreatment.

As well as using a plasma as an excitation source for atomic emission spectrometry, they may be used as an ion source for mass spectrometry. Inductively coupled plasma mass spectrometry (ICP MS) has achieved world wide acceptance as a flexible analytical technique for trace element determinations in a wide range of sample types. The early ICP MS instruments used a

quadrupole mass analyser and the vast majority of modern commercial instruments still use this form of analyser to scan through a large mass range over a very short time, making it ideal as an analyser for signals which vary with time.

1.2.2 Plasma Formation

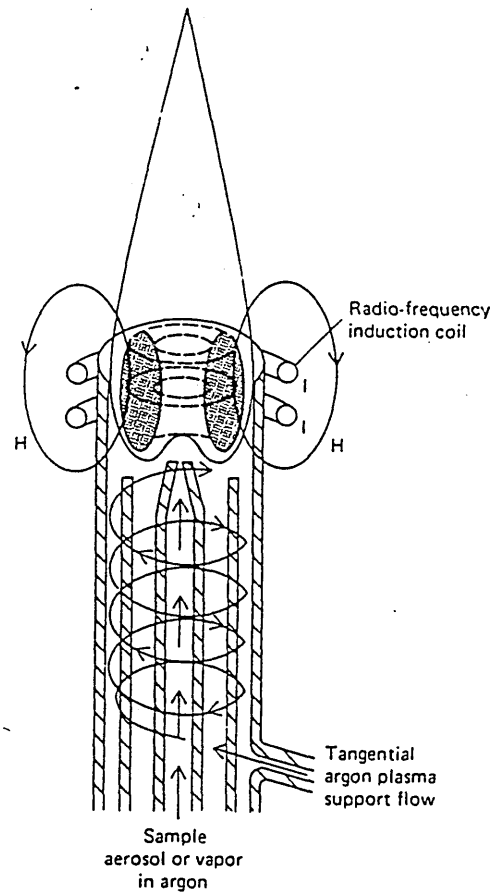
A plasma is defined as a volume of gas in which a significant portion is ionised. Magnetic fields may then interact with the plasma. One such interaction is that of an inductive coupling of a magnetic field with the plasma. The concentration of the cations and electrons formed as a result of the ionisation is equal so that the net charge approaches zero. In the argon plasma, argon ions and electrons are the principal conducting species, although cations from the sample will also be present in lesser amounts. Argon ions, once formed in a plasma, are capable of absorbing power from an external source so as to maintain the temperature at a level at which further ionisation sustains the plasma indefinitely. Temperatures as great as 10,000 °K are encountered.

Three power sources have been employed in argon plasma spectroscopy. The first power source uses dc electrical power which is capable of maintaining a current of several amperes between electrodes immersed in a stream of argon. The second and third are powerful radio frequency and microwave frequency generators through which argon flows. Of the three, the radio frequency or inductively coupled plasma source appears to offer the greatest advantage, in terms of sensitivity and freedom from interference. On the other hand, the dc plasma source has the virtue of simplicity and lower costs.

Figure 1.1 shows a schematic diagram of an inductively coupled plasma source. The method of forming a plasma is to use a torch, consisting of three concentric tubes, the inner sample carrier tube, an intermediate plasma gas tube and an outer coolant gas tube. The diameter of the largest tube is about 2.5 cm. This is placed inside a water cooled copper coil connected to a high frequency generator, which is capable of producing 2 kW of energy at about 27 MHz. With argon gas flowing through the torch and the power switched on, there is no interaction, since argon is a

non-conductor. In order to initiate the plasma it is necessary to plant a 'seed' of electrons in the coil space. Modern instruments use a tesla coil. When the plasma is initiated it takes up a shape of a cone, and is formed within the space above the coil.

Figure 1.1 A typical inductively coupled plasma source (from Fassel (19))



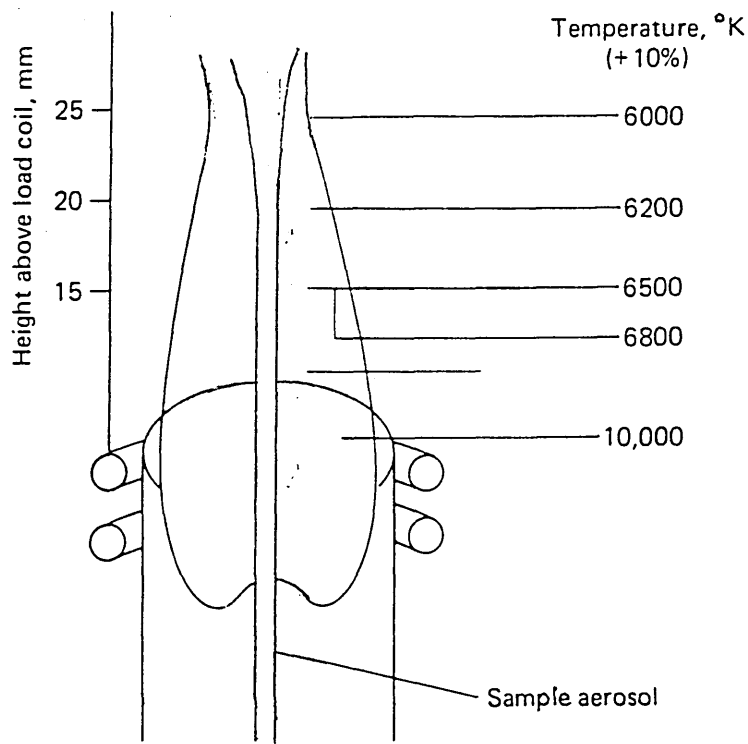
1.2.3 Plasma temperatures

The temperature of a plasma formed in this way varies between 9,000 and 10,000 °K. It is important, therefore, that the apparatus supporting the plasma is prevented from melting. This is achieved by using a coolant gas flowing at about 10 to 16 L per minute. Argon as the coolant gas, is introduced tangentially, the gas streams helically upwards cooling the tube and also shaping the plasma. The inner glass tube in the torch allows the sample carrier gas in. This carrier gas is said to punch a hole through the centre of the plasma. The temperature of this central hole is about 4,000 to 5,000°K. This high temperature coupled with a relatively high residence time of a few milliseconds, creates an atmosphere suitable for volatilisation and atomisation of aerosols during their passage through the plasma. Atomic emission is usually detected in a region of the plasma about 15 mm above the coil. The efficiency of atomisation depends on the power output and the velocity of the sample carrier gas. The intermediate tube allows for introduction of an optional gas flow called the 'plasma gas' which may be used to adjust the vertical position of the plasma.

Figure 1.2 shows temperatures at various parts of the plasma. By the time the sample atoms have reached the observation point, they have resided in the plasma for about 2 ms at temperatures ranging from 6,000 to 8,000°K. These times and temperatures are roughly two or three times as great as those found in the hottest combustion flames (acetylene/nitrous oxide) employed in flame methods. As a consequence, atomisation is more complete and fewer chemical interference problems arise.

Several other advantages are associated with the plasma source. First, atomisation occurs in a chemically inert environment which tends to enhance the lifetime of the analyte by preventing oxide formation. In addition, and in contrast to arc, spark, and flame sources, the temperature cross section of the plasma is relatively uniform. Because the sample is confined to a narrow cross section, self absorption and self reversal effects are not encountered. Thus linear calibration curves over several orders of magnitude of concentration are often observed.

Fig 1.2 Temperatures in a typical inductively coupled plasma source



1.2.4 Plasma emission

An examination of the emission produced by a high energy source such as a plasma reveals three types of superimposed spectra: continuous, band and line. The continuum apparently arises from a recombination of thermally produced electrons with argon ions. Spectral observations are often made at a height of 15 to 20 mm above the induction coil; here, the background radiation is remarkably free of argon lines and is well suited for analysis. Band spectra, are made up of a series of closely spaced lines, observed in certain wavelength regions, due to molecular species such as OH, NO and CN.

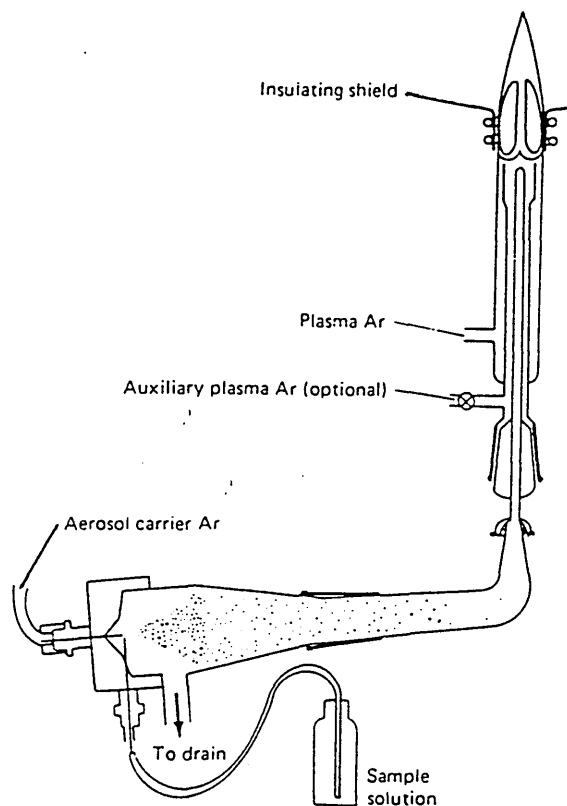
Emission spectroscopy is based upon line spectra produced by excited atoms and ions. Spectra generated by using a plasma excitation source are generally richer in lines than lower energy emission sources such as flames, because of the higher energy involved. Many of the lines observed in a plasma spectrum arise from ions rather than atoms.

1.2.5 Instrumentation

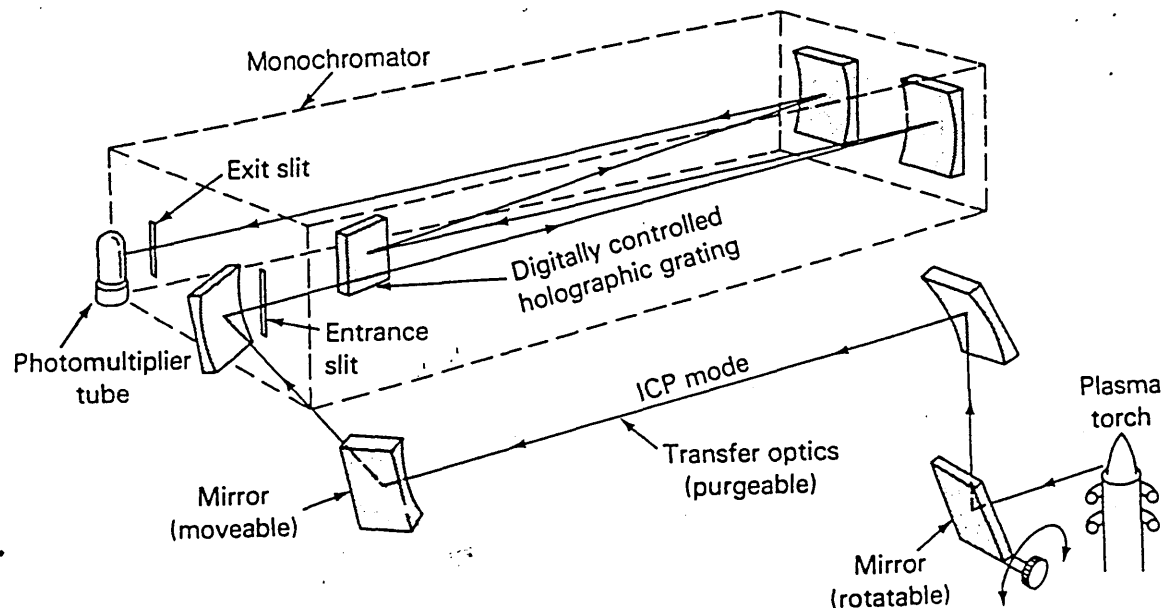
Instruments for elemental emission analysis by plasma excitation are manufactured by several instrument makers. Their wavelength ranges vary considerably; some include the entire ultraviolet/visible spectrum from 180 to 900 nm. Most do not operate above 500 to 600 nm, in as much as the majority of useful element emissions occur at shorter wavelengths. A few instruments are equipped with vacuum chambers which permit detection of ultraviolet radiation down to 170 nm. This may be used to analyse for such elements as carbon, phosphorous, and sulphur.

The sample is carried into the hot plasma at the head of the torch by argon flowing at about 1 L per minute through the central quartz tube. The sample may be an aerosol, a thermally generated vapour, fine powder, or ablated particles. The most widely used apparatus for sample injection is similar to the nebuliser employed for flame methods. **Figure 1.3** shows a typical arrangement. Here the solution is nebulised by a flow of argon, and the resulting finely divided droplets are carried into the plasma.

Fig 1.3 A typical nebuliser for sample introduction into an ICP source

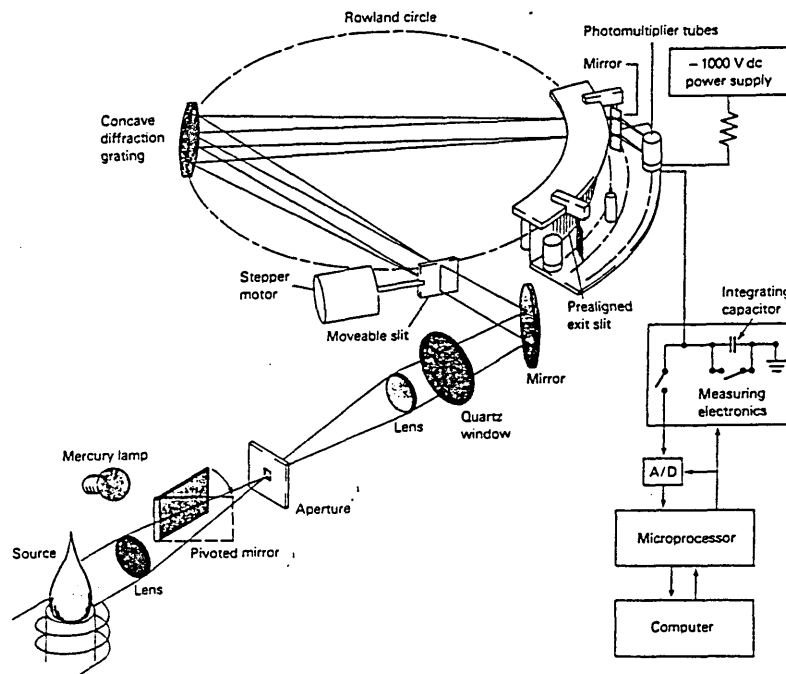


Instruments are of two basic types: sequential and simultaneous multi channel designs. Sequential instruments are less complex, and less expensive. Here, the instrument is programmed to move from the line of one element to that of a second. In contrast, multi channel instruments are designed to measure simultaneously the intensities of emission lines for a large number of elements (up to 60). Figure 1.4 shows a typical sequential instrument. A series of mirrors are used to direct the emission from the plasma source into the monochromator. The holographic grating is driven by a stepper motor with each step corresponding to a change in wavelength. Up to 20 elements can be analysed at one time in a few minutes.



Multi channel instruments incorporate as many as 60 photomultiplier tubes located behind fixed slits along the curved focal plane of a concave grating monochromator. A typical diagram of such a device is shown in Figure 1.5. Here the entrance slit, the exit slit, and the grating surfaces are located along the circumference of a 'Rowland circle', the curvature of which corresponds to the focal curve of the concave grating. Radiation from several fixed slits is reflected by mirrors to photomultiplier tubes. The slits are factory fixed to transmit lines for elements chosen by the customer, but can be altered to accommodate other elements. The signals from the several photomultiplier tubes may then be integrated. The entrance slit can be moved tangentially to the Rowland circle by means of stepper motors. This device permits scanning through peaks and provides information for background correction.

Fig 1.5 A plasma multichannel spectrometer based upon Rowland circle optics



Spectrometers such as the one shown in Figure 1.5 have been used both with plasma and with arc and spark sources. For rapid routine analysis such instruments are often ideal. In addition to speed, photoelectric multichannel spectrometers often offer the advantage of good analytical precision. Under ideal conditions reproducibilities of the order of 1% relative of the amount present can be achieved. Several of the newer instruments are provided with a second monochromator that permits spectral scanning thus adding a versatility that was absent in some earlier instruments. Generally, multichannel instruments are not as versatile as the sequential instruments. Modern skew grating sequential instruments now allow for rapid and accurate scanning through the range of wavelengths, being almost as fast as simultaneous instruments. Multichannel emission instruments based upon the multichannel photo diode detection systems (which are more sensitive than traditional photomultiplier tubes) are now commercially available. Also the echelle monochromator with its greater linear dispersion and resolution compared to previously used grating systems would appear to offer considerable potential for the development of instruments of this kind. Most modern instruments have been reduced in size and have become benchtop instruments, whose entire operation is controlled by microcomputer.

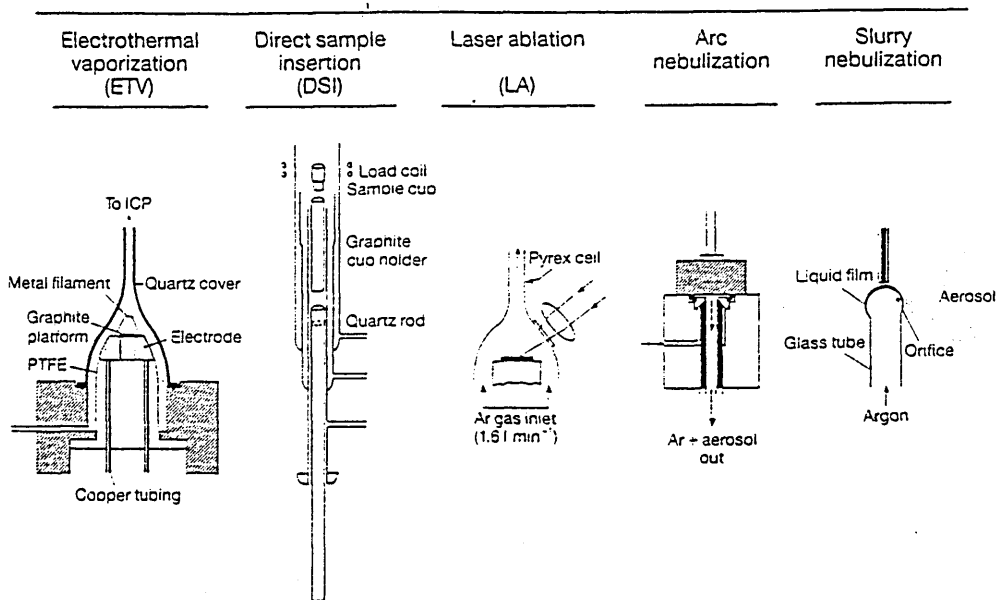
1.5 Solid sample introduction for inductively coupled plasma spectrometry

Solid sampling devices have been used to vaporise liquid and solid samples into flames and plasmas for many years. Applications of such devices have been mainly in the field of inductively coupled plasma spectrometry and have been reviewed by Thompson et al (20), Ng and Garuso (21), and Matuisiewicz (22). In principle, any sample introduction method which can be used with plasma emission spectrometry is also suitable for plasma mass spectrometry. Today, there are commercial solid sampling systems which have been developed from research devices. Some notable ones are described below.

Overview and nomenclature

There are five most commonly used solid sampling systems which have been used for direct measurement of solid samples with plasma spectrometry. These are illustrated in Figure 1.6. The five techniques are electrothermal vaporisation (ETV), direct sample insertion technique (DSIT), arc nebulisation, slurry nebulisation, and laser ablation (LA).

Fig 1.6 Examples of solid sample introduction techniques for ICP spectrometry



Electrothermal vaporisation (ETV) which has already been described for liquid sample introduction, is a technique which was developed very early on and has so far been most commonly used. Many of these devices were simple modifications of equipment used in electrothermal vaporisation atomic absorption spectrometry. Graphite platforms or metal filaments, which are resistively heated, are employed for the evaporation of samples. The sample vapour is transported by an inert gas stream to the plasma via a short transport tube.

In the direct sample insertion technique (DSIT), the sample is placed in a graphite or metal cup which is inserted directly into the plasma. There, the cup is inductively and thermally heated to high temperatures and the sample is evaporated into the plasma. This technique of sample introduction has also been known as the "sample elevator technique, (SET)".

The use of a high voltage interrupted arc has been described for the generation of a sample vapour which again was transported into a plasma by an Ar carrier gas flow. There are few applications and few publications produced, with little academic interest so far.

In slurry nebulisation, the sample is introduced into the plasma by a conventional pneumatic nebulisation system. This technique can in principle also be regarded to be a solid sample introduction technique. The sample is not digested as in conventional nebulisation but is finely ground and suspended in a solvent and is thus introduced as an aerosol of fine hydrated solid particles.

The final technique is laser ablation (LA). The use of a laser beam for evaporating, atomising, and ionising a sample has been known for many years. In laser ablation inductively coupled plasma spectrometry evaporation and ionisation take place at different places and by different energy sources. The sample which is evaporated and partially atomised and ionised by the laser is transported into the plasma via a transfer tube.

Electrothermal vaporisation (ETV)

Electrothermal vaporisation using a resistively heated graphite rod as a means of sample introduction in plasma emission spectrometry was first described by Gunn and Millard et al (23) in 1980. Actually this system was not used for direct introduction of solids but for micro amounts of liquids. However, these ETV devices can in principle also be used for insertion of solid samples. Gunn and Millard (23) also found that the most critical parameters effecting sensitivity were the carrier gas flow rate, the RF power to the ICP, and the filament vaporisation temperature. They found that the optimum flow rate reduces as the filament temperature goes up because of the "piston effect" (expansion of the carrier gas due to the heating pulse applied to the filament). A disadvantage of the ETV sample introduction technique compared to pneumatic nebulisation is that precision is degraded, presumably due to worse reproducibility of the evaporation efficiency. Park (24) obtained a precision of between 13 and 15 %RSD for integrated signals of Mo and W, in solutions of geological materials after decomposition by fusing them with a $\text{Na}_2\text{CO}_3/\text{NaNO}_3$ flux. The melt was leached with water and 5 μl aliquots of the solution were pipetted into the ETV. Detection limits of 0.03 ppm for Mo and 0.06 ppm for W were found. However, memory effects were experienced with W due to carbide formation and the authors did not recommend the electrothermal vaporisation as preferable to conventional nebulisation.

Gray (25) used a similar system to that of Gun and Millard (23) for sample introduction into an ICP MS. Gray demonstrated that the background spectrum of a dry argon gas shows much less interferences from molecular species than does a plasma with high solvent loading. Absolute detection limits for the elements Pb, Zn, Cd, As, and Se were reported to range from 1 pg to 12 pg. The determination of the principal isotope of sulphur was feasible with a precision better than 1 % RSD. Such performance is not achievable with pneumatic nebulisation due to the high background levels of dimer oxygen molecular ions originating from water.

The suitability of electrothermal vaporisation for simultaneous determination of trace elements (Cd, Mg, Pb, and Zn) in Ni base alloys was undertaken by Clarke (26). Precise control of furnace temperature was used to achieve a selective volatilisation of trace elements from the involatile host matrix. Relatively high furnace temperatures were necessary for the efficient release of As and Se. It was found that by increasing the graphite cup temperature to a point at which the solid Ni based sample melted completely (1600 to 1800^o C), the volatile trace elements Cd, Mg, Pb, and Zn were released from the molten matrix. The response from the matrix elements at this temperature was minimal and spectral interferences were not observed. The metalloid elements As and Se, were not vaporised under these conditions. However, it was possible to increase the temperature further so as to release them from the matrix. Signals recorded for the matrix elements Al, Co, Cr, and Ni were very intense and the possibility of spectral interference on the As and Se channels was investigated. It was found that by using two different certified reference materials (BAS 345 and BAS 346), which have the same nominal matrix, but different trace element concentrations (BAS 346 had enhanced trace element concentrations). The results showed the greater signal from the alloy with the higher Se content. This suggested that the signal was a true analyte response and not a spectral interference.

Darke et al (27) investigated the merits of an ETV device based on a design by Gunn and Millard (23) for use with inductively coupled plasma emission spectrometry. Drying, ashing, vaporisation temperatures and the carrier gas flow rates were optimised, and the use of matrix modifiers was tested for the determination of lead in fly ash samples. The detection limit with the ETV showed an improvement over the solution nebulisation by a factor of 10 (0.01 ng ml⁻¹ cf. 0.1 ng ml⁻¹). Quantitation was performed by the method of standard additions for fly ash analysis by the electrothermal vaporisation technique and the results showed good agreement compared to values obtained by solution nebulisation.

Direct sample insertion devices (DSID)

A direct sample insertion device was first developed by Horlick, Salin, and Sing for use with inductively coupled plasma emission spectrometry (28). A Fassel type torch was modified to accommodate the sample probe which consisted either of home made graphite, tantalum or tungsten cups or of graphite sample cups utilised in classical dc arc emission spectroscopy. The cups sit on top of a quartz rod which is fixed on the sample cup holder. The bottom of the torch is sealed by a glass shutter, except during sample insertion, so as to maintain the gas pressure in the central tube of the torch and keep the plasma discharge at its normal position. During insertion, the glass shutter is opened. When insertion is complete a teflon stop at the end of the quartz rod seals the bottom of the central tube. The samples can be dried or ashed at a position of 35 mm below the load coil. When fully inserted, the top of the cup is aligned with the top of the load coil. At this position, the sample cup can attain a temperature of 2000⁰ C. But even at these temperatures non volatile analytes such as carbide forming elements do not vaporise completely. Sample size is in the order of some 20 µl or a few mg. The direct sample insertion system is fully automated, and the total time for a full insertion is 5 s.

Boomer et al (29) used a wire loop direct sample insertion device. They found that all inductively coupled plasma mass spectrometry parameters were found to be rather different from those with solution nebulisation and had to be carefully optimised. For the analysis, 10 µl volumes of sample were deposited onto a wire loop which was inserted into the plasma. Detection limits for the elements Mn, As, Pb, Cd, Li, Ag and Cu were improved by a factor of 40 over conventional nebulisation. For 100 ng ml⁻¹ solutions, precision in the range of 5 to 13 %RSD was achieved for 5 repetitive insertions.

Hall et al (30) compared the electrothermal vaporisation device system designed by Park (24) and a wire loop direct insertion device designed by Salin and Sing (28) with regard to their applicability to the analysis of river water reference material SLRS 1. They concluded that, although introduction by the direct sample introduction technique is not subject to loss of analyte

during the transport to the plasma, DSI was less applicable to the analysis of solutions with high (> 1 %) salt concentrations. Although better precision and slightly better detection limits could be achieved with direct sample introduction in the analysis of "clean" solutions, the electrothermal vaporisation technique proved to have greater flexibility for more complex matrixes.

Arc nebulisation

In 1986 Jiang and Houk (31) described a technique for direct elemental analysis of solid conducting materials. The sample was used as the cathode in an intermittent arc. The arc was generated between the Cu anode and the sample cathode. The eroded sample material was transported through a plastic tube (2 m long, 3 mm inner diameter) into the torch of a plasma mass spectrometer by Ar carrier gas flow. For the steels used in their study, the sample material was removed at a rate of approximately 1 mg min^{-1} . Standardisation was performed with steel standard reference materials whose elemental composition was certified with NBS standard reference materials. Similar background spectra were recorded as in laser ablation inductively coupled mass spectrometry, enabling the determination of non metallic impurities. Detection limits in the lower $\mu\text{g g}^{-1}$ range were often achieved for the elements: Al, Si, Ti, V, Cr, Co, Ni, As, Zr, Nb, Mo, Sn, Ta and W. Precision was found to be ca. 5 % RSD.

Slurry nebulisation

Another way of introducing solid samples into the plasma is the technique of slurry nebulisation. The feasibility of slurry nebulisation has been studied by Williams et al (32). Slurries were prepared by shaking 1 g of sample with 10 g of zirconia beads in 2 ml of sodium pyrophosphate solution (0.05 g per 100 ml) for 24 hours. The finely ground samples (particle size $<3 \mu\text{m}$) were then washed from the beads and diluted to 100 ml with tetrasodium pyrophosphate solutions. Good agreement was achieved for the concentration values which were determined by slurry nebulisation plasma emission spectrometry and plasma mass spectrometry with the certified values for the elements Si, Al, Fe, Mg, Mn, Cr, V, Ni, Cu, Co and Zn in certified reference material soils (BCR CRM 142, SO 1 and SO 2).

For aspiration of the slurries a Babington or V groove type nebuliser should be used (33-35). Calibration can be performed simply with aqueous standards. However, internal standardisation is strongly recommended to be applied in order to correct for possible signal suppression.

Darke et al (36), who scrutinised the performance of laser ablation and slurry nebulisation as a means for sample introduction in plasma emission spectrometry as well as plasma mass spectrometry, found poor agreement between the results obtained for slurry nebulisation and the certified values in a South African reference material rock sample (SARM 5). They suggested that particle size effects might cause analytical errors in slurry nebulisation plasma spectrometry.

Laser ablation (LA)

In this technique a laser beam is focused onto a sample which is contained in an ablation chamber. When the beam strikes a solid, a small plasma is formed at the surface and the intense heat vaporises a small portion of the sample. Ablated material is entrained and transported to the plasma by an Ar carrier gas flow. The plasma injector gas is normally used as carrier gas. The laser beam vaporises both conductive and non conductive materials. Ideally, the elemental composition of the vapour in the plasma mirrors that of the sample. In practice, however, fractional ablation of different elements occurs, and particles of different sizes have different transport efficiencies. Losses during the transport through the transfer tubing have also been observed. Because of the excellent focusing characteristics of a laser beam (down to a few tens of microns) microsampling on a surface with a high spatial resolution and analysis of inclusions can be performed. The topic of LA ICP spectroscopy is the central concern of this project.

1.4 Basic characteristics of lasers

The first laser was constructed in 1960 (37). Since that time, chemists have found numerous useful applications for these sources in high resolution spectroscopy, kinetic studies of processes with lifetimes in the range of 10^{-9} to 10^{-12} s, the detection and determination of extremely small concentrations of species in the atmosphere, and the induction of isotopically selective reactions. In addition, laser sources have become important in several routine analytical methods, including: Raman spectroscopy, molecular absorption spectroscopy, emission spectroscopy, and as part of instruments for Fourier transform infrared spectroscopy.

The term laser is an acronym for *light amplification by stimulated emission of radiation*. Lasers operate through a process of stimulated emission, which results in the amplification of the incident radiation by inducing a transition from a higher to a lower level, resulting in the emission of a resonant photon. Stimulated emission occurs when the population of the higher state exceeds the lower one. This produces an intense beam of highly directable, monochromatic, coherent light.

The essential elements of a laser are: a lasing medium, which may be a solid crystal such as a ruby, a semiconductor such as gallium arsenide, a solution of an organic dye or gas; a pumping process to excite the atoms in the lasing medium to higher energy levels, which will trigger the formation of a cascade of photons of the same energy (pumping can be achieved by radiation from an external source, an electrical current, or an electrical discharge); and suitable optical feedback components that allow the beam of radiation to pass once through the laser medium (as in a laser amplifier) or bounce back and forth repeatedly through the laser medium (as in a laser oscillator). A discussion into the detailed workings of a laser was considered outside the scope of this introduction. There are numerous texts which cover the basic operation and use of lasers (38, 39). However, a glossary of the most commonly used terms in analytical chemistry is given in Table 1.3.

Radiance

The observed effects of laser radiation on the sample are clearly dependant upon the radiant flux, or power output of the laser, and the irradiance upon the sample surface. These quantities are defined as follows:

$$\text{Radiant Flux} = \frac{\text{Pulse energy}}{\text{Pulse length}}$$

$$\text{Irradiance} = \frac{\text{Radiant flux}}{\text{Area}}$$

Irradiance is dependant on the area of interaction of the laser beam with the sample. This in turn is governed by the focusing criteria applied to the beam. The irradiance of a laser beam is defined as the power emitted per unit area. The units are Watts per square cm (W cm^{-2}).

Laser modes

If the output beam of a laser is examined with a highly resolving spectrometer it becomes apparent that the beam consists of a number of closely spaced discrete frequency components covering a moderately broad spectral range. These discrete components are laser modes. They cover a spectral range approximately equal to that of the atomic transition producing laser output. Single mode operation produces a laser output whose linewidth can be very narrow. It is directly related to a quantity called the quality factor (Q) of the cavity. Q switching refers to changing the Q value of the cavity. The Q value is inversely proportional to the energy dissipated per cycle. Q switching is a method by which very short but intense bursts of radiation are produced by a laser. A single laser pulse from a laser such as a NdYAG can be shown to consist of many random spikes of about $1 \mu\text{s}$ duration and with a separation of $1 \mu\text{s}$. These spikes are due to relaxation oscillations representing the competition between populations of the upper laser level by the pumping source and depopulation of it by stimulated emission. The total length of the train of

spikes is dependent upon the duration of the pumping source, generally about 1 ms. The peak powers of these spikes are in the order of kilowatts. Q switching produces a single spike whose power is in the megawatt range with a duration of 10 to 100 ns. However, the total energy emitted is less than that emitted in non Q switched operation due to the losses associated with the Q switching. The free running or normal mode of laser operation emits a much higher peak power than Q switching.

Q switching may be achieved by simply placing a shutter within the laser cavity. Once the laser has been pumped and a high gain achieved, the shutter is then quickly opened. A popular method of Q switching a laser is to use an electro optical pockel cell used in conjunction with a polariser.

There are many different laser types used in analytical chemistry, including ruby, CO₂, excimer and most commonly NdYAG lasers (Neodymium yttrium aluminium garnet). What ever laser type is used, most can be operated under computer control.

Table 1.3 A list of useful definitions for laser terminology

| | |
|------------------------------|-----------------------------------------------------------------------------------------------------------------------------------------------------------------------------------------------------------------------------------------------------------------------------------------------------------------------|
| Blow off | Physical ejection of solid or molten materials during the ablation process |
| CW | Continuous wave. A laser operating with a continuous output for a period > 0.25 s is regarded as a CW laser. |
| Excimer Laser | Rare gas halide or rare gas metal vapour laser emitting in the UV region. The word excimer is actually a contraction of 'excited dimer' |
| Fluence | Also known as energy density. Unit: J cm ⁻² |
| Free running laser | Also known as normal mode. A laser emits peak powers of the order of mode 1x10 ⁴ to 1x10 ⁵ W in pulses lasting several hundred milliseconds |
| Irradiance | Radiant flux incident per unit surface area. Also called radiant flux density or power density. Unit: W cm ⁻² |
| Laser plasma | A plasma (luminous gas having a fraction of its atoms or molecules ionised) generated by laser induced breakdown of a gas or formed on the surface of materials irradiated by high power pulsed or CW lasers. May also be referred to as laser plume |
| Mode | A stable condition of oscillation in a laser |
| Pulsed laser | A laser that delivers its energy in the form of a single pulse or a train of pulses. The duration of the pulse is < 0.25 s |
| Q | The figure of merit of a laser cavity, known as the quality factor, and defined as $(2\pi) \times (\text{average energy stored in the resonator}) / (\text{energy dissipated per cycle})$. The higher the reflectivity of an optical resonator, the higher the Q and the less the energy loss from the desired mode |
| Q switch | An optical device which changes the Q of a laser cavity, typically raising it from a value below laser threshold by prevention of laser action until a high level of inversion is achieved in the laser medium. Q switches can be based on acousto optic devices, rotating mirrors, or frustrated internal reflection |
| Q switched mode laser | A laser employing an element with variable loss within the laser cavity and emitting peak pulses of the order of 1x10 ⁷ to 1x10 ⁸ W and lasting several tens of nanoseconds |
| Sputtering/Spattering | Forcible or explosive emission of particles, for example during irradiation of material with a laser beam |

1.5 Role of lasers in trace element analysis

Since the 1960s analysts have been aware of the possibilities for the introduction of solid materials into spectrometers using the interaction of laser radiation with a sample. Laser ablation has many desirable features which have been described. It is also capable of providing spatially resolved information about chemical composition together with the ability to handle small samples. However, there seems little agreement on the optimisation of laser operating parameters required by the analytical scientist, such as laser power, wavelength, beam profile, focusing optics, beam convergence, spot size, laser mode and repetition rate. In addition a variety of ablation chambers and transport systems have been proposed and some workers have reported some difficulties relating to calibration.

In addition to laser ablated sample introduction into plasmas and flames, direct optical and mass spectrometric measurements of laser generated plasmas in the form of "laser microprobes" is an alternative methodology.

1.5.1 Laser microprobes

Laser microprobe analysis was first developed by Brech and Cross in 1962 (40). The instrumentation generally consists of a pulsed laser for sample ablation, an optical microscope for sample examination (the optics of which are also used for focusing the laser radiation) and a system for detection and analysis of the ablated material. The early work (41) utilised a ruby laser for ablation and recorded the emission spectra of the laser induced plasma by the interaction of the laser beam with the sample. Since then the ablated material produced by laser microprobes has been analysed by atomic absorption spectrometry, mass spectrometry, and most recently by optical multi channel analysers using a gated diode array detection system. In this section, laser microprobe optical emission spectrometry is reviewed.

Direct spectrochemical measurement of the plasma enables rapid in situ analysis. The emission signals from the laser induced plasma are complex and vary greatly with time. Time resolved

measurement is usually essential for the separation of the analyte emission response from the intense plasma background. Basic characterisation of the laser induced plasma and systematic studies concerning the effect of key parameters such as the wavelength of the laser light and the type and pressure of the buffer gas have been reported (42-44). Niemax and Sdorra (44), concluded that a wavelength of 1064 nm was more suitable than 266 nm for analysis of glass and steel samples. They (44) also found a reduced pressure of Ar gas, typically 1.33×10^3 Pa, offered improved analytical performance.

A pulsed nitrogen laser was used by Kagawu and co workers (45, 46) for the ablation of various samples. Time resolved emission spectra of the laser induced plasma were measured. Their results showed that there was a linear relationship between the ablated mass and the emission intensity of the laser induced plasma. The number of atoms vaporised from the sample was estimated from the volume of the ablation crater. Calibration graphs were plotted of the emission intensity measured for pure elemental standards against laser energy. The intensity of the emission lines produced by the laser plasma were measured for sample materials and the concentrations of the elements were determined from the calibration graphs. The results were reported as having %RSD values of up to 30%. It was concluded that using this method of standardisation the intensity of a normalised analyte emission line was proportional to the analyte concentration in the sample and independent of the sample matrix. Limits of detection were reported for Cr, Mn, and Cu as 20, 50 and $10 \mu\text{g g}^{-1}$ respectively.

Leis et al (47) recorded time resolved spectra of laser induced plasmas in argon atmospheres. They found that the spectra were significantly dependant on the observed time after laser interaction with the sample (Q Switched Nd YAG, 1064 nm, up to 250 mJ per 8 ns pulse, 2 Hz repetition rate). At 500 ns after the pulse, the recorded spectrum consisted of a continuum and ion emission lines. At $10 \mu\text{s}$ the ion lines had decreased in intensity and the atom lines were more intense. These observations were attributed to the plasma temperature decreasing with time owing to mixing with the argon. A series of iron chromium binary metal samples were ablated. The spectral observations from these ablations allowed plasma temperature measurements to be

made. These values showed that the plasma temperature decreased with time. It was found that as the chromium concentration increased, more material was ablated per laser shot. This work also showed that for a calibration method to be successful standards and samples must be closely matrix matched.

Time resolved laser induced breakdown studies of iron ore samples were carried out by Grant et al (48). The period of the plasma lifetime, which was optimum for maximum signal to background ratio (S/B) for Fe, Mg, Si and Ca, was determined to be between 2 and 3 us. Ablation was carried out with a XeCl laser (308 nm, 28 ns pulse, 40 mJ per pulse, irradiance $1.6 \times 10^6 \text{ W mm}^{-2}$). It was stated that the time resolved spectra showed an improvement in the signal to background ratio compared with the value obtained with time integrated spectra, even if the latter were obtained in an inert atmosphere at low pressures. Using this information Grant (48) carried out quantitative analysis of iron ore samples. The precision of the results was reported to be in the range of 2 to 25 % and LODs were reported at 0.01%. Although the results did not compare favourably with those obtained with spectrometric techniques such as inductively coupled plasma emission spectrometry with aqueous nebulisation, it was concluded that with a more detailed study this technique could lend itself to a field based application.

Anderson (49,50) applied laser induced plasma emission spectrometry to the analysis of polyvinyl chloride materials (49). The effects of key parameters such as laser energy, sample position and repetitive firings at given sites were examined. Quantitative data was also obtained for Sb, Ca, and P in polyvinyl chloride. A Q switched Nd YAG (1064 nm) laser was used operating at 10 Hz. The laser induced plasma was monitored using a gated diode array optical multichannel analyser (OMA). The laser was fired during alternate flashes of the flashlamp, (i.e. at 5 Hz) and the optical multichannel analyser recorded a blank spectrum during the flashlamp cycles when the laser did not fire. Each blank spectrum was automatically subtracted from the previous emission spectrum to yield a net signal from the plasma. It was found that a high laser energy (flashlamp energy of 70 J, irradiance of $3.1 \times 10^{11} \text{ W cm}^{-2}$) produced a more intense, longer lived plasma that required a different optic viewing position than for a lower energy setting of 40 J (irradiance of

8.0x10¹⁰ W cm⁻²). A relatively low energy setting of 40 J was chosen, which inflicted minimal laser damage to the sample but produced suitable emission responses. Quantitative measurement was limited by the availability of well characterised standards. Basic performance data was reported for Ca (LOD 0.016 %m/m and a precision of 4.8 %RSD) and Sb (LOD 0.04% m/m and a precision of 4.8 %RSD).

Depth profile studies using the same technique were also carried out by Anderson (50) for measurement of Zn/Ni and Sn coatings on steel samples. With preferred operating conditions, linear calibration against coating thickness for Zn/Ni (2.7 to 7.2 µm) and Sn (0.38 to 1.48 µm) on steel were achieved with good precision (3.5 %RSD). An ultra thin coating of Cr (20 nm) on steel was also detected by this technique. The depth profile performance and rapid measurement times, typically less than 60 s, indicated that this technique may have useful industrial applications. The applications of laser microprobes are summarised in Table 1.4.

Table 1.4 A summary of laser microprobe applications

| Sample | Elements | LOD | Precision | Ref |
|--------------------|-------------------|-----------------------|---------------|-----|
| Iron steel | Cr | 20 µg g ⁻¹ | Up to 30 %RSD | 45 |
| | Mn | 50 µg g ⁻¹ | | |
| | Cu | 10 µg g ⁻¹ | | |
| Fe/Cr binary steel | Cr | 24 µg g ⁻¹ | not reported | 47 |
| | Si | 30 µg g ⁻¹ | | |
| Iron ores | Fe,Si,Mg,Ti Ca | 0.01% m/m | not reported | 48 |
| PVC | Sb | 0.04% m/m | not reported | 49 |
| | Ca | 0.016% m/m | | |
| | P | not reported | | |

1.5.2 Laser ablation inductively coupled plasma atomic emission spectrometry

As mentioned previously, material removed from a sample by the interaction of a laser beam with the sample surface can be analysed spectroscopically. In addition to the use of laser ablation in combination with atomic absorption spectrometry, it has been combined with plasma excitation sources for analysis by optical emission and mass spectrometry. Although this section will concentrate on the use of optical emission spectroscopy some examples of laser ablation coupled to ICP mass spectrometry will be discussed.

The first application of laser ablation inductively coupled plasma atomic emission spectrometry reported in the literature was for the analysis of airborne particulates (51, 52). The airborne particulates were collected on the adhesive surface of flexible Mylar tape and then vaporised by a CO₂ laser. The vapour was transported in a stream of argon through a sample cell and into the plasma. A similar method was attempted by Thompson et al (53). They found that the rock samples crushed on to adhesive tape gave unsatisfactory results when ablated by a ruby laser. Further rock samples were prepared as lithium metaborate fusions or pressed powder pellets using epoxy resins as binding agents. Some improvement in the sample introduction method was reported. Other workers have prepared powdered samples as pellets, (54, 55). Lin and co workers (56, 57) mixed powdered samples with a diluent mixture prior to pelletising. This allowed a series of calibration standards to be prepared. Calibration graphs were shown to be linear over at least two orders of magnitude for Nb, W, Zr, and eleven rare earth metals.

Since the first publications on laser ablation inductively coupled plasma emission spectrometry, the choice of laser for the ablation process has varied between workers. Various laser operating parameters have also been used for a variety of different samples. Thompson and co workers (58, 59) used a ruby laser with a maximum pulse energy of 1 J. They operated the laser with variable degrees of Q switching in order to study the particulate matter produced by the laser ablation process. The work showed the applicability of laser ablated material to analysis by

plasma spectrometry. Results for stainless steel showed that the composition of laser ablated material compared favourably with bulk sample composition.

Chan and Russo (60) used ICP ES to study the effects of changing various laser parameters on the laser sample interaction. Several observations were reported, including that the amount of material removed by laser ablation was dependant on the surface characteristics. This was demonstrated by pretreating the metal surfaces with nitric acid. Surface oxidation resulted in improved coupling between the laser beam and the metal. The presence of spikes recorded in many of the emission spectra, were attributed to the ablation of large particles transported into the plasma. It was suggested that it might be possible to correlate these spikes with particle size.

The use of a single laser pulse to vaporise samples may lead to micro local sampling for the bulk sample. This may be used as one of the strongest properties of the technique. Probing the sample with a laser beam provides a route for studying the lateral distribution of elements in the solid sample. In some cases, depth gradients can be profiled for comparing surface and bulk constituents. Laser ablation inductively coupled plasma emission spectrometry has a sampling spatial resolution on the order of 20 to 50 μm . Sample imaging is similar to optical microscopy, but inferior to the electron imaging available with Auger spectroscopy. The depth profiling resolution is on the order of 1 to 10 μm per laser pulse; therefore laser ablation cannot provide the high depth resolution information that is available with surface analysis techniques such as, secondary ion mass spectrometry (SIMS) and Auger spectroscopy. None the less, concentration gradients of interest are often on the micrometer scale and would be accessible with laser ablation. However, as with any depth profiling technique, considerable attention should be paid to concentration gradient calibration which can be difficult to establish.

Ramsey et al (61), using laser ablation inductively coupled plasma emission spectrometry, provided quantitative determinations of element ratios in the concentrated brines contained within fluid inclusions. Fluid inclusions are small droplets of fluid trapped and preserved in minerals during their primary growth, larger than 30 μm in diameter, in topaz and halite. Inclusions formed

at different stages could therefore, be analysed separately and differentiated. This proved to be an advantage over previous bulk sampling methods that only provided composite analysis of all inclusion types present. The laser ablation system used was a Carl Zeiss Jena LMA 10, Q switched ruby laser microprobe coupled to an ICP ES. The laser was operated in a single shot mode, with a repetition rate of up to one shot every 15 s. The power settings were in the range 700 to 800 V and an intermediate beam stop was found to be most effective in reducing the crater size to around 50 μm . The accuracy of the average element ratios estimated from the analysis of a single fluid inclusion was generally well within 10% for the six elements determined (Ca, Ba, K, Li, Mg, and Sr). The element ratio showed a poor level of precision of between 20 to 45 %RSD.

Marshall and Franks (62) analysed trace elements in solid plastic materials using a LA ICP MS technique. The system was applied to the examination of polypropylene, polyester, poly(vinyl chloride), nylon, and polyethylene, containing a variety of fillers and other additives. A Q switched Nd YAG laser (1064 nm) was used. It was found that by using carbon 13 as an internal standard, in order to adjust for variations in ablation and transport of the different sample types, semi quantitative analysis could be achieved with an accuracy that was within a factor of 2 of the known value for most of the elements investigated. Quantitative measurements were made using a matrix matched standards, which showed good agreement with certified values. Relatively good sensitivity at the low $\mu\text{g g}^{-1}$ level was achieved, but the levels of precision were relatively poor and were typically in the order of 10% RSD.

Watling et al (63) used laser ablation inductively coupled plasma mass spectrometry to investigate its potential to provide data on relative trace elemental compositions of glass and steel samples. Glass and steel samples frequently occur as physical evidence in forensic analysis, and represent two dissimilar sample types. A fine focus Nd YAG (1064) laser was used enabling specimens of approximately 50 μm in diameter to be examined. Ablation protocols and optimum laser operating parameters were established. Sixty two glass samples were examined of which thirty one were float glasses, four were sheet glasses and twenty seven were container glasses. The steel samples examined were drillings from sixty nine sources and included steel from safes,

firearm barrels, tools, angle iron, rods and crowbars. The technique used was essentially qualitative and relied on comparison of trace element assemblages or ratios. Samples could be compared either by direct overlay of spectra or using interactive software.

Quantitative analysis of glasses was achieved by Moenke Blankenburg (64) using a novel calibration technique, for laser ablation inductively coupled plasma emission spectrometry and laser ablation inductively coupled plasma mass spectrometry, using an aqueous multielement solution as a calibrant. In the first step, aqueous standard solutions were nebulised in the normal manner but carried to the plasma by only one part of the divided argon stream. The other part of the gas stream was allowed to flow through the laser ablation chamber, but without laser action. Intensities were measured and calibration graphs constructed for the element to be determined and for a reference element. In the second step, intensities for the laser ablated solid (analyte and reference element) were measured using both flow streams, one flowing through the ablation chamber transporting the aerosol and the other transporting a blank solution. The two argon streams were mixed below the torch so that the water or liquid introduction into the plasma was the same, thus maintaining similar plasma conditions. With this novel calibration technique it was possible to obtain accuracies close to that of wet chemical techniques. Precision too was improved and was typically below 5% RSD.

Bulk analysis of biological standard reference materials by laser ablation inductively coupled plasma mass spectrometry was undertaken by Ward et al (65). NIST SRM 1571 Orchard leaves and 1573 Tomato leaves were analysed using a Q switched ruby laser using a beam energy of up to 1.5 J at repetition rates of up to 1 Hz. The method was considered to be semi quantitative. The results presented were mainly within a factor of 2 of the certified values of all levels from well below $1 \mu\text{g g}^{-1}$ to several % m/m. Some were much closer.

A non destructive sampling method for steels and alloys for laser ablation inductively coupled plasma spectrometry was described by Raith (66). The steel rubbing technique involved polishing the surface of metal components of interest with a diamond lapping film disc (15 μm diamond

particles) and then ablating the material transferred onto the disc using laser ablation. The advantages of the method are that it is essentially non destructive, components can be virtually any shape or size, and the sampling is safe requiring no electrical equipment. Furthermore, samples could be taken by non specialist staff anywhere in the world and then the samples posted back to the laboratory for analysis. Investigations carried out on steel standards (CRM 455, 456, 458, and 460) showed a precision generally better than 10% RSD. Limits of detection were in the range of 1 to 10 $\mu\text{g g}^{-1}$. The sample was ablated by using a raster of 5x5 points with a defocused laser (10 mm beneath the sample surface to achieve larger crater sizes and lower ablation rates to avoid damage to the disc). A Q switched Nd YAG laser operating at 4 Hz was used.

Finally a method for rapid survey analysis of polymeric materials was achieved by Booth and McLeod (67). A Nd YAG laser (1064 nm, output energy of up to 250 mJ per pulse and a maximum repetition rate of 15 Hz) coupled to an ICP emission spectrometer was used for the analysis of polymers, dry and liquid paints. Transient emission signals were studied as a function of laser operating modes, i.e. laser duration and flashlamp energy. Experiments performed on dried paint samples gave relatively imprecise transient signals (33 %RSD in contrast to that for ablation of the liquid sample (4 %RSD). This was thought to be due to greater homogeneity of the liquid sample. A near linear dependence of emission intensities on flashlamp energy was noted and the results suggested a direct correlation between the mass of ejected material and the amount reaching the plasma. A similar correlation was seen for laser duration. Some other typical examples of laser ablation inductively coupled plasma spectrometry are given in **Table 1.5**.

Table 1.5 Summary of typical examples of laser ablation inductively coupled plasma spectrometry

| Sample | Elements | LOD | Precision | Ref |
|-----------------------------------|----------------------------------------|------------------------|-----------------------------------|-----|
| SARM rock standards SRM 1 to 5 | Al,Ba,Ca,In, K,Mn,Na,Si, Sr,Ti,Y | --- | 1.8 to 40% typically below 10% | 68 |
| Pressed powder rock standards | 17 rare earth | 100 ng g ⁻¹ | <10% | 69 |
| Fluid inclusions in rocks | Na,K,Ca,Fe | --- | --- | 70 |
| Uranium oxides | 23 impurity elements | 1 µg g ⁻¹ | <8 % | 71 |
| Single mineral Grains | La,Ce,Nd,Sm Eu,Dy,Er,Yb | sub ppm | <10% | 72 |
| Fluid inclusions in rocks | 13 major and minor | --- | 7 to 32% | 73 |
| U Zr metal alloy | ²³⁵ U, ²³⁸ U | --- | 0.17% with IS 7.2% without | 74 |
| Zeolites Glass fibres | Li,B,Al,Si,Ti | --- | about 10% | 75 |
| High purity Quartz, Glasses | B,Co,Sr,Pb | < 1 µg g ⁻¹ | 3 to 7% | 76 |
| Mineral Zeolites | Hf,Y,Th,U | < 1 µg g ⁻¹ | <12% | 77 |

1.6 Laser interaction with materials

Since the first lasers became available, physicists have made extensive investigations of the interaction of laser radiation with all forms of matter and there are a considerable number of publications concerned with solids. The fundamental processes are of interest if an understanding of the event is to be obtained. This information is useful to a chemist wishing to evaluate the possibilities of using laser ablation sampling for quantitative analysis. Despite the very large number of papers, it is perhaps still the case, at least as far as chemists are concerned, that "the mechanism of vaporisation of a solid by a laser beam is a complex process which, at present, is not fully understood" (78).

In this section, topics of relevance in analytical science are considered. They are, the ablation event and its products, the influence of various laser operating parameters and the influence of target properties.

1.6.1 The ablation event

When a laser beam is focused on to a solid surface, the irradiance in the target spot area can lead to a variety of effects including heating, evaporation and degradation. Two effects are of particular concern are the formation of a plasma which expands out from the surface when the power density or fluence exceeds some threshold value, typically of the order of $1 \times 10^8 \text{ W cm}^{-2}$. The second is the ejection of material from the surface due to the ablation pressure generated by the expansion of the gas in contact with the surface and the expansion of gas within the sample and/or vaporisation/degradation of the sample. This formation of a surface plasma is not necessary for ablation to occur; indeed, such plasmas may absorb the incoming radiation very strongly and thereby reduce the effectiveness of the radiation for the purposes of ablation.

There has been sustained interest in the use of spectroscopic techniques for the study of the laser produced plasma. As early as 1964, Archibald et al (79), obtained time resolved spectrograms of the plasma produced by the interaction of a 1 MW Q switched ruby laser with a variety of metal

targets. More recently, Lee Salvin and Sneddon (80) described experiments in which a radiometer was used to monitor the total light emission signal from several NIST standard reference metals using an ArF excimer laser at 193 nm for a 20 us duration (with a repetition rate of between 1 and 50 Hz). A correlation was found between the radiation emission intensity and the laser energy, and evidence obtained in support of a model for the calculation of mass of material removed. As a continuation of their study Sneddon et al (81) made spatial measurements of the emission intensity from laser induced plasmas. They reported that copper (a metal with a high thermal conductivity, $4.01 \text{ W cm}^{-1} \text{ K}^{-1}$, and a high boiling point, 2567° C) produced a relatively confined, high excitation temperature (13,200 to 17,200 K) laser induced plasma, whereas lead (low thermal conductivity, $0.353 \text{ W cm}^{-1} \text{ K}^{-1}$, and a low boiling point, 1740° C) produced an expanded laser induced plasma of low excitation temperature (11,700 to 15,300 K). These observations indicated that the optimum position for spectrochemical measurements of laser induced plasmas was very dependent on the target metal.

Dienstbier et al (82), showed that optothermal methods could be usefully applied for the study of the ablation process produced by UV laser radiation (193 nm). Both pyroelectric and photoacoustic measurements of aluminium and polymethyl methacrylate were made and it was noted that all possible mechanisms of signal generation must be included in the interpretation of the results. Acoustic emission has also been used as the basis for internal standardisation in inductively coupled plasma emission spectrometry (83). The workers showed that earlier results obtained from experiments involving a static low pressure ablation cell could be applied to a flowing atmospheric pressure cell. Measurements of the pressure developed during the ablation event were made by two methods: a ballistic target pendulum and shifted X ray emission images, showed that pressures of up to $1 \times 10^9 \text{ kPa}$ were developed above a thin foil when irradiated with light from a CO_2 laser at $10 \mu\text{m}$ (84). A combination of reflectance and mass spectrometric measurements has been used (85) to follow the ejection of charged particles from a silicone crystal under the action of 20 ps pulses at 532 nm. Above 0.26 J cm^{-2} , equal amounts of positively and negatively charged species were produced. Ablation events have also been used

to produce neutral atomic and molecular beams (86). Fluxes of 1.3×10^7 atoms $\text{cm}^{-2} \text{s}^{-1}$ were obtained from uranium, aluminium, and bismuth fluoride targets.

Huie and Yeung (87) were able to claim in 1986 the first study of the spatial and temporal distribution of particles formed by laser vaporisation of metallic surfaces. An acousto optic deflector was used to scan the direction of a probe laser beam which interrogated the particles 100 us after the ablation event produced by a Nd YAG laser (1064 nm, 140 mJ, 1 Hz, 10 ns pulse) and a metallic surface (aluminium, copper, molybdenum or tantalum). They concluded that particle formation was dependant on power density, laser wavelength, surface characteristics (rough or smooth in comparison with the 0.1 mm laser spot diameter) and the volatility of the material. However, it was suggested that several other factors might be important, including laser mode, reflectivity, and absorption at the laser wavelength, and thermal conductivity.

Scanning electron microscopy has been used to characterise the material produced after ablation of metals, pyrite, a ceramic tile and "Perspex" by Thompson (88), by a Q switched ruby laser. A variety of laser conditions were used, ranging from maximum Q switching to (0.1 J, 200 μs) to free running (1 J, 500 μs). The collected particles could be divided into a number of categories including, spheres and angular fragments (typically produced by metals and ceramics). The production of spheres was considered to be due to the explosive removal of the molten surface, amorphous material consistent with condensation from the gaseous state. Angular fragments (observed for ceramics) thought to be due to shock processes (thermal and mechanical). In addition, agglomerates of spheres were observed for metals which were considered to be further evidence for the explosive removal (blow off) of molten sample. Explosive removal was also considered responsible for the production of a "spherical particle with a tail" from ceramic targets. The particle number and mass distributions for various degrees of Q switching were also presented from which it could be seen that although most of the particles were less than 5 μm in size, most of the mass was associated with particles greater than 5 μm in size.

1.6.2 Influence of laser parameters

Most fundamental studies of the interaction of the interaction of laser radiation with solids address the question of the role of the properties of the laser radiation. Of, particular relevance to the generation of ablated material are pulse energy, duration, spot size, repetition rate and wavelength, although other features such as the laser mode and angle of incidence have a role to play. Also there is an association between laser properties and both the nature of the atmosphere above the sample and the sample surface. For example, it may be possible for the laser radiation to produce a breakdown plasma in the gas above the sample surface or the sample may release sufficient material from the surface at the start of the event to cause the formation of the plasma.

It is evident that a laser power density of around $1 \times 10^8 \text{ W cm}^{-2}$ represents a threshold value for the change over from one mechanism of interaction to another, in that for values below this threshold no plasma is formed and therefore the ejection of bulk material is by a process of melting and blow off, whereas above this threshold the surface temperature is much higher than the boiling point of all elements and material evaporates directly into a plasma. However, the transition from one situation to the other is heavily dependent on the type of sample, the laser, and how the power density is achieved (long duration high energy pulse or short duration low energy pulse and spot size). The individual photon energy is also involved, i.e. the wavelength of the laser light is a relevant property.

To some extent, for moderate energy lasers two different interactions may be distinguished depending on whether the laser pulse is free running or is Q switched. Most lasers operate using one of two modes of laser operation: Q switching and free running. Q switching produces very short but intense bursts of radiation pulses that are of a few nano seconds duration, although the energy is reduced compared with that available in the free running pulse from the same laser. Whereas a free running laser pulse may have an energy up to 100 times greater, the duration of the pulse may be up to 10^6 times longer (i.e. several hundred microseconds) and the power density of a Q switched pulse is higher than that of the free running pulse.

The two pulse modes (Q switched and free running) can lead to significantly different analytical outcomes. The physical characteristics of the laser crater produced by the two laser pulse modes can be used to achieve different sampling objectives. A single free running pulse produces a deep narrow crater whereas the Q switched mode creates a shallower wider crater, yielding a greater proportion of material than the free running mode, thereby increasing sampling sensitivity. The shallow crater produced by Q switching is also more representative of the analytical composition of the sample, and for this reason most research groups have opted for the Q switched mode, when undertaking laser analysis.

Several factors may contribute to the difference observed. In the Q switched mode, the intense plasma generated early in the pulse can absorb some of the laser energy itself. The laser induced plasma then transfers some of the energy to the sample surface. As a result of this energy transfer, the dimensions of the sample crater are determined to a large extent by the dimensions of the plasma, rather than the dimensions of the focused laser beam. Thus the effective dimensions of the crater may be several times larger than the laser beam itself.

As early as 1965, optical and electron microscopy were used to study the damage caused by the action of radiation from a Q switched ruby laser to metal surfaces (89). Two different types of crater were identified, and designated as ejection craters and surface craters. The former were characterised by a central peak surrounded by a concentric zone of different surface structure. The latter were similar to impact craters, having no central peak, and were observed to form along surface defects such as scratches. The physical dimensions of the craters produced in various metal surfaces by the action of radiation from a free running ruby laser (1.4 J, 270 μ s and the mean power density of 10^7 W cm⁻²) were measured by Klocke (90), who considered that the depth was primarily a function of energy density and power density in the spikes, whereas the diameter was primarily a function of the focal spot size and power density.

It is generally seen that an increase in the laser energy will result in an increase in the amount of ablated material. Work performed by Booth and McLeod (67) for laser ablation inductively coupled plasma emission spectrometric analysis of wet and dry paint samples, showed that the analytical signal increased as a function of the laser beam energy. It has been suggested, however, that the analytical signal may not be proportional to the mass of ejected material. Transport efficiency is important in determining the analytical signal. Arrowsmith and Hughes (78), proposed that transport efficiency is controlled by particle size which are dependent on the laser type and operating conditions. It was concluded that large particles resulting from a high energy laser pulse would have poor transport efficiency. The most desirable method, therefore, is to use a low energy laser burst with a high repetition rate operating in the Q switched mode of operation. This should produce much finer particles facilitating a higher transport efficiency.

In studying the effect of laser beam spot size, Eyett and Bauerle (91) confirmed what might have been expected, namely that ablation rates were heavily dependant on the laser beam spot size. An XeCl laser (308 nm, 11 ns pulse, maximum repetition rate 10 Hz, power density of $2.8 \times 10^8 \text{ W cm}^{-1}$) was used and the spot size varied between 24 and 175 μm in diameter while maintaining a constant fluence of 3.1 J cm^{-2} . The target materials included lead, polyvinyl chloride and two metal oxides.

Until recently most commercially available instruments for laser ablation were equipped with a pulsed Nd YAG laser operating in the infrared at its first harmonic (1064 nm). This choice of laser was based on two essential reasons: firstly, it was and still is the cheapest and simplest choice of laser for these kinds of applications and secondly, the results of (for example Arrowsmith and Hughes (78)) have shown that high sensitivities can be achieved, typically in the $\text{sub } \mu\text{g g}^{-1}$ range for solid samples. It is, however, now the case that UV laser ablation using both frequency quadrupled Nd YAG, excimer and frequency doubled lasers have found to give superior sampling compared to infra red lasers in every analytical aspect and therefore the use of UV lasers have now superseded infra red lasers.

Geertsen et al (92) found that by studying the plasma ignition in air and argon buffer gas as a function of laser wavelength, laser ablation is a major process responsible for removal of material in the case of UV lasers, as opposed to IR lasers, where shielding of the laser radiation by the laser induced plasma (which absorbs some of the incident laser radiation) limits direct laser ablation and increases the temperature of the plasma. The consequences of this difference between IR and UV laser radiation were found to be considerable and lead to a superior performance of UV laser sampling i.e. reproducibility, matrix effects, quantitation, spatial resolution and sensitivity.

Most previously published work dealing with laser ablation was based on the use of Nd YAG lasers operating at the fundamental wavelength of 1064 nm, it has been shown by Geertsen (92), that the use of lasers operating in the UV region of the spectrum minimise possible selective volatilisation and enhanced ablation efficiency. Work performed by Gagean and Mermet (93) using a 308 nm XeCl excimer laser for the analysis of metal standards showed good limit of detection values in the sub $\mu\text{g g}^{-1}$ range together with good precision i.e. 0.2 to 0.3 %RSD.

Gunther et al (94) also found that fractionation effects due to different ablation rates of various elements which have prevented quantification without the use of matrix matched standards when using 1064 nm Nd YAG lasers are reduced but not eliminated using shorter UV wavelength lasers (e.g. quadrupled Nd YAG 266 nm lasers). Excimer lasers with wavelengths below 200 nm are expected to reduce fractionation effects further, but they present a series challenge to the design of optical systems, especially if high resolution UV ablation needs to be combined with high quality visual observation. The laser ablation system employed by Gunther (94, 95) utilised a 193 nm, Argon Fluoride excimer laser in combination with a Perkin Elmer 6000 ICP MS instrument. The optical system allowed imaging of both visible and UV laser light onto the sample surface at the same time. Laser operating parameters were studied using glass reference materials (NIST SRM 612/610). These experiments using the Argon Fluoride laser system demonstrated a greatly reduced matrix dependence of the ablation process, which facilitates in situ analysis of unknown samples.

1.6.3 Influence of target properties

Clearly from the analytical chemists perspective, the role of the nature of the target is of prime importance as the object of the various experimental experiments in the determination of the bulk elemental composition from measurements either of the photons emitted from the plasma at the surface or from subsequent spectroscopic measurements made on the transported material. Ideally the ejection of material from the surface should be independent of sample properties, but unfortunately all the experimental evidence suggests that these parameters are of critical importance. In some respects all the fundamental studies by analytical chemists of the various laser based techniques are motivated by the desire to achieve an understanding of the processes by which a representative sub sample of the surface is transferred to either the laser induced plasma or a remote spectroscopic device. A further complication arises from the dimensions of the surface area probed by the laser beam. For many sample materials this spot may be of a size at which the material exhibits considerable inhomogeneity.

Surprisingly, relatively little work appears to have been done in gaining a full understanding of the factors governing sub sampling by laser radiation. At present efforts to perform quantitative analytical measurements rely on the often unrealistic requirement of matrix matched standards. It is clear that the analytical requirement of being able to handle a variety of samples whose properties range from those of high purity metals to polycrystalline minerals is unlikely to be met by a single set of laser operating parameters, apart from those in which the sample is totally vaporised.

Many basic studies of the analytical use of the laser solid interaction start with a consideration of metal samples, which to a first approximation may be considered as a homogenous solid. In addition to heat capacity, melting and boiling points, density, thermal conductivity and heat of evaporation, properties such as hardness, reflectivity (which in turn depends on surface chemistry and morphology) and particle size are also important. Again there is a problem of scale; bulk

properties may have little relevance to the outcome of the ablation event when heterogeneous sample material is of interest.

For studies in which the ablated material is transported some distance before atomisation, the role of the sample properties on the transport of material is of interest. Sneddon and Mitchell (96) found that for a systematic study of copper compounds of different densities, a decrease in the density produced atomic emission signals with increasing intensity. The samples were prepared so as to have the same copper concentration and particle size. The reduced signal with the high density sample was found to be due to reduced transport efficiency.

Some sample properties, such as reflectivity, are also functions of the properties of the incoming laser radiation and thus extremely difficult to separate entirely the factors affecting the production of sub sampled material into categories which are purely due to the target and purely due to the laser. As has already been mentioned, there are numerous experimental parameters associated with analysis by laser ablation and thus any completely systematic optimisation is time consuming. However, it is evident from the literature that for any analysis using laser ablation, it is essential that optimisation of the operating parameters associated with laser ablation is undertaken for different sample types. This is particularly true for samples which to date have never before been analysed by laser ablation inductively coupled plasma spectrometry, which is the essential feature of this thesis, where laser ablation of aqueous solutions, oils and gels is performed.

1.6.4 Laser interaction with liquids

Although the interaction of lasers with liquids has long been studied (97-101), it was not until recently that analytical applications have been developed (102-104). These applications are based on the so-called Laser Induced Breakdown Spectroscopy (LIBS) of liquid samples. This technique observes emission from a spark produced by the focussing of an intense laser pulse into a liquid. Cremers and Radziemski (105) used this technique for the analysis of synthetic

aqueous multielement solutions in order to evaluate the characteristics of the laser spark in water and to determine the limits of detection for several elements in solution (Li, Na, K, Rb, Cs, Be, Mg, Ca, B, and Al). They found that most of the elements were only detectable at levels above $1 \mu\text{g ml}^{-1}$, although the detection limit for Li was found to be as low as $0.006 \mu\text{g ml}^{-1}$. The precision for replicate sample analysis varied between 4 to 8 %RSD. A pulsed 10 Hz, NdYAG laser operating at 1064 nm was used to produce a spark directly in the liquid. The emission from the spark was observed using a spectrometer. It was proposed that a laser pulse incident upon the liquid has a characteristically strong electric field which induces dielectric breakdown of the medium. A spark is produced and shock waves emanate from the focal volume. Dielectric breakdown of pure water and some organic solvents occurs with focussed laser powers of 10^{10} to $10^{11} \text{ W cm}^{-2}$. However, the breakdown threshold is thought to be influenced by the presence of particles or dissolved materials. In many cases, the laser spark was produced in liquids with the use of 1 to 2 J laser pulses of 10 to 30 ns duration. Stable sparks can be produced, however, with the use of 40 to 50 mJ laser pulse energies at powers of about 3 MW, which is well in the range of most small commercially available lasers operating at 10 to 20 Hz. Cremers and Radziemski concluded that the laser spark method of liquid analysis would be useful in situations requiring real time non-invasive monitoring of species at high or moderate concentrations where the liquid is at least partially transparent to the laser beam wavelength.

Cheung and Yeung (106) performed elemental analysis of liquids based on laser vaporisation at fluences below breakdown, together with acoustic normalisation for improved precision. By using an ArF laser operating at 193 nm for the analysis of NaCl solution, a dynamic range of 3 orders of magnitude with a limit of detection of $0.23 \mu\text{g ml}^{-1}$ for Na was realised. Laser vaporisation of KCl and BaCl_2 was also investigated and detection limits of 1.5 and $130 \mu\text{g ml}^{-1}$ respectively were established. When discussing a variety of intensity dependent phenomena that occur when lasers are focussed into liquids, they concluded that these phenomena include dielectric breakdown and plasma production which is thought to cause ablation of the liquid and generation of high pressure acoustic waves with the ejection of liquid from its container. However, they also concluded that laser induced breakdown spectroscopy has a few shortcomings associated with the strong laser

fluence used. First, because of the formation of hot plasma, there is a strong continuum emission that masks the line signal during the first few hundred nano seconds. Secondly, splashing of the liquid samples due to the formation of high acoustic pressure waves resulted in the wetting of nearby optics and removal of unpredictable amounts of sample mass resulting in poor reproducibility. Signal averaging using acoustic normalisation was therefore needed to obtain improved precision (a precision of less than 9 %RSD was achieved).

1.7 Conclusions

There are a number of advantages to techniques used in the direct introduction of samples into plasma spectrometers. These include the reduction in the time involved in sample preparation procedures, avoiding the risk of potentially hazardous reagents, and reducing the risk of contamination. In addition, separation or concentration steps are not necessary and there is little risk of diluting the analyte below its limit of detection or of losing volatile elements during the digestion process. Solid sampling techniques, provide the capability of analysing solutions with high concentrations of acids, dissolved solids or organic solvents, because the matrix can be removed prior to analysis by fractional evaporation of the sample components. Organic solutions can be analysed without adding oxygen to the plasma or risking carbon deposition on the torch sample injection tube. With electrothermal vaporisation vapours generated during the drying or ashing step can be vented to waste, whereas these vapours reach the plasma with direct sample introduction techniques and can cause depositions.

There is also the potential for improvement in absolute detection limits using solid sampling techniques by increasing sample transport efficiency. Microamounts of solids or liquids can be analysed and extremely low limits of detection can be achieved. Due to high sample transport efficiencies of up to 80 %, electrothermal vaporisation, direct sample introduction techniques, laser ablation, and arc nebulisation provide sensitivities and, consequently detection limits which are approximately one order of magnitude better than those achieved by conventional pneumatic nebulisation. When even higher sensitivity is required, replicate aliquots of sample can be added

upon drying; this is more easily performed with electrothermal vaporisation than with direct sample introduction. Matrix modification, a technique frequently used with graphite furnace atomic absorption spectrometry, is possible with electrothermal vaporisation and direct sample introduction techniques.

The main disadvantage of solid sampling techniques is that, in general, the reproducibility of the measurements is much worse than with pneumatic solution nebulisation. Additionally, calibration is often difficult, and the use of standards or reference samples which are identical to the analyte samples in the matrix composition is necessary. As far as electrothermal vaporisation and direct sample introduction techniques are concerned many problems which are caused by matrix interferences and which are well known from graphite furnace atomic absorption spectrometry will be similar in ICP spectrometry.

Calibration of the laser ablation technique is based on the ablation of solid standards. The greatest limitation of this technique as with all other solid sampling techniques for quantitative analysis is the availability of well characterised matrix matched calibration standards. Unless closely matched calibration standards are available the accuracy of determinations will be poor. In the absence of commercial solid calibration standards semiquantitative data for laser ablation can be obtained (i.e. accuracy within a factor of 2 to 3) by internal standardisation. On the whole solid sampling systems are very suitable for rapid semiquantitative survey analysis. Solid sampling systems extends the application of plasma spectrometry, and can be expected to provide some of the best analytical detection limits available.

Despite the shortcomings of laser ablation as an accurate solid sampling technique it is clear that it has considerable uses in examination and characterisation of solid materials. It is extremely easy to generate information about the elemental composition of a sample; at least to characterise the constituents as major, minor or trace elements. Laser ablation comes into its own as a technique for measuring the distribution of elements in inhomogeneous materials or multilayers or for in-situ microanalysis. It is a technique which allows micro sampling on a surface or analysis of

inclusions. In contrast to single step microprobe techniques where excited atoms and ions produced in the laser microplasma are utilised for atomic emission, fluorescence or mass spectrometry, in laser ablation inductively coupled plasma spectrometry vaporisation and ionisation take place sequentially. The single step techniques suffer from severe matrix influences, low and widely varying yields of analytically useful species (10^{-3} to 10^{-15}), compound formation, and poor precision, whereas in laser ablation plasma spectrometry each step (ablation, transport, and excitation) can be optimised independently, giving rise to simpler and quicker optimisation.

It is unlikely in the near future that laser ablation inductively coupled plasma spectrometry will be an alternative to dissolution procedures in order to obtain accurate information about bulk elemental composition. The technique will, however, be used for the initial examination for unknown solid materials, for rapid semiquantitative characterisation of elemental composition, for identification of trends in concentration. It is only after more information is obtained about the effects of laser operating parameters for different materials that the technique may become a fully quantitative analysis technique for solids. It is apparent from the literature on laser ablation that most analysis has been performed on metallurgical or geological samples. This leaves a great deal of scope to expand the possible applications of the technique.

1.8 Aims

The overall aim of this project is to determine and critically evaluate optimum conditions for sampling a range of materials by laser ablation. A variety of operating conditions associated with the ablation process will be investigated including laser energy, ablation time and laser focusing. A number of materials which have not previously been sampled by laser ablation will be analysed. These include aqueous multielement solutions, oils, gels, biological samples, as well as a range of glasses and thin coated steel samples.

Initial work will be performed on glasses and will critically evaluate the effectiveness of the basic experimental setup as well as the relative criticality of the operating parameters on analytical performance.

Laser ablation will be evaluated for microsampling synthetic multielement solutions as a novel means of calibration for samples that are difficult to introduce into the plasma by conventional means, such as solutions with a high solids content and viscous organic liquids. Optical emission intensity from an inductively coupled plasma will be studied as a function of various operating parameters for sampling optimisation and to develop understanding of the ablation process. Work will also include microsampling of mineral oils, with the aim of using aqueous standards for calibration purposes. A comparison of ablation process between aqueous solutions and oils will be made.

Laser ablation will be used for depth profiling of a range of coated steel and glass samples. The criticality of various operating parameters will be studied in order to gain optimised depth resolution using the experimental setup.

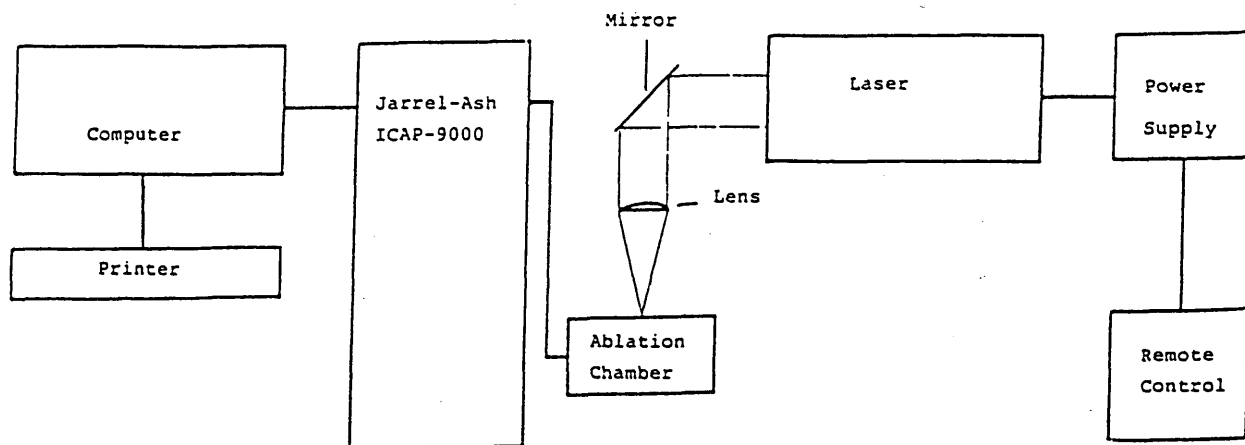
Finally laser ablation of thin sections of biological tissue and the possible use of gel multielement standards as a novel means of calibration for the quantitative analysis of such samples will be investigated.

2.1 INTRODUCTION

Two laser ablation ICP spectroscopy systems were used. The first was a custom made laser ablation inductively coupled plasma emission spectrometer, which was used for bulk analysis of glass materials, liquids, and depth profiling. The second was a laser ablation inductively coupled plasma mass spectrometer, which was used for the analysis of gel multielement standards.

The laser ablation ICP emission spectrometry instrumentation was configured using a high power laser with a multichannel ICP emission spectrometer (Figure 2.1 shows a schematic for the laser ablation ICP spectrometer system). A high power, pulsed laser beam was directed down onto the sample using an infrared reflecting mirror and a focussing lens (50 mm f.l.). The sample was held in one of two ablation chambers, which were in turn mounted on manual XYZ translation stages. The vapour which resulted from the interaction of the laser with the sample was swept into the plasma via a length of tubing ('Tygon' 5 mm i.d.) into a customised plasma torch interface. The carrier gas flow rate was controlled by a flow meter (0.0 to 2.5 L per minute). The whole system was enclosed in a steel safety cabinet which prevented any leakage of laser radiation into the environment. A microcomputer was used to control the data acquisition, the results being presented either as emission-time profiles and/or as raw counts based on the integration of the signals. The laser was contained in a specially built laser laboratory which was separated from other workers. This section will describe each component of the system in greater detail.

Fig 2.1 Schematic of the laser ablation inductively coupled plasma emission spectrometer components



2.2 The laser

The laser was a 'Spectra Physics Quanta-Ray™ DCR-11' pulsed NdYAG class IV high power laser, with an output wavelength of 1064 nm. The laser consisted of three parts: a power supply box, a remote control module, and the laser head. All the precautions for safe operation, maintenance, and operation were given in the 'Spectra Physics' instruction manual. The general specifications of the laser are given in **Table 2.1**.

The laser is capable of Q-switching, which is used to shorten the pulse duration and raise its peak power. The DCR-11 utilises an electro optic Q-switch comprising a polariser, a quarter wave plate and a "Pockels" cell. During Q-switched operation the flashlamp excites the neodymium ions for approximately 200 microseconds to build up a population inversion, a fast high voltage pulse applied to the pockel cell changes the Q-switch from high loss to low loss. The resultant pulse width is approximately 9 ns.

Table 2.1 Specifications of the DCR-11 laser, operating in the Q-switched mode of laser operation

| | |
|---------------------------------|------------------------------------|
| Wavelength | 1064 nm |
| Pulse width (Q-switched) | 8-9 ns |
| Pulse energy | 415 mJ |
| Pulse energy stability | +/- 4 % |
| Repetition rate | 10 Hz optimum, 1-15 Hz total range |
| Beam diameter | 6.4 mm |
| Line width | <1.0 mm |
| Linear polarisation | >98 % |
| Divergence | <0.5 mrad |

The laser is mounted on a custom made optical bench. The bench was constructed of stainless steel, which has been painted mat black so as to reduce the possibility of laser beam reflections. The laser beam was directed through a steal tunnel which prevented any possibly leakage of laser radiation. All the laser functions are controlled from a remote control panel. Consequently, the beam may be completely enclosed and the laser operated in the Class 1 mode.

2.3 The ICP emission spectrometer

The ICP emission spectrometer used in these studies was the 'Jarrell-Ash ICAP 9000'. The ICAP 9000 consists of a 0.75 m direct reading spectrometer, a radio frequency generator, an inductively coupled plasma source and appropriate data aquisition and handling computer software (Thermospec).

The spectrometer, is a rugged, heat treated, cast iron, A-frame base to which the entrance slit, grating and focal curve are mounted. To the right of the instrument is the plasma source assembly. The plasma source consists of a plasma torch surrounded by a water cooled induction coil. A 2.5 kW crystal controlled R.F. generator operating at 27.12 MHz provides energy to the torch and creates an oscillating magnetic field, which sustains the plasma. Radiation emitted from the plasma is directed through the entrance slit, diffracted by the grating, refocused on the exit slits and projected onto the photomultiplier tubes. The photomultiplier tubes convert light energy to electrical signals which are digitised and processed by the computer.

The instrument is fitted with a fixed cross flow nebuliser where the sample injection needle and the sample gas flow needle are set at right angles to each other. The argon collides with the sample and nebulises it. For this work, the spray chamber, plasma torch interface was modified and is illustrated in **Figure 2.2**. This facilitated conventional solution nebulisation and sample introduction by laser ablation without making any adjustments to the instrument configuration.

The spectrometer is equipped with 30 fixed channels, each corresponding to a different element and each identified by a physical channel number recognised by the software. The instrument technical specifications are given in Table 2.2. The elements, channels and analytical wavelengths are given in Table 2.3.

Fig 2.2 The Jarrell-Ash ICP torch and spray chamber assembly, and the chamber torch interface

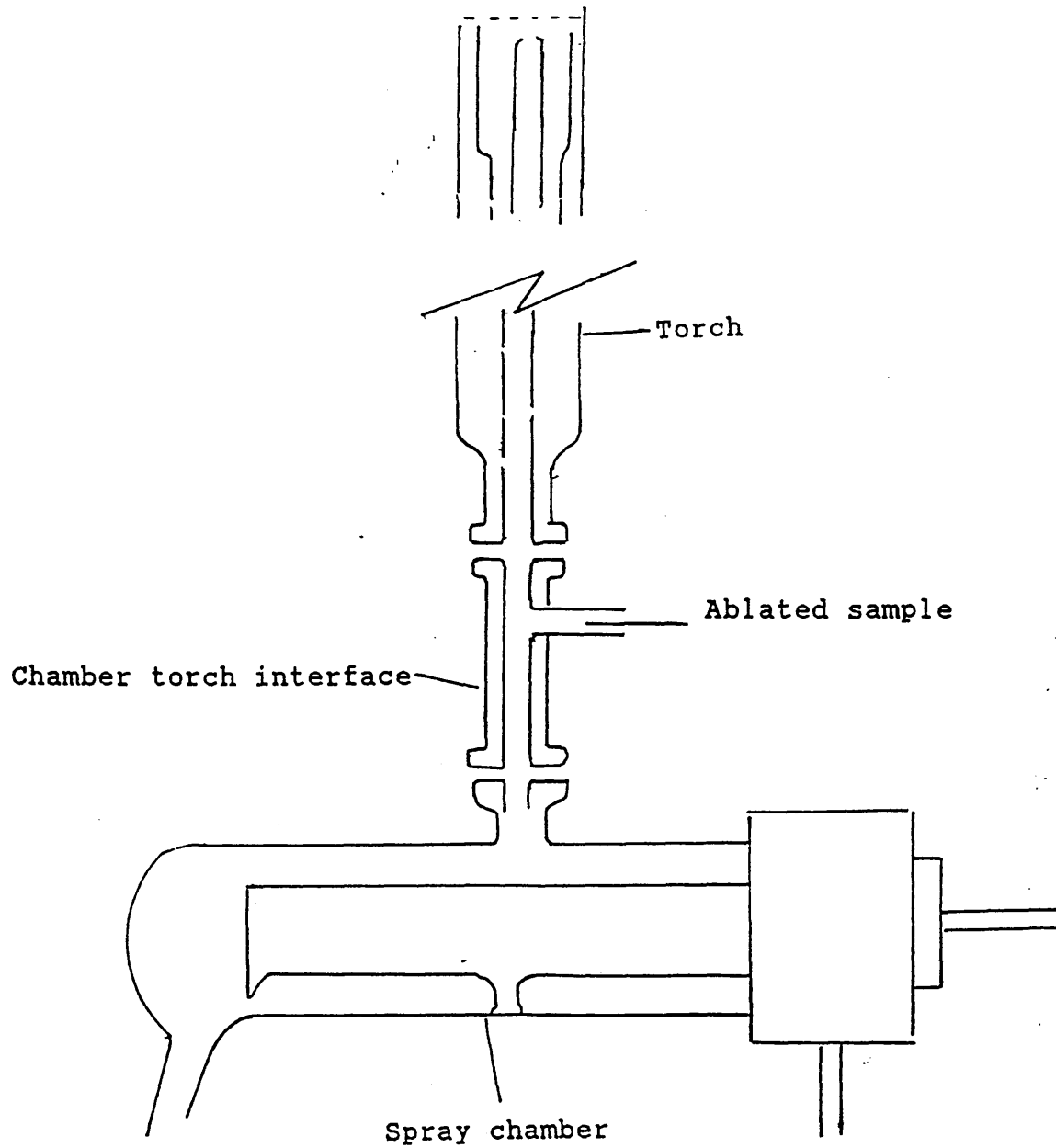


Table 2.2 Technical specifications of the 'Jarrell-Ash ICAP 9000' spectrometer

| | |
|------------------------------------|------------------------------------------------------------------------------------------------------------|
| Optics | 0.75 m Rowland circle, Paschen-Runge mount. 1510 lines per mm ruled grating at 500 nm. |
| Linear dispersion | 0.92 nm per mm first order 0.46 nm per mm second order 0.31 nm per mm third order |
| Resolution | 0.045 nm first order 0.023 nm second order 0.015 nm third order |
| Wavelength range | 190-800 nm |
| Variable wavelength channel | 0.5 Ebert. 190-900 nm |
| Background correction | 63 available steps on a computer controlled scanning refractor plate covering a 0.5 nm range (first order) |
| Source | 2.5 kW R.F. generator operating at 27.12 MHz with automatic tuning. |
| Nebuliser | Cross flow pneumatic. |
| Torch | Quartz |

Table 2.3 Available spectrometer channels

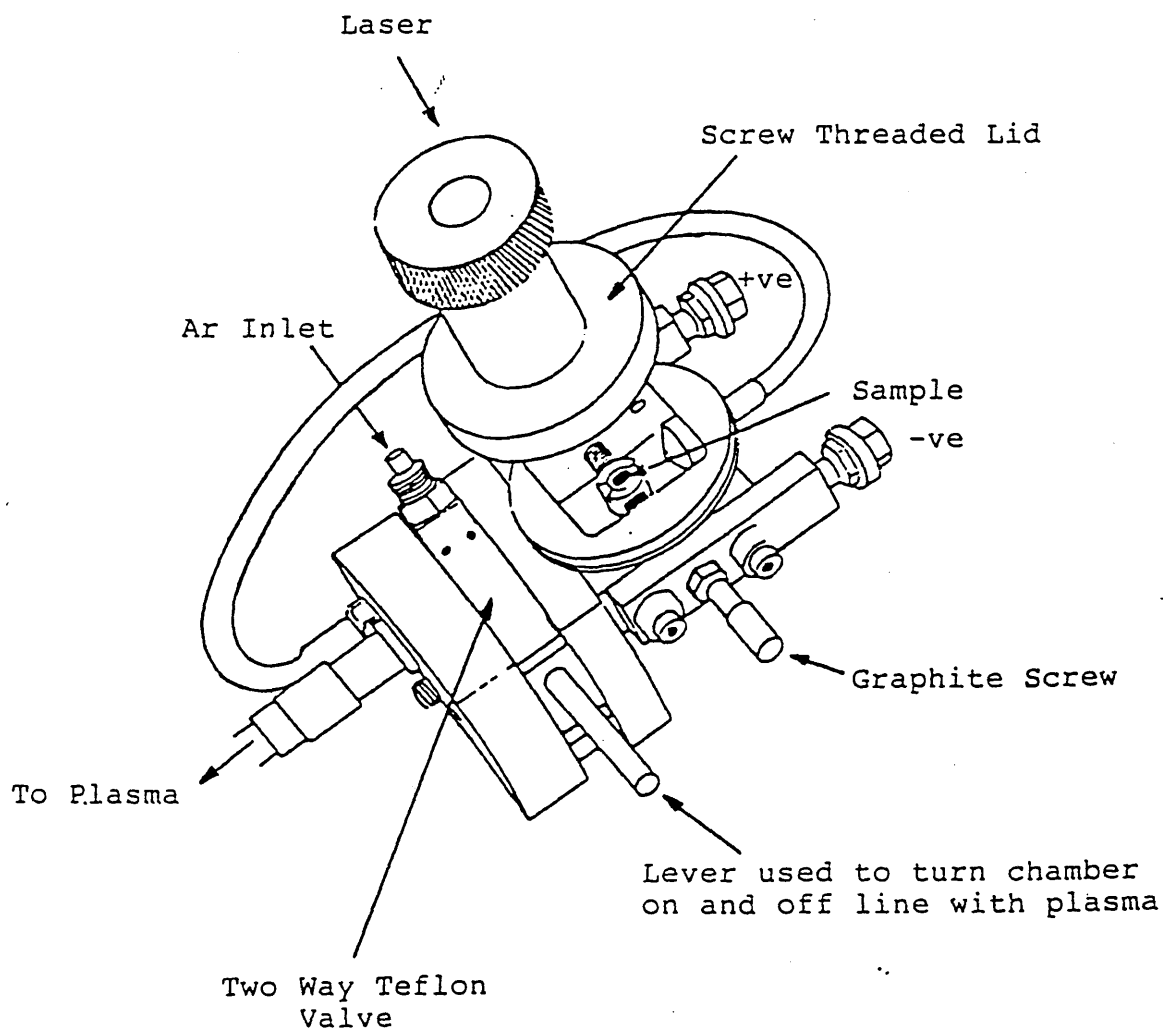
| Element | Channel No | Wavelength |
|---------|------------|------------|
| Ag | 19 | 328.07 |
| Al | 14 | 308.22 |
| As | 11 | 193.70 |
| B | 9 | 249.70 |
| Ba | 6 | 493.40 |
| Ca | 35 | 317.93 |
| Cd | 23 | 228.80 |
| Co | 45 | 228.62 |
| Cr | 42 | 267.72 |
| Cu | 34 | 324.75 |
| Fe | 8 | 259.94 |
| Ge | 16 | 209.42 |
| Hg | 4 | 194.22 |
| K | 25 | 766.49 |
| Li | 21 | 670.78 |
| Mg | 10 | 279.08 |
| Mn | 44 | 257.76 |
| Mo | 38 | 202.03 |
| Na | 12 | 588.99 |
| Nb | 17 | 319.50 |
| Ni | 28 | 231.60 |
| Pb | 32 | 220.35 |
| Se | 46 | 196.03 |
| Si | 41 | 288.16 |
| Sn | 48 | 189.99 |
| Ti | 2 | 334.94 |
| V | 40 | 292.40 |
| W | 36 | 207.91 |
| Zn | 5 | 213.86 |
| Zr | 30 | 339.20 |
| N+1 | 26 | Variable |

2.4 The laser ablation chambers

Two different designs of ablation chamber were used. The first ablation chamber is constructed from two sections of stainless steel illustrated in **Figure 2.3**. The upper section is detachable from the main body by a screw thread to allow sample change over. This section houses a 1 cm diameter quartz window through which the laser radiation passes. The window is slightly tilted so that any reflected radiation from the laser does not pass back and damage the laser. The window was detachable which allowed for easy cleaning or replacement.

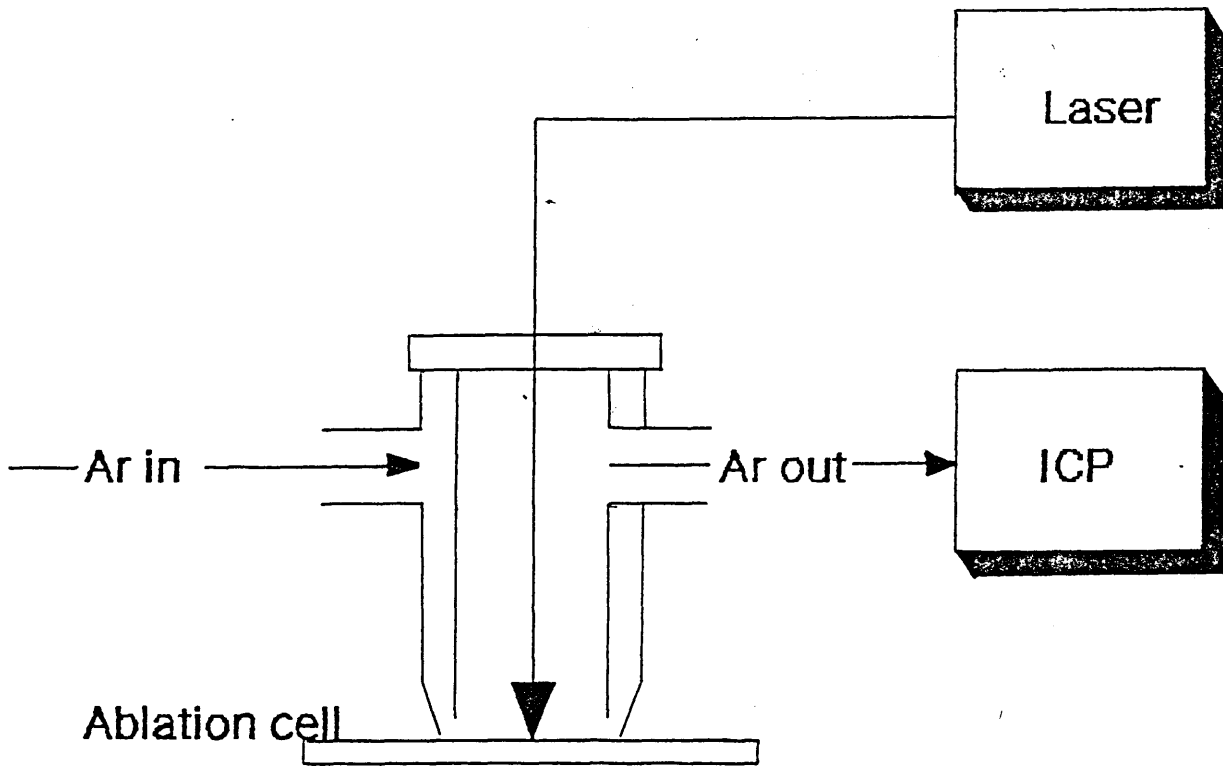
A switching valve enabled the chamber to be brought off-line to allow for sample loading and change over without disturbance of the plasma. The chamber volume was kept small (20 ml) to prevent sample vapour dilution and condensation. The laser ablation chamber is fixed to a XYZ manual translation stage, whose movement allowed for positioning of the laser beam onto the sample and focussing of the laser beam onto the sample surface.

Fig 2.3 Ablation chamber design 1



A second ablation chamber illustrated in Figure 2.4, which was based on the design by Arrowsmith (78) was constructed. The chamber is designed to sit over the surface of a flat sample and a seal made from draft excluder is used to make an air tight seal between the chamber and the sample. The chamber was constructed from two concentric glass tubes, with an internal volume of approximately 2.5 ml. The carrier gas streams down the space between the two tubes, at the bottom of the cell a portion of the gas carries the ablated material into the inner tube and into the plasma via a length of tubing. A removable window allows for cleaning of deposited material produced by laser sampling.

Fig 2.4 Ablation chamber design 2



2.5 The laser ablation ICP mass spectrometer

The basis of ICP mass spectrometer system (VG PlasmaQuad) may be summarised very simply. The sample to be analysed is dispersed into a stream of gas. This gas stream is injected into the core of a high temperature plasma sustained by radio frequency fields. Energy is transferred from the plasma to the sample, dissociating, atomising and ionising it in turn. The plasma core containing the sample ions is extracted into a reduced pressure region through a small orifice. A portion of this extracted plasma passes through a further orifice and there is a further drop in pressure. A system of electrostatic lenses extracts the positively charged ions and transports them to a quadrupole mass filter, which only transmits ions of a particular selected mass to charge ratio an ion detector registers the transmitted ions. Each naturally occurring element has a unique and simple pattern of nearly integer mass to charge ratios corresponding to its stable isotopes, so allowing easy identification of the elements in the sample. The number of registered ions from a given isotope of course depends directly on the concentration of the relevant element in the sample, so quantitation is straightforward.

The quadrupole is a high performance unit with high transmission (giving good sensitivity) and resolution. Different parts of the spectrometer are held at different pressures to ensure correct operation of the plasma sampling interface and the quadrupole mass filter. In order to maintain these pressures a combination of rotary and diffusion vacuum pumps are used. The interface between the plasma and the mass spectrometer has two cones; first, the sampling cone, followed by the skimmer cone. Behind these cones are a series of cylindrical electrodes designed to extract and focus ions from the interface into the mass spectrometer.

The VG LaserLab is an accessory for the VG PlasmaQuad ICP-MS, which allows for the direct analysis of samples using laser ablation. The system consists of a pulsed NdYAG laser producing the fundamental wavelength of 1064 nm, and associated optics and control electronics. The laser light is folded through 90° by means of a dielectric coated mirror, onto a 75 mm focal length lens. The focussed radiation is directed onto a sample mounted within a quartz sample cell

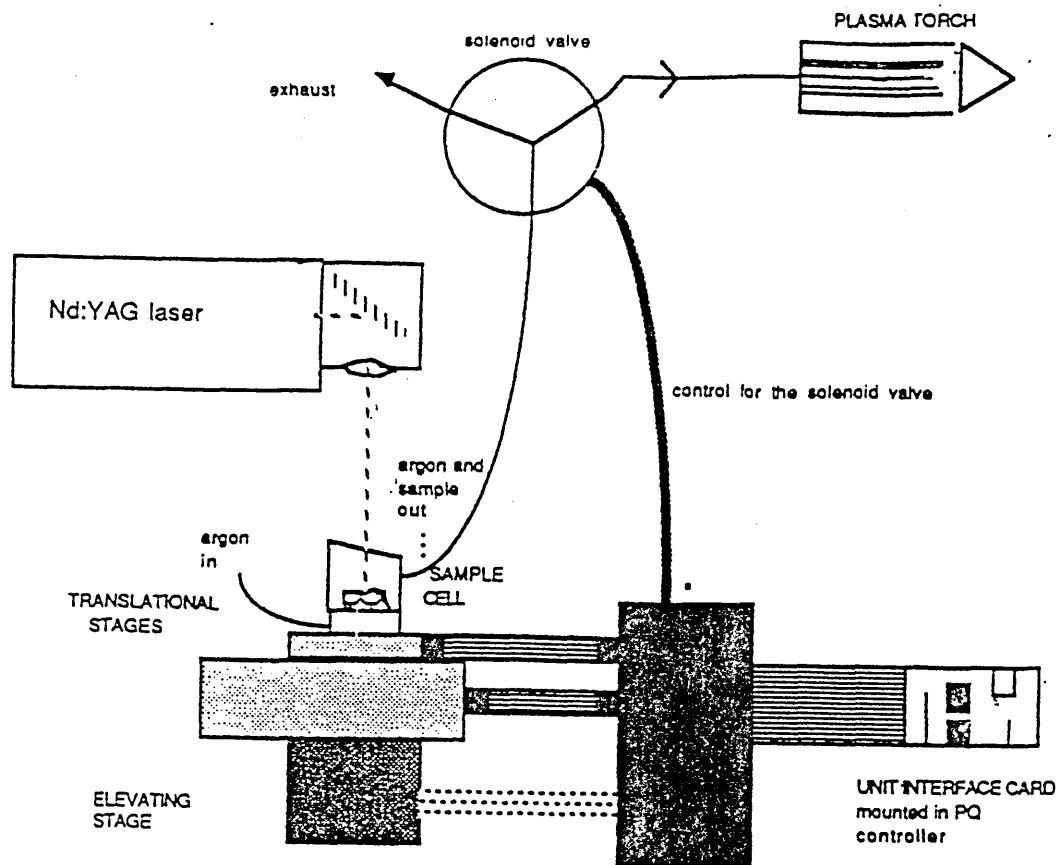
which has a controlled flow of argon carrier gas, transporting vaporised material to the inductively coupled plasma. The sample cell is mounted on precision stepper motor driven translation stages, which can be computer controlled manually by means of a joystick or remotely by the computer using suitable software module.

Sample viewing is facilitated by means of a video camera, allowing all control to be made from the keyboard of the PQ data station. The complete package is fully interlocked such that it is impossible for any laser radiation to escape into the environment.

The laser output is focussed onto the surface of the sample mounted within a quartz sample cell, with a volume of approximately 50 ml. The ablation chamber is mounted on a PTFE cell holder which in turn is mounted on a pair of perpendicularly mounted translation stages. A flow of argon into the cell through the PTFE holder is taken from the nebuliser carrier gas in the VG PlasmaQuad gas panel. The gas and microparticulate matter is taken from the cell to the ICP via a solenoid controlled valve, which can be switched to redirect flow from the torch at times of sample change over.

Positioning the sample and activating the purge system can be facilitated from a joystick or via the PlasmaQuad data station. Sample illumination is by a fibre optic light guide, with the power supply and lamp mounted beneath the sample cell enclosure. The interface between the computer (user) and LaserLab is made via the laser management unit, mounted in the bench of the ablation unit.

Figure 2.5 shows a schematic of the laserlab system.



2.6 Reagents, materials and procedures

Glasses

The following certified reference material glass samples were used: fluoride-opal glass, soda lime magnesia silica glass, soda-lime glass, and lead oxide-potassium oxide glass. The following standard reference material glasses were also used: NIST SRM 611, 613, and 614.

The samples were held in ablation chamber design 1. The lower section of the ablation chamber accommodated the sample holder. Both solid and liquid samples could be sampled. Solid samples i.e. the glass samples were placed into the ablation chamber.

Aqueous solutions

Aqueous multielement standards were prepared from a $1000 \mu\text{gml}^{-1}$ Spectrapure grade reagents, and distilled deionised water obtained with a Milli-Q system (Millipore) to obtain the desired concentrations. The test solutions consisted of $100 \mu\text{g ml}^{-1}$: B, Ti, Zn, and Na. Volumes of between $20 \mu\text{l}$ and 1 ml were pipetted into a carbon cup with a maximum volume of $40 \mu\text{l}$.

Oils

A multielement oil standard (Conostan S 21, $100 \mu\text{g ml}^{-1}$) was used. $20 \mu\text{l}$ portions were pipetted into the carbon cup. Samples were diluted using xylene. Two certified lubricating oils were also ablated as well as a certified engine oil containing wear metal particulates.

Depth profiling

The following steel coated samples were examined: titanium nitride on steel ($1, 3, 5, 7$ and $10 \mu\text{m}$ coating depth), zirconium nitride on steel ($3 \mu\text{m}$ coating depth), titanium/zirconium nitride on steel ($1 \mu\text{m}$ coating depth), a multilayered coating of titanium on zirconium nitride on steel ($3 \mu\text{m}$ coating depth), two ultrathin coated samples of tin (2.8 g m^{-2}) and chromium on steel (20 nm) and a tin oxide coated glass.

The Ti and Zr Nitride coatings were prepared by Arc bond sputtering, using the appropriate metal targets onto a steel substrate producing a very even coating. The samples came in varying coating thicknesses from 1 to $10 \mu\text{m}$ on steel strips of 2 mm thickness. The Sn and Cr coated steel samples came as large sheets which were cut into more manageable strips measuring 10 by 2 cm lengths. The tin oxide coated glass was obtained as a low emissivity glass section.

Biological samples

Electrophoresis gels were prepared containing 23 elements (Ag, Al, B, Ba, Bi, Ca, Cd, Co, Cr, Cu, Fe, Ga, In, K, Li, Mg, Mn, Na, Ni, Pb, Sr, Tl, and Zn) at concentrations of 0.01, 0.1, 1.0, 10, 50, and $100\ \mu\text{g g}^{-1}$, also a blank gel was prepared. The preparation of the multielement gels was as follows.

0.5 g of immunoelectrophoresis gel (Indubiose A) was dissolved in 50 ml of distilled water. The solution was heated and gently stirred on a hot plate until boiling. The solution was then heated for a further 10 minutes so that a clear solution was seen. Known amounts of multielement standard (Merk Multi element standard containing the above elements at $1000\ \mu\text{g ml}^{-1}$) were weighed out into glass vials. The heated solution of gel was then weighed out into the vials to give a final mass of 2 g. The gel solution was then poured onto the surface of a glass slide so that the entire surface was coated. The slides were then allowed to air dry overnight. Each standard was prepared in duplicate and a blank slide containing only the gel solution was prepared.

Biological microtome tissue samples were prepared by freezing the tissue in liquid nitrogen and then sectioning the tissue samples using a microtome knife (sections as thin as 5 μm were cut). These sections were then placed onto a microscope slide and ablated using ablation chamber design 2.

For the sampling of the electrophoresis gels and the steel coated samples chamber design 2 was used. The chamber was placed onto the surface of the flat samples and held in position with a clamp.

3.1 Introduction

The term glass refers to a class of materials of great practical usefulness, with a number of characteristic properties such as transparency, brittleness, and the property of softening progressively and continually when heated. Chemically these materials are mixtures of inorganic oxides. They are made by fusing sand, soda, and potash. A number of other metal oxides may also be added in order to enhance the properties of the glass. The nominal glass composition consists of the matrix elements 60-80 % SiO_2 , 2-12 % CaO , 14% Na_2O , and 1-2 % Al_2O_3 (107-111). Glasses may also contain a proportion of minor elements, which may be classed as major elements in some glass types, typically these include; Fe, Pb, B, Ti and K. The concentration of minor elements varies largely from $\mu\text{g g}^{-1}$ levels to percentage levels. Also there may be a number of elements at trace level, these may include a number of transition metals which are used primarily to add colour to the glasses.

As the number of formulations and applications of glass materials increase, the need for rapid, accurate and precise determination of the concentrations of major, minor, and trace elements of glass samples becomes important. When forensic scientists wish to establish the origin of a glass fragment they resort to the measurement of physical properties, such as refractive index, and density, and to wet chemical analysis for major and minor elements. However, modern glasses are made by carefully controlling the composition of the major elements for batches of the same glass and any differences are revealed in the minor and trace element composition.

Glass analysis usually requires the sample to be in a liquid form but silicate containing materials are not easy to prepare for elemental analysis. In most cases preparation of glasses involves the use of fusion fluxes (108-111) or complex acid digestion techniques, using open top, hotplate, acid digestion techniques followed by atomic absorption spectrometry (112-114). Many of these procedures are time consuming and also very laborious, requiring constant supervision during operation, and the use of hazardous chemicals, such as hydrofluoric acid. Many instrumental techniques have been employed for characterisation of glass samples including neutron activation

analysis (115-117), D.C. arc atomic emission spectroscopy (118-120), and X-ray fluorescence spectroscopy (120-122).

In recent years inductively coupled plasma spectrometry has been employed in trace element analysis of glasses. Advantages of the technique include the applicability to metals and non-metals, a high sensitivity for all elements, a simultaneous multielement capability, a large linear working range of the plasma and a relative absence of matrix interference. Catterick et al (123) used ICP emission spectrometry to determine minor and trace concentrations in forensic glass fragments of Al, Ba, Fe, Mg, and Mn with concentrations of 500, 5, 50, 500, and $10\ \mu\text{g g}^{-1}$ respectively. However, trace elements are also present at concentrations lower than this as shown by Headridge et al (124) who determined the levels of Pb, Ag, and Bi for forensic and archaeological glass samples using a graphite furnace atomic absorption technique. Limits of detection were found to be less than $5\ \mu\text{g g}^{-1}$.

Direct solid analysis of trace elements in glasses has been performed using laser ablation inductively coupled plasma mass spectrometry by Franks et al (125). The analysis, however, suffered from poor precision of about 10 %, owing to signal fluctuations. These fluctuations are most likely due to shot to shot variation in the amount of ablated material reaching the plasma. Another problem associated with laser ablation, like all solid analysis techniques is calibration. Satisfactory calibration is only possible where standards of a similar matrix are available. For these reasons laser ablation has only been used as a fast semi- quantitative method for the analysis of solids.

In this research a variety of glass samples are examined. Experiments will show whether analytical signals can be produced as a function of laser operating mode (Q switched or free running). Laser surface pretreatment for metals analysis from (126, 127) has shown to increase signal sensitivity, therefore such sample pre-treatment will be carried out. Results will be produced as emission-time signals for the matrix elements Si, Na, Ca and Al, for soda lime glass.

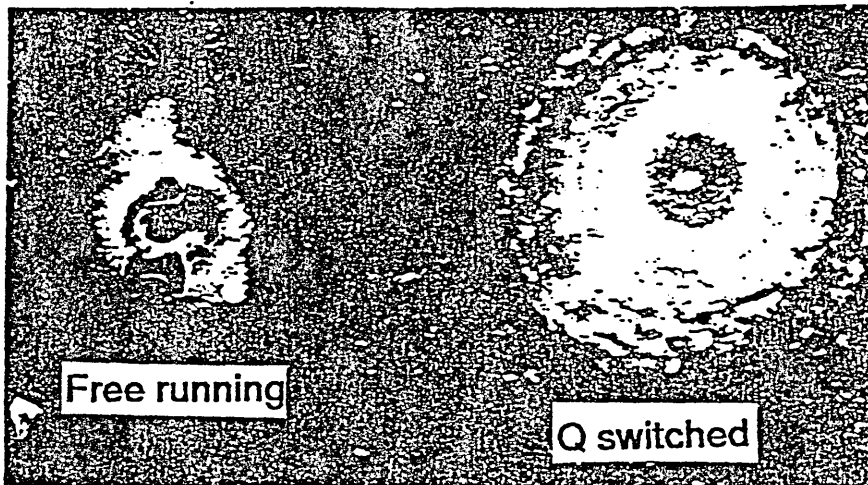
Systematic studies investigating the laser operating parameters as a function of the analytical signal include the effect of laser ablation time, the degree of laser beam focussing, and the laser beam energy. These studies will be used to optimise the sampling of glasses and to investigate the nature of the signals for the matrix elements.

Limits of detection and precision were calculated for a range of trace elements in glass standard materials. The effect of internal standardisation on precision was also investigated. Finally quantitative analysis of different glass samples was undertaken for a range of major, minor and trace elements.

3.2 Preliminary experiments

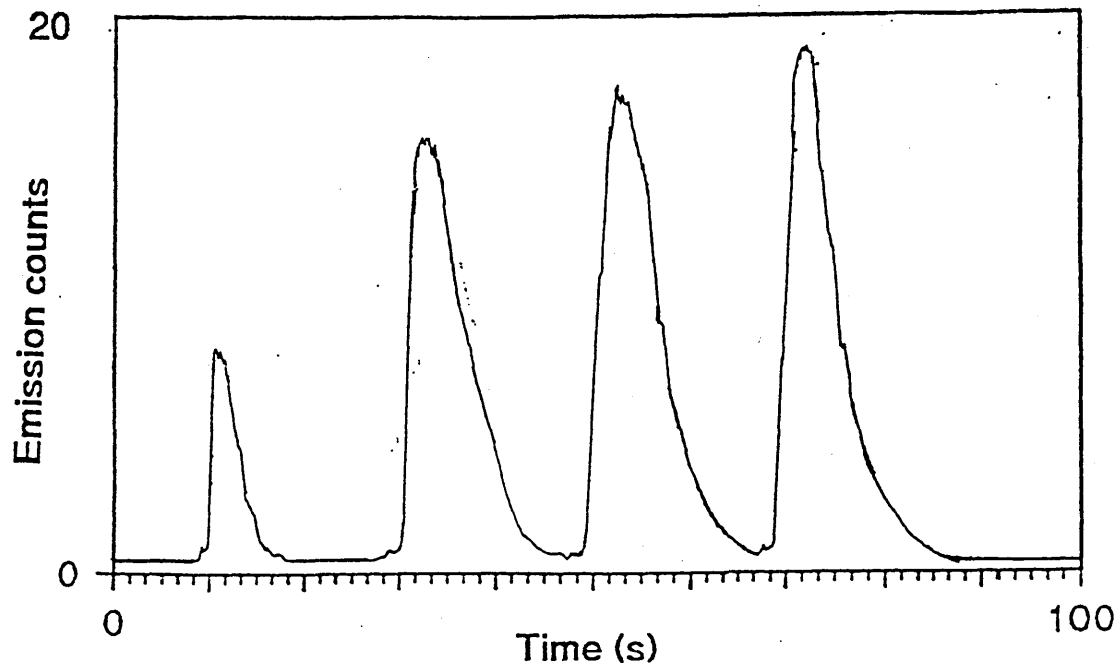
The NdYAG laser may be operated in two modes of operation Q-switched and free running. Initial experiments performed by firing the laser at soda lime glass for a 5 s ablation period and a laser lamp energy of 60 J, showed that no signal was obtained with the laser operating in the free running mode. A visual inspection of the craters is illustrated in **Figure 3.1** as a photomicrograph of the two types of crater formed after ablation of a silica glass sample for an ablation time of 5 s formed by the two modes of laser action. The photomicrograph shows that with the free running mode deep narrow craters are produced (less than 1 mm width). Where as with the Q-switched mode of laser operation a shallow relatively wide crater is formed (more than 3 mm). Clearly, both modes of laser operation produce cratering of the surface, so the difference in the emission signals for the two modes of laser operation must be due to the difference in transport efficiency of the particles formed. From the literature (128, 129) it is known that the free running mode of laser operation produces melting of the sample surface. Relatively large amounts of sample are ablated from the ablation site but little material gets to the ICP because the ablated material which exist have a poor transport efficiency and hence a small emission signal results. Conversely, the Q-switched mode of laser operation produces vaporised material with a high transport efficiency. Therefore, in all these experiments it was decided to operate the laser in the Q-switched mode of operation.

Fig 3.1 Photomicrograph of laser ablation craters on silica glass, for left the free running mode and right Q-switched laser pulses; (NdYAG laser, 60 J laser lamp energy, ablation time of 5 s)



The rate of ablation is determined by the degree of absorption of laser radiation at the particular wavelength used. In the case of glass samples, such as soda lime faint tunnelling through the material and ablation of the base on which the sample was placed was seen. Such ablation resulted in low sensitivity. This suggests that there was little coupling of the laser beam energy with the sample surface. However, when the surface of the glass sample had been previously ablated for a minimum of 5 s using a high laser lamp energy (60 J) this produced a rough opaque crater, which when fired on by the laser resulted in an increased emission signal with no ablation of the base. Clearly, such sample surface pretreatment increases the coupling of the laser beam with the sample surface. The effect of laser surface pretreatment is illustrated in Figure 3.2, which shows the emission time response for four transient signals for silicon in soda lime, using a laser lamp energy of 60 J for a 5 s ablation period. The first peak was much smaller than the subsequent peaks due to little laser coupling with no surface pre-treatment. The peak heights for the last three peaks showed a precision of 8 % RSD, for the soda lime glass. Differences in the peak heights were thought to be due to changes in laser focussing as the sample was ablated. A similar trend is seen for the other matrix elements, Na, Ca and Al.

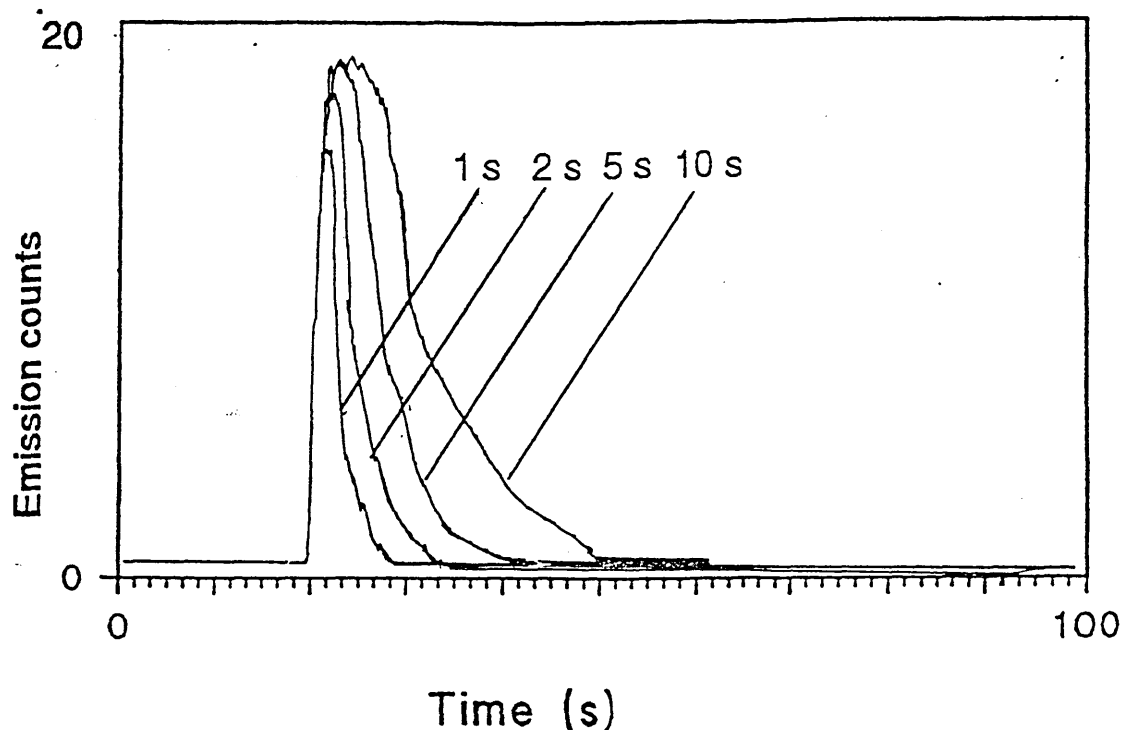
Fig 3.2 Emission time profiles for laser ablation of soda lime showing four emission signals for silicon. A laser lamp energy of 60 J was used and the sample was ablated four time for 5 s at 20 s intervals at the same site



3.3 Effect of laser ablation time

The first parameter investigated was the effect of ablation time on the signal response. A sample of soda lime glass was placed into the ablation chamber with the laser focussed on the surface. Ablation times of 1, 2, 5, 8, and 10 s were used as well as single shot laser firing. A laser lamp energy of 60 J was used, together at 10 Hz repetition rate. Emission time profiles for ablation times of 1, 2, 5 and 10 s were overlaid for Si, illustrated in Figure 3.3. Results are similar for all the other matrix elements Na, Ca and Al.

Fig 3.3 Emission time profile for laser ablation of soda lime glass showing emission signals as a function of the ablation time (1, 2, 5, 10 s). A laser lamp energy of 60 J per pulse was used. The results shown are for silicon



Ablation times of 1 to 10 s gave transient signals. It is found that when the ablation time is increased from 1 to 5 s the peak height and the peak width both increase as well as the peak area. The increase in the peak height and especially the peak width corresponds to an increase in the total amount of sample ablated for an increased ablation time. For ablation times of over 5 s there is no further increase in base peak height and very little increase in the peak width. Examination of the emission time signals (1 to 10 s) shows that memory effects are negligible as the peak is seen to return quickly to the baseline after the laser is switched off. Ablation times of over 5 s may cause the sample temperature to increase long enough to produce a greater degree of melting. Melting of the sample would result in the ejection of relatively large molten droplets which are not transported into the plasma.

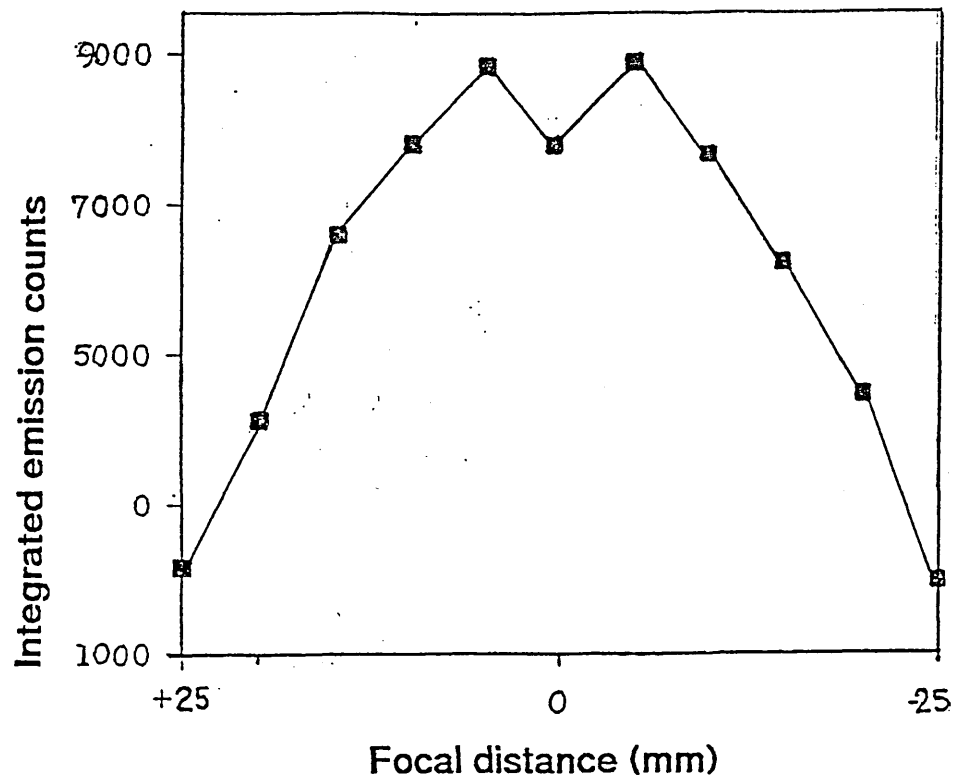
These experiments show that there are two factors to consider. First in order to gain enough sensitivity for bulk analysis the ablation time must be long enough to ablate sufficient sample into the plasma. Second an ablation time of greater than 5 s results in melting of the sample producing material which is no longer transported into the plasma. It was decided that a 5 s ablation period is sufficient for future experiments for glass samples.

3.4 Effect of laser focusing

Defocusing of the laser will alter the laser beam spot size and hence will also alter the laser energy incident on the sample. This decrease in the energy density of the beam due to defocusing of the laser is often used to provide a more representative sampling of bulk samples.

Up till now the laser has been focussed on the sample surface. The analytical signal as a function of laser focus was studied for ablation of a silica glass sample. The other laser ablation conditions were kept the same throughout the course of the experiment for example a laser lamp energy of 60 J was used for a 5 s ablation time. Each of the ablation sites were subjected to surface pretreatment by ablation. Changes in laser focus was achieved by moving the sample in the vertical direction, between 25 mm above and below the focal point of the laser. This gave laser spot sizes of 0.106, 0.169, 0.232, 0.358, and 0.421 mm in diameter, corresponding to defocusing the laser by 0, 5, 10, 15, 20, and 25 mm respectively. The results were produced graphically as raw counts based on the integration of the transient signal as a function of the laser focus, and are illustrated in **Figure 3.4** for silicon.

Fig 3.4 Graph showing the raw counts based on integration of the transient signal as a function of the laser focusing distance (0 to 25 mm above and below the surface of the sample). The results shown are for silicon



These results showed that a maximum signal was obtained when the laser was defocused from the surface of the sample by 5 mm. When the laser beam is focussed on the sample surface, melting is the predominant process. The laser bores relatively deeply into the sample ejecting molten particles. Very little of the ablated material is carried into the plasma. When the sample is moved 5 mm from the focal point vaporisation becomes more significant. Melting may still occur but at these lower laser beam densities more ablated material reaches the plasma. At position still further than 5 mm the laser energy densities fall still further and the degree of ablation falls, resulting in lower emission signals.

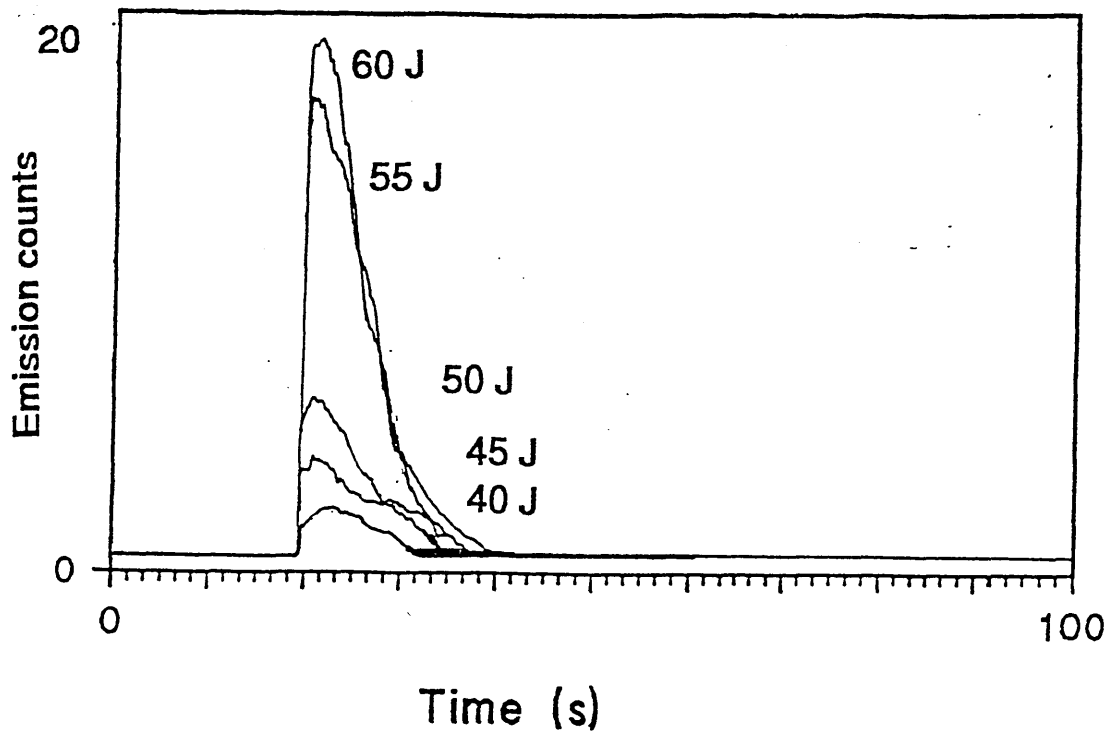
3.5 Effect of laser energy

Laser energy is an important parameter controlling the sampling amount of ablated material and is typically reported along with the experimental data. The amount of sample ablated could be controlled by varying the laser energy and/or the laser focussing onto the sample. The most common and easiest method of controlling the laser output energy is to control the energy delivered to the flashlamp. This control can be varied continuously over the operating range of the laser. However, because there is a threshold energy required for lasing, a lower limit is set which in this case varied but was seen to be about 35 J flashlamp energy.

Although the calculations gave a laser spot size of radius 5.3 μm , the observed craters appeared to be significantly larger than this. Scanning electron micrographs of craters produced on the glass surface after ablation show that a crater as large as 2 mm may be produced (illustrated in **Figure 3.1**). This is due to the conduction of heat through the sample and the expansion of heated material from the heated area, and is related to the dimensions of the plasma rather than the diameter of the focussed laser beam.

The flashlamp energy was varied from 40 to 70 J per pulse, giving laser pulses of between 196 and 345 mJ per pulse. The laser was operated for a 5 s ablation period. Emission time profiles were overlaid for laser energies of 40, 45, 50, 55 and 60 J laser lamp energy for Si are illustrated in **Figure 3.5**. The results were similar for the other matrix elements Na, Ca and Al.

Fig 3.5 Emission time profile for laser ablation of soda lime glass showing emission signals as a function of laser lamp energy (40, 45, 50, 55, and 60 J). A 5 s ablation time was used. The results shown are for silicon



Examination of the emission time profiles show that it is the peak height as well as the peak area that increases with increasing laser beam energy, corresponding to an overall increase in the amount of ablated material entering the plasma. This increase in peak height was seen most dramatically for laser lamp energies of over 50 J. Although the laser is capable of producing higher beam energies, it is seen that at beam energies higher than 60 J the sample shatters, resulting in no signals.

The results show a dramatic increase in the analytical signal for laser lamp energies of over 50 J. This large change in the ablation signal may be caused by different sampling processes at different laser beam energies. At lower laser energies two processes occur. Plasma sampling, where the plasma induced by each laser pulse vaporises material from the surface. Secondly direct laser/material interaction which occurs because at lower laser energies the laser induced plasma is optically thin allowing significant laser radiation to pass through to the sample surface.

At higher laser lamp energies the predominant ablation process would be due to the interaction of the laser induced plasma with the sample surface. As has been mentioned earlier the size of the crater produced by a Q-switched laser is determined principally by the size of the laser induced plasma formed over the surface. At laser lamp energies of 55 J and over such laser induced plasma formation would result in a significantly larger crater and hence a dramatic increase in the amount of material ablated.

An increase in sensitivity may be obtained for bulk sampling of glasses by increasing the laser energy incident on the sample. However, very high laser energies were seen to shatter the glass samples. Therefore, it was found that for practical purposes, a maximum sensitivity could be obtained using a laser lamp energy of 60 J.

It is concluded that in order to achieve optimum sensitivity the optimum instrumental operating parameters were as follows: A Q-switched laser beam operating at a laser lamp energy of 60 J, a 5 s ablation period, and defocusing 5 mm above the sample surface. It was also noted that pre-ablation of the sample surface greatly improved coupling between the sample and the laser beam and hence greatly improved sensitivity.

3.6 Calibration

The optimised instrumental operating parameters were used as the basis of experiments to analyse glass materials. Calibration graphs were constructed to determine the dynamic linear range, the limits of detection and precision. The use of internal standardisation to improve sampling precision was undertaken.

Calibration curves for several elements were constructed over three orders of magnitude in concentration. The calibration standards that were used were NIST SRM's 610, 613, and 614 for the elements Fe, Pb, Ag, Cu, B, and Co, these elements were all common to the three standards. The concentration of each element are given below in **Table 3.1**. Each sample was ablated for

5 s using a laser lamp energy of 60 J. Each point represents the mean of five measurements.

The calibration graphs are illustrated in Figure 3.6.

Table 3.1 Concentration of the elements Fe, Pb, Ag, Cu, B, and Co in SRM glasses (NIST SRM 610, 613, and 614)

| Element | NIST standard element concentration / $\mu\text{g g}^{-1}$ | | |
|---------|------------------------------------------------------------|-------|------|
| | 610 | 613 | 614 |
| Fe | 458 | 51 | 13.3 |
| Pb | 426 | 38.57 | 2.32 |
| Ag | 254 | 22.0 | 0.42 |
| Cu | 444 | 37.7 | 1.37 |
| B | 351 | 32 | 1.30 |
| Co | 390 | 35.5 | 0.73 |

Glass nominal composition: 72 % SiO_2 , 12 % CaO , 14 % Na_2O , and 2 % Al_2O_3 .

Fig 3.6 Calibration graphs for laser ablation of glass standard reference materials (NIST SRM 610, 613, and 614) for Fe, Pb, Ag and Cu

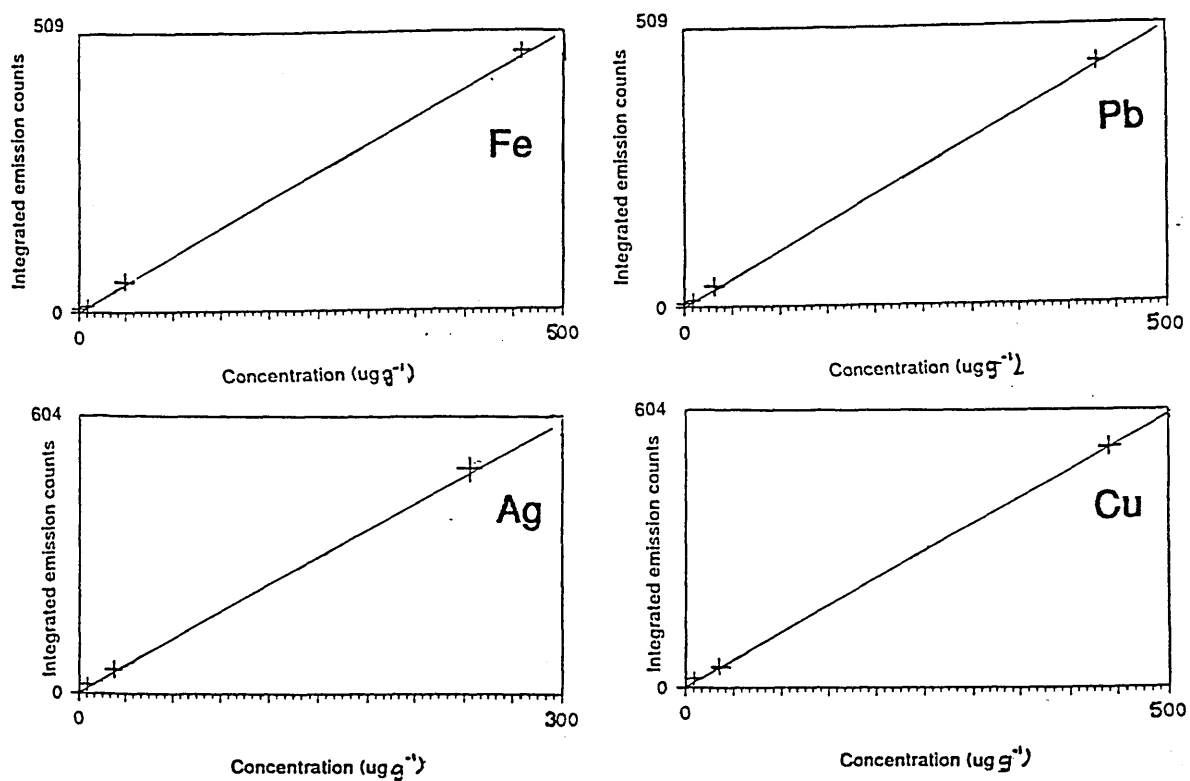
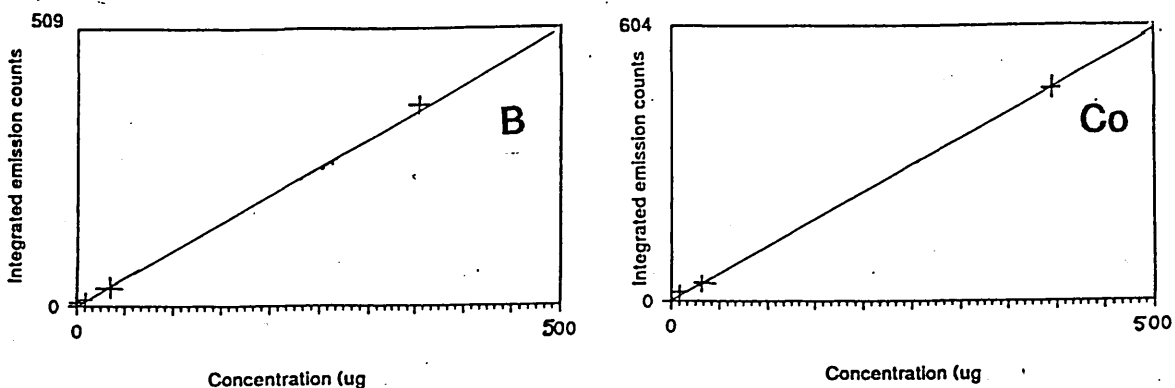


Fig 3.6 Calibration graphs for laser ablation of glass standard reference materials (NIST SRM 610, 613, and 614) for B and Co



Limits of detection were calculated for all elements for which concentration data was available. Limits of detection, in this case were calculated as the minimum reading that was statistically distinguishable from the background. Detection limits were determined by the concentration obtained for the blank plus 3 SD. The blank signal, was calculated as the signal produced for ablation of a high purity quartz glass sample. Table 3.2 shows the results obtained from the calibration studies.

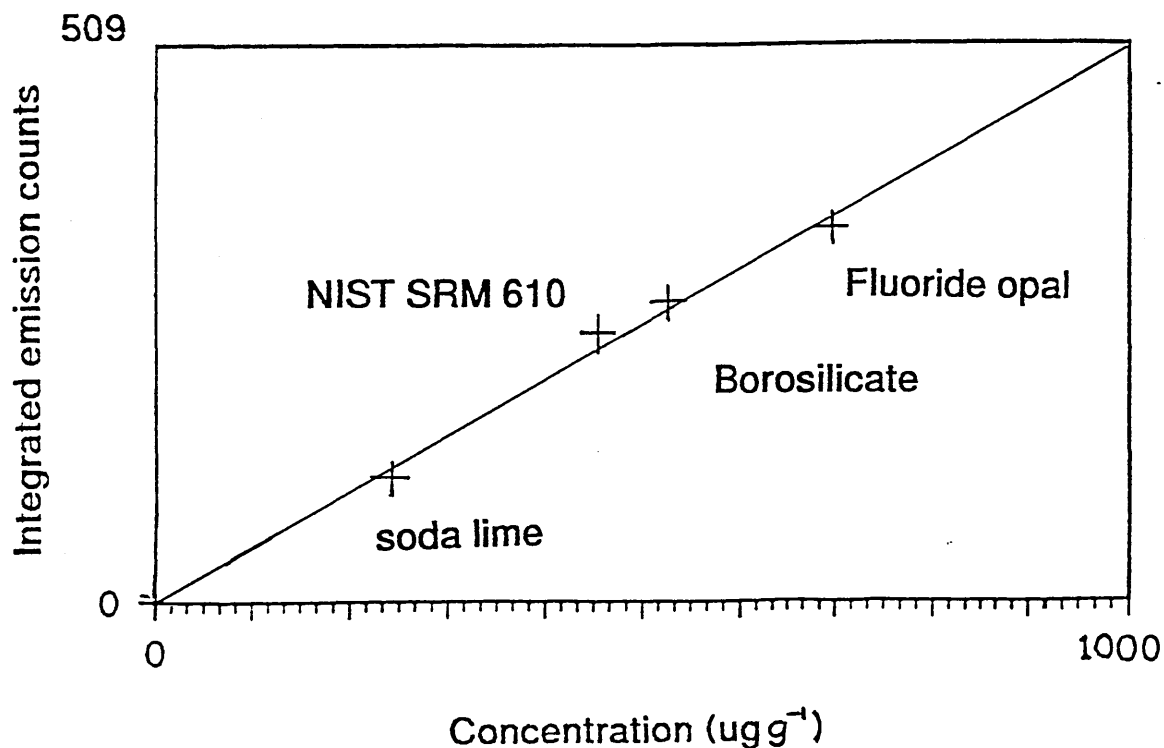
Table 3.2 Calibration data and detection limits calculated for laser ablation of glass standard reference materials (NIST SRM 611, 613, 614)

| Element | Equation of line | Correlation coefficient | Detection limit $\mu\text{g g}^{-1}$ |
|---------|------------------|-------------------------|--------------------------------------|
| Fe | $y=171.1x + 97$ | 0.987 | 0.015 |
| Pb | $y=27.6x + 43$ | 0.986 | 0.084 |
| Ag | $y=16.2x + 27$ | 0.996 | 0.11 |
| Cu | $y=25.6x + 103$ | 0.992 | 0.11 |
| B | $y=55.6x + 39$ | 0.985 | 0.023 |
| Co | $y=68.6x + 104$ | 0.996 | 0.050 |

The values for limits of detection show that the results achieved using laser ablation are typically below $0.1 \mu\text{g g}^{-1}$, and are in many cases at the double digit $\mu\text{g g}^{-1}$ level. These low detection limits allow comprehensive discrimination of glass materials, without the need for sample dissolution and subsequent dilution and loss of sensitivity. The calibration curves also show that linearity was achieved for all elements over the concentration ranges for each of the standards. The system is capable of distinguishing concentrations below $1 \mu\text{g g}^{-1}$ up to and over $500 \mu\text{g g}^{-1}$.

In order to obtain analytical data for glass samples, borosilicate glass, fluoride opal glass, and soda lime glass as well as a standard reference material glass (NIST SRM 610) were examined. Experiments were performed to investigate whether the different matrix composition of these different glasses will affect the signal for the same trace element. The samples were all ablated under the same conditions (60 J laser lamp energy, for 5 s) after pre-ablation of the sample surface. Results produced as a graph of the integrated peak area as a function of the Fe concentration for the above glass samples, are illustrated in Figure 3.7.

Fig 3.7 Integrated emission signals for four different glass samples for Fe, shown as a graph showing signal intensity against Fe concentration as a function of different glass types (borosilicate, fluoride opal, soda lime and a standard glass NIST SRM 610)



The results show linearity for Fe. The signal is proportional to the element concentration which is independent of the glass matrix. These results suggest that it would be possible to produce quantitative data for trace element analysis using external calibration standard, in this case NIST SRM 610.

3.7 Precision

Precision was evaluated using 10 different sites after pre-ablation. The use of an internal standardisation for signal normalisation to improve precision was also investigated.

A standard glass (NIST SRM 610) was employed and the following elements determined: Fe, Pb, Ag, Cu, B, and Co, at concentrations of 458, 426, 254, 444, 351, and 390 $\mu\text{g g}^{-1}$, respectively.

The data is presented in Table 3.3 below.

Table 3.3 Precision study data for laser ablation of SRM (NIST SRM 610)

| Raw counts based on the integration of the transient signals Counts x 1000 | | | | | | |
|-------------------------------------------------------------------------------|------|------|------|-------|------|------|
| | Fe | Pb | Ag | Cu | B | Co |
| 1 | 78.6 | 14.9 | 6.2 | 12.3 | 19.9 | 27.4 |
| 2 | 92.6 | 11.5 | 4.2 | 14.5 | 25.6 | 34.1 |
| 3 | 87.4 | 13.8 | 5.1 | 13.8 | 22.5 | 32.9 |
| 4 | 68.9 | 10.0 | 3.8 | 13.0 | 22.2 | 31.9 |
| 5 | 72.4 | 10.8 | 4.0 | 13.4 | 22.5 | 32.0 |
| 6 | 96.4 | 11.9 | 4.3 | 15.9 | 26.8 | 37.6 |
| 7 | 79.4 | 15.0 | 7.3 | 12.5 | 20.7 | 27.5 |
| 8 | 69.0 | 10.1 | 3.8 | 13.1 | 22.2 | 32.1 |
| 9 | 72.5 | 11.0 | 4.0 | 13.6 | 22.7 | 32.1 |
| 10 | 75.3 | 12.0 | 4.1 | 13.8 | 22.9 | 33.0 |
| Mean | 79.2 | 11.9 | 4.69 | 13.6 | 22.8 | 32.1 |
| S.D. | 9.29 | 2.22 | 1.11 | 0.997 | 1.95 | 2.82 |
| %RSD | 11.7 | 18.6 | 23.6 | 7.3 | 8.6 | 8.8 |

The precision data shows similar levels of precision for the elements Fe, Cu, B, and Co where as the precision for Pb and Ag is significantly poorer. This difference in precision may be accounted for by the relative difference in the melting and boiling points of the elements; Pb and Ag have relatively low melting and boiling points compared to the other elements which may result in losses due to condensation of these analytes on the walls of the transfer tubing, shown by a simple experiment in which the transfer tube was acid washed, followed by analysis of the solution. These losses are not reproducible and will therefore result in a reduction in sampling precision.

The precision data also indicates similar trends for each element. The implication is that the use of an internal standard may improve precision. However, careful choice of the most suitable internal standard must be made. When choosing an appropriate internal standard for a particular element the laser sampling characteristics of both elements will have to be similar. Hence both elements would have similar melting and boiling points to ensure similar rates of ablation of both elements. The melting and boiling points of each element is given below in **Table 3.4**.

Table 3.4 Melting and boiling points of the following elements; Fe, Pb, Ag, Cu, B and Co

| Element | Fe | Pb | Ag | Cu | B | Co |
|-----------------|------|------|------|------|------|------|
| MP \uparrow C | 1539 | 328 | 962 | 1083 | 2327 | 1455 |
| BP \uparrow C | 2887 | 1780 | 2212 | 2582 | 2547 | 2837 |

Precision were recalculated using the element to Co ratios. The precision for each element using Co as an internal standard are given below in **Table 3.5**.

Table 3.5 Precision data using cobalt as an internal standard

| Element | Fe | Pb | Ag | Cu | B |
|---------|-----|------|------|-----|-----|
| %RSD | 5.7 | 13.5 | 18.2 | 4.2 | 4.8 |

The results using internal standardisation show that improvements in precision can be achieved. However, the improvement in using Co as an internal standard was most significant for the less volatile elements with similar melting and boiling points as Co such as Fe, Cu, and B. Where as very little improvement was seen for the more volatile elements Pb and Ag. The Pb to Ag ratios, however, give a precision of 7.4 %RSD. This further confirms that for internal standardisation to be effective elements of similar volatility must be used.

3.8 Analysis of glasses

For the analysis of glass a single point calibration curve technique was used using a glass SRM (NIST SRM 611, 500 ppm) as an external calibration standard. Both the standard and the sample were subjected to the same laser ablation conditions, 60 J lamp energy for a 5 s ablation period. Results were obtained as raw counts based on the integration of the transient signal and the mean of ten values. The following glass samples were analysed: soda lime, fluoride opal and borosilicate. All elements certified for the three glass types were determined: Si, Ca, Na, Al, Ti, Fe, B, K, and Zn. Results are given in **Table 3.6**.

Table 3.6 Results for analysis of glass by laser ablation

Borosilicate glass

| Element | Certified concentration / $\mu\text{g g}^{-1}$ | Found concentration / $\mu\text{g g}^{-1}$ | % Agreement (+/- %) |
|---------|---------------------------------------------------|-----------------------------------------------|------------------------|
| Si | 370000 | 337807 | -9 |
| Ca | 1400 | 1371 | -2 |
| Na | 28500 | 26462 | -7 |
| Al | 1300 | 1257 | -3 |
| Ti | 210 | 206 | -2 |
| Fe | 525 | 529 | +0.8 |
| B | 77000 | ---- | ---- |
| K | 2000 | 2098 | +5 |

Table 3.6 Results for analysis glass samples by laser ablation - continued

Fluoride opal glass

| Element | Certified concentration $\mu\text{g g}^{-1}$ | Found concentration $\mu\text{g g}^{-1}$ | % Agreement (+/- %) |
|---------|-------------------------------------------------|---------------------------------------------|------------------------|
| Si | 320000 | 316920 | -1 |
| Ca | 30000 | 28950 | -4 |
| Na | 114000 | 117325 | +3 |
| Al | 16000 | 15985 | -0.1 |
| Ti | 250 | 266 | +6 |
| Fe | 700 | 693 | -0.01 |
| B | 600 | 589 | -2 |
| K | 4750 | 4987 | +5 |
| Zn | 26000 | 27932 | +7 |

Soda lime glass

| Element | Certified concentration $\mu\text{g g}^{-1}$ | Found concentration $\mu\text{g g}^{-1}$ | % Agreement (+/- %) |
|---------|-------------------------------------------------|---------------------------------------------|------------------------|
| Si | 340000 | 338500 | -0.4 |
| Ca | 71000 | 72600 | +2 |
| Na | 108000 | 106530 | -1 |
| Al | 9000 | 9250 | +3 |
| Ti | 120 | 128 | +6 |
| Fe | 238 | 250 | +5 |
| K | 830 | 798 | -4 |

Figures in parenthesis are the % RSD for conventional analysis of glasses (n=5)

The results for laser ablation show that good agreement was observed between the found and the certified values with % agreement varying between -9 and +7%. It was not possible to measure B in borosilicate glass as the intensity signal went off scale. This technique gives better accuracy than that commonly encountered in conventional analysis of glass samples. Catterick et al (123) produced data for analysis of small glass fragments using an acid digestion technique followed by inductively coupled plasma emission spectrometry which showed an accuracy of between -23 and +18 % for five glass samples for Al, Ba, Fe, Mg and Mn. These results were improved compared to those obtained by other workers using laser ablation. Denoyer (76) analysed a standard reference glass (NIST SRM 612) using other standard glass calibrants (NIST

SRM 610, 614 and 616). He showed results around the 50 ug g^{-1} level which varied between -19 and +15% of the certified concentration.

4.1 Introduction

In this chapter the analysis of small volumes of liquid typically between 20 and 40 μl , is investigated. The technique is called laser ablation microsampling.

The technique, analogous to electrothermal vaporisation, is one in which small volumes of liquid are vaporised into a plasma using a focussed pulsed laser beam instead of a heated filament. With only minor changes to the experimental set-up the laser ablation chamber can handle solids as well as liquids. Laser ablation ICP-spectrometry of liquids has hardly been exploited for analytical purposes. The possibility of liquid sample introduction by laser ablation may help to overcome some of the problems associated with conventional liquid sample introduction techniques. Feasibility studies were undertaken to investigate this novel approach to liquid sampling. Experiments were designed to gain more information of the basic underlying processes that occur during laser vaporisation of aqueous multielement solutions, such as the mechanism by which aqueous solutions are ablated with reference to laser operating parameters and the effect of different thermochemical properties of analytes.

ETV devices coupled to ICP spectrometers (23-25) have been successfully used to sample small volumes of liquid, typically 5 to 100 μl . These devices have shown improvements in transport efficiency over pneumatic nebulisation and improvements in detection limits of 1 to 2 orders of magnitude. The reason for this significant improvement in detection power has been attributed to the result of an increased concentration of analyte already desolvated and vaporised by the heated filament. However, it can be seen that the analytical sensitivity for different elements is affected by the thermochemical properties. Important mechanisms which affected transport of the elements to the plasma are identified by Park et al (24) as the formation of non volatile carbides on the graphite cup, and the formation of other refractory compounds and the deposition of volatile materials on the sample transport tubing and walls of the ETV chamber. Therefore, for this study it was considered important to investigate elements with a wide range of thermochemical properties with respect to melting and boiling points, and the formation of refractory compounds. A

synthetic aqueous multielement solution was prepared containing Ti, B, Zn, and Na at 100 µg ml⁻¹.

Table 4.1 shows the different thermochemical properties of the chosen elements.

Table 4.1 Thermochemical properties of Ti, B, Zn and Na

| Element | Melting point/ °C | Boiling point/ °C | Formation of refractory compounds |
|---------|-------------------|-------------------|-----------------------------------|
| Ti | 1677 | 3277 | Carbide and Oxide |
| B | 2327 | 2547 | Carbide |
| Zn | 420 | 908 | None |
| Na | 97.5 | 892 | None |

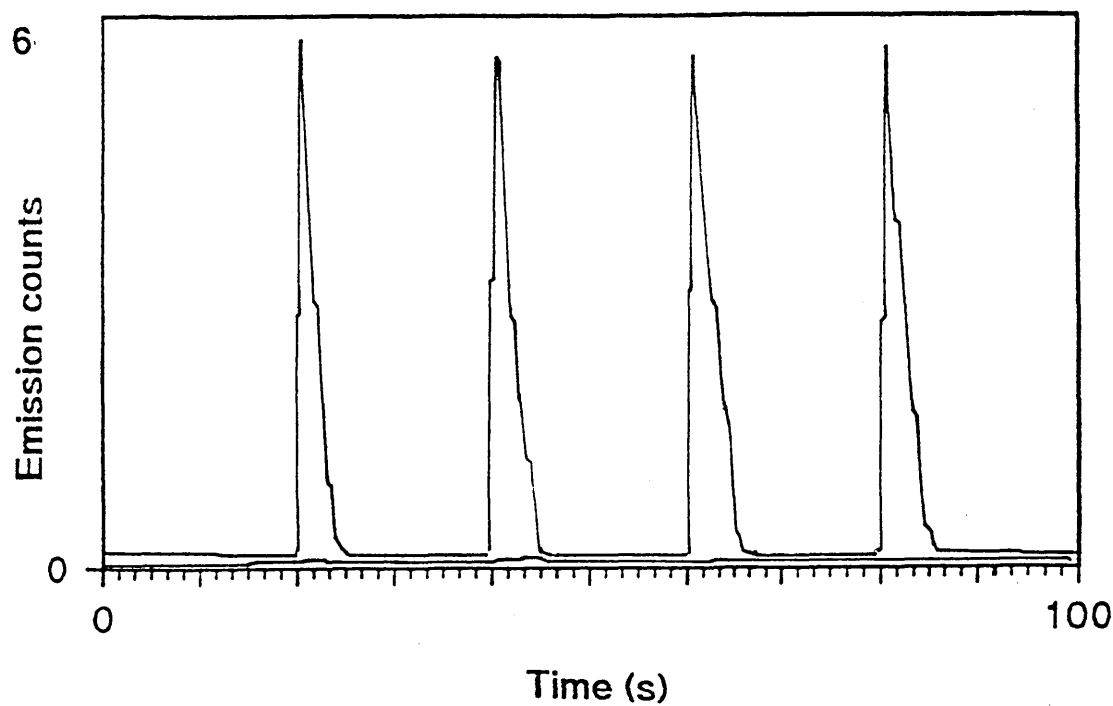
Hence the solutions used contained two relatively non volatile elements, Ti and B, along with two relatively volatile elements, Zn and Na. Furthermore, Ti and B readily form refractory compounds.

4.2 Preliminary experiments

Most fundamental studies of the interaction of laser radiation with materials address the question of the role of the properties of laser radiation. The laser beam wavelength, pulse energy, ablation time, degree of laser focussing, and the laser beam mode of operation are of particular relevance to the generation of ablated material. Additionally there is a relationship between laser properties and sample properties such as reflectivity, absorption at the laser beam wavelength, and thermal conductivity. In order to evaluate laser ablation for the sampling of aqueous micro samples, the optical emission intensity from the plasma was measured as a function of laser operating parameters: pulse energy; ablation time; degree of laser focusing; and the sample volume.

Preliminary studies were performed to ascertain whether or not analytical signals could be obtained from laser ablated synthetic aqueous multielement standards. The procedure was as follows: 20 μl solution were contained in a carbon cup with a maximum volume of 40 μl . A pulsed laser beam operating at 10 Hz was focussed onto the surface of the liquid and fired using a laser lamp energy of 60 J, for each of four consecutive single shots. The same conditions were used for the ablation of a distilled water blank. Emission time profiles are shown in figure 4.1 for titanium, for both the aqueous multielement standard and the distilled water blank.

Fig 4.1 Emission time profile for laser ablation of an aqueous multielement solution ($100\mu\text{g ml}^{-1}$: Ti, Zn, Na and B) ($20\mu\text{l}$ sample was subjected to 4 single laser shots using a Q switched laser at 60 J laser lamp energy). The results shown are for titanium



The results show that transient signals are obtained for each of the four laser shots for the aqueous multielement standard. The peaks are of a short duration (typically 6s) and there is no carry over between them. No signals were seen for the distilled water blank. The shot to shot precision calculated from measurements of peak heights, gave values between 9 and 12 %RSD for each element.

A visual check made on the contents of the carbon cup after laser ablation showed that some liquid remained after the four single shots. It is seen therefore, that in order to improve sampling sensitivity an increased ablation period is needed to remove all the sample. Sample spattering on the ablation chamber walls was also observed. It is likely that sample spattering is the primary cause of the relatively poor precision, of between 9 and 12 %RSD, compared to <1% RSD for conventional sample introduction. The spattering is probably caused by the generation of high pressure acoustic waves produced by dielectric breakdown of the sample as described in **Section 1.6.4 (105, 106)**. The possibility of reducing the amount of spattering by reducing the incident energy of the laser beam and/or by defocusing the laser is reported later.

The aqueous solutions are transparent to laser radiation at 1064 nm and therefore there would be little or no interaction of laser radiation at this wavelength with the water. However, the main mechanism by which the analyte is vaporised is likely to be by a thermal process, where the laser energy heats the base of the carbon cup thereby transferring thermal energy to the liquid so that a portion of it is vaporised. A laser plume, formed at high incident laser energies (laser power densities of around $1 \times 10^8 \text{ W cm}^{-2}$ (90)), may interact with the thermally ablated material and cause further breakdown and atomisation of the sample.

4.3 Calculation of analyte mobility

It was important to examine how laser ablation signals compared to the steady state signal obtained for pneumatic nebulisation of the aqueous multielement solution. By calculating the analyte introduction rate for pneumatic nebulisation, the introduction rate of analyte for laser ablation could be calculated by comparing the signals for each element. Differences in individual element introduction rates will indicate any element suppression due to the thermochemical nature of the element. For example, the loss of elements due to formation of refractory compounds, or loss of volatile elements condensing on the chamber walls.

The analyte introduction rate into the plasma by pneumatic nebulisation was calculated as follows: A sample uptake rate of 2 ml per minute was measured. From the volume of liquid going to waste it was estimated that the transport efficiency was about 2 %. Thus, the analyte introduction rate was calculated to be approximately $0.067 \mu\text{g s}^{-1}$ for a $100 \mu\text{g ml}^{-1}$ solution for Ti, Zn, B and Na.

It was found by visual inspection of the sample cup, following ablation times of 1, 2, 3, 4, and 5 s of a 20 μl sample using a Q switched laser at 60 J, that a 5 s ablation period was sufficient to remove all the liquid from the cup and hence maximise sampling sensitivity. Emission time profiles for both methods of sample introduction are shown in **Figure 4.2** for Titanium. Similar results were obtained for Zn, Na and B. The transient signal produced by laser ablation was integrated over 30 s, which corresponded to the base line width of the transient peak. The steady state signal produced by pneumatic nebulisation was integrated for the same 30 s. The results were derived from the mean of 5 samples. The integrated signal for laser ablation was divided by the integrated signal for pneumatic nebulisation. This ratio was then multiplied by the total mass of analyte that would enter the plasma calculated for pneumatic nebulisation over 30 s. This was $30 \times 0.067 \mu\text{g s}^{-1} = 2 \mu\text{g}$. This allows the calculation of the mass of each element entering the plasma by laser ablation for a 5 s ablation time. Results are given in **Table 4.2**.

Fig 4.2 Overlays of emission time profiles for an aqueous multielement solution ($100 \mu\text{g ml}^{-1}$: Ti, Zn, Na and B) by laser ablation ($20 \mu\text{l}$ was ablated using a Q switched laser for a 5 s ablation time at 60 J laser lamp energy) and pneumatic nebulisation of the same solution. The results shown are for Ti and Zn

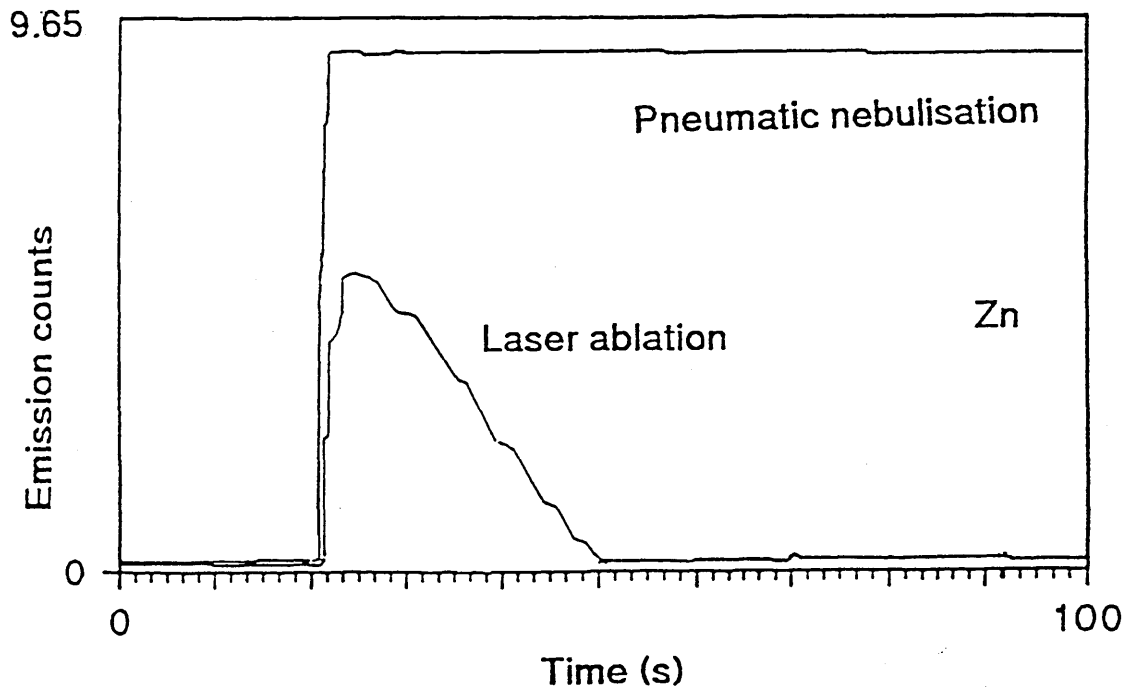
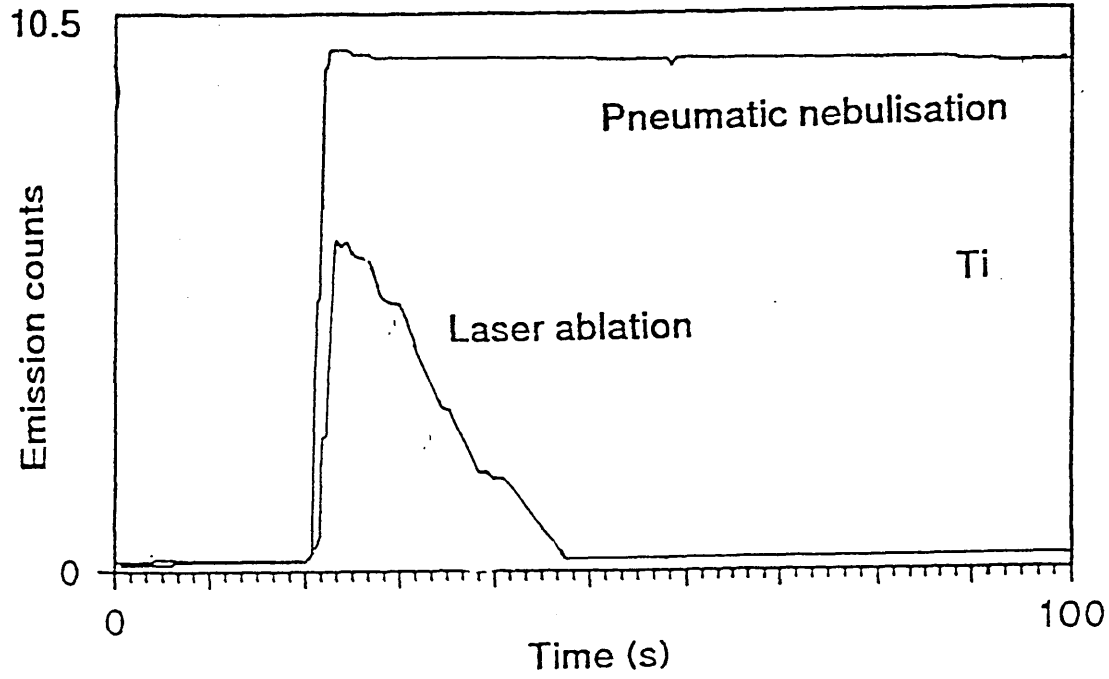


Table 4.2 Raw counts based on the integration of signals produced by laser ablation and pneumatic nebulisation of an aqueous multielement solution

| Element | Laser ablation (LA) signal counts x 1000 | Pneumatic nebulisation (PN) signal x 1000 | LA/PN ratio | Mass of analyte entering the plasma for a 5 s ablation time / μg |
|---------|------------------------------------------|-------------------------------------------|-------------|-----------------------------------------------------------------------------|
| Ti | 103 | 295 | 0.35 | 0.70 |
| B | 8.7 | 25 | 0.34 | 0.68 |
| Zn | 91 | 253 | 0.36 | 0.72 |
| B | 3 | 8.4 | 0.36 | 0.72 |

LA signal is the mean of the results for integration of the laser ablation signal for 5 samples. PN signal is the mean of the results for integration of the signal obtained by pneumatic nebulisation.

These results show that the average mass of an element introduced into the plasma from a 5 s ablation was approximately 0.7 μg . The mass of an element in a 20 μl solution is 2 μg . Therefore, approximately 30 % of the analyte reaches the plasma. The initial work reported in Section 4.2 showed that some of the sample was lost through spattering, and some of the vaporised material may have condensed out on the sample introduction tubing. However, the results for each element are similar showing that there is little or no suppression of analyte due to factors such as the formation of refractory compounds and loss of volatile elements. The reasons for this may be due to a relatively low temperature at which vaporisation occurs for laser ablation, when compared with ETV where the sample is atomised at temperatures as high as 3000⁰ C (24). At these higher temperatures problems arise from the formation of refractory compounds and the loss of volatile elements. With laser ablation it is suggested that the volatilisation temperatures due to laser heating of the carbon cup are only sufficient to vaporise the analytes into the plasma. What little atomisation occurs will be due to the interaction of the vapour with the laser induced plasma.

4.4 Effect of laser ablation time

The laser was operated for extended time periods of between 1 and 10 s, and a 20 μ l sample was ablated using a laser lamp energy of 60 J. Emission time profiles for 1, 3, and 5 s ablation times were overlaid. The results were similar for Ti, Zn, Na and B. The emission time profile produced for titanium is illustrated in **Figure 4.3**.

The emission time profiles for each of the elements for 1, 3, 5 and 10 s ablation periods produced transient signals. It was seen that increasing the ablation from 1 to 5 s resulted in an increase in the base peak width from about 20 to 30 s. This is due to an increase in the total quantity of sample ablated for longer ablation times. For ablation times over 5 s no further increase in the peak width was seen, suggesting that all of the liquid had been ablated at 5 s. This confirms results from visual observations in the earlier studies reported in **Section 4.2**. It is noted that the peak height also shows a small increase as the ablation time increases. This suggests an increased rate of sample entering the plasma for longer ablation periods. This may be explained by an increase in heating of the carbon cup, resulting in an increased rate of sample vaporisation.

Figure 4.4 shows a graph of the raw counts, based on the integration of the transient signal, as a function of laser ablation time. The integration period was started at the time of laser firing. The total integration time was 30 s, and each data point used for the graph is the mean of 5 samples. The levels of precision are given in **Table 4.3**. As the results obtained with each of these elements were similar, only those of Titanium are given.

Fig 4.3 Emission-time profile for laser ablation of an aqueous multielement solution ($100 \mu\text{g ml}^{-1}$: Ti, Zn, Na, and B) showing emission intensity as a function of laser ablation time: 1, 3, and 5 s ($20 \mu\text{l}$ was ablated, using a Q switched laser at 60 J laser lamp energy). Results are shown for titanium

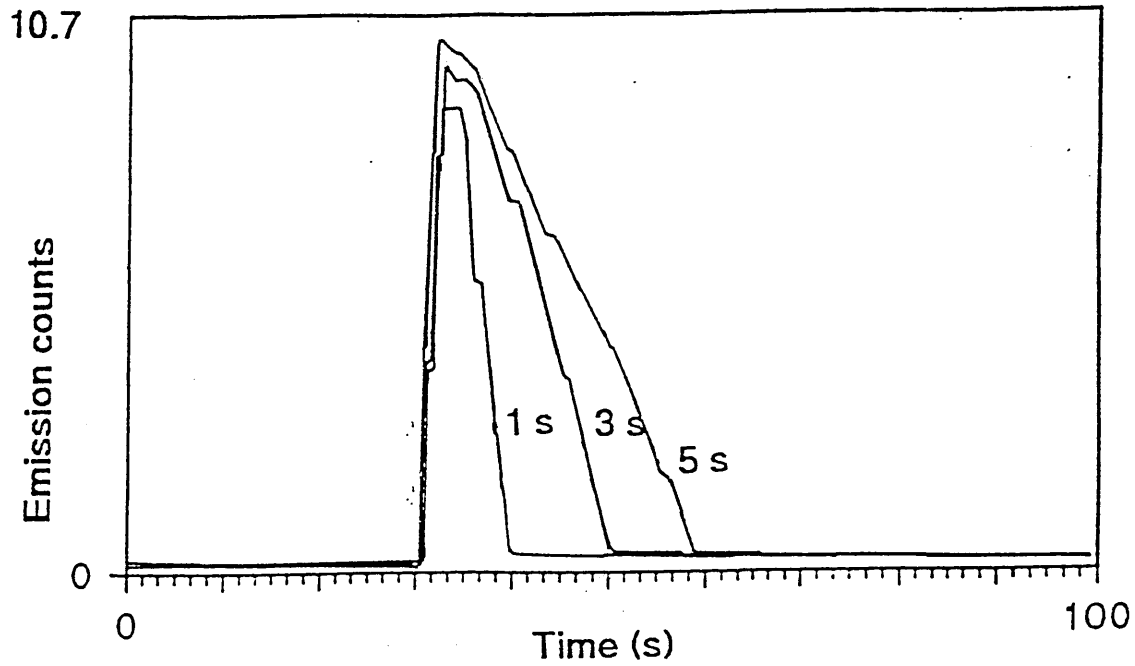


Fig 4.4 Graphs showing the raw counts based on integration of the transient signal as a function of ablation times: 1 to 10 s for laser ablation of an aqueous multielement solution containing $100 \mu\text{g g}^{-1}$ Ti, Zn, Na and B ($20 \mu\text{l}$ was ablated using a Q switched laser operating at 60 J) for Ti

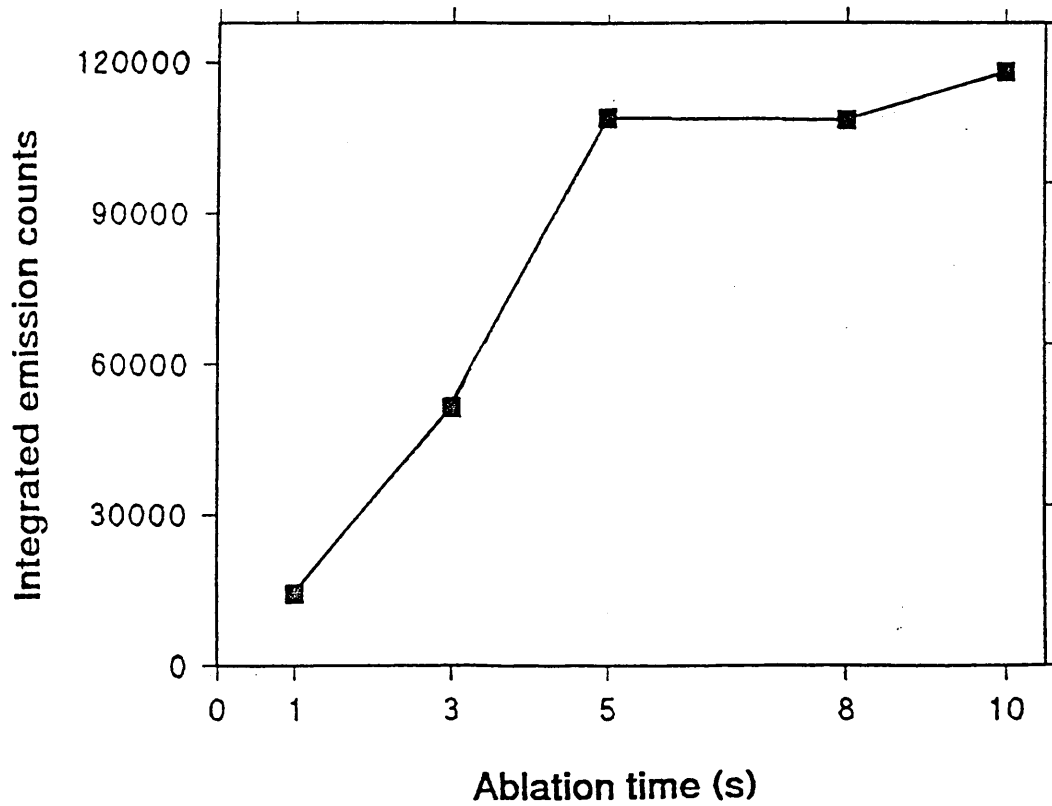


Table 4.3 Table showing the level of precision (as the %RSD n=5) for raw counts based on the integration of the transient signals obtained as a function of the laser ablation time (1 to 10 s) for the elements Ti, Zn, B and Na

| Element | Ablation time / s | | | | |
|---------|-------------------|------|-----|-----|-----|
| | 1 | 3 | 5 | 8 | 10 |
| Ti | 13.5 | 12.0 | 6.0 | 6.2 | 6.0 |
| B | 12.0 | 11.2 | 5.8 | 6.0 | 5.8 |
| Zn | 13.0 | 12.0 | 7.5 | 6.5 | 6.4 |
| Na | 14.2 | 12.8 | 6.8 | 7.0 | 7.0 |

The graphical data (see Figure 4.4) indicates a direct correlation between duration of laser operation and the amount of analyte entering the plasma up to a maximum duration of 5 s with no further increase beyond 5 s. For ablation times of 1 and 3 s an average precision of about 12 %RSD is seen. However, for an ablation time of 5 s and beyond the average precision is about 6 %RSD. A dramatic improvement, which is expected, because all the sample is used up at ablation times of 5 s and beyond. A similar correlation between ablation time and analytical signal was found by Booth and Mcleod (67) for the ablation of liquid paint samples. The volume of paint was approximately 30 μ l and there was an increase in the analytical signal up to 10 s ablation time. Laser ablation of glasses in Section 3.3, showed a direct correlation between laser ablation time and the signal, with a maximum signal produced for an ablation time of 5 s.

It is concluded that to obtain the maximum sensitivity and precision for 20 μ l sample ablated with a laser lamp energy of 60 J, a minimum ablation period of 5 s has to be used. Additionally it was observed that ablation times greater than 5 s result in damage of the carbon cup.

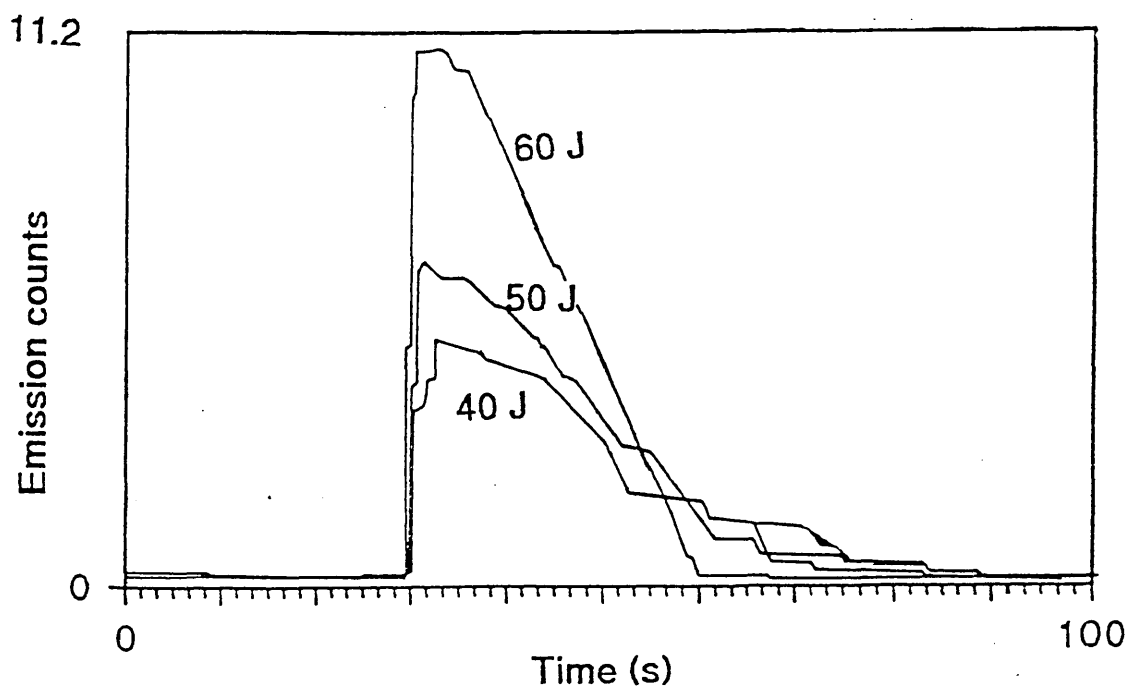
4.5 Effect of laser energy

The previous study showed that an ablation period of 5 s using a laser lamp energy of 60 J was sufficient to ablate all of the 20 μ l aqueous sample from the sampling cup. The next series of

experiments were undertaken to ascertain the effect of varying laser energy on the ablation yield and rate of ablation.

Varying the laser energy output is done most easily by varying the laser flashlamp energy. The flashlamp energy could be varied from 40 to 70 J per pulse giving a laser pulse energy of between 196 and 345 mJ per pulse (Laser lamp energies of 40, 50, 60 and 70 J gave the corresponding laser irradiance of 9.69×10^{10} , 1.21×10^{11} , 1.45×10^{11} , and 1.71×10^{11} W cm⁻²). The laser was operated for 5 s ablation periods. The result produced for Ti is illustrated in Figure 4.5. Results were found to be similar for Ti, Zn, Na and B.

Fig 4.5 Emission time profile for laser ablation of an aqueous multielement solution ($100 \mu\text{g ml}^{-1}$: Ti, Zn, Na and B) showing emission intensity as a function of laser lamp energy: 40, 50 and 60 J ($20 \mu\text{l}$ was ablated, using a Q switched laser operating for 5 s). Results are shown for titanium

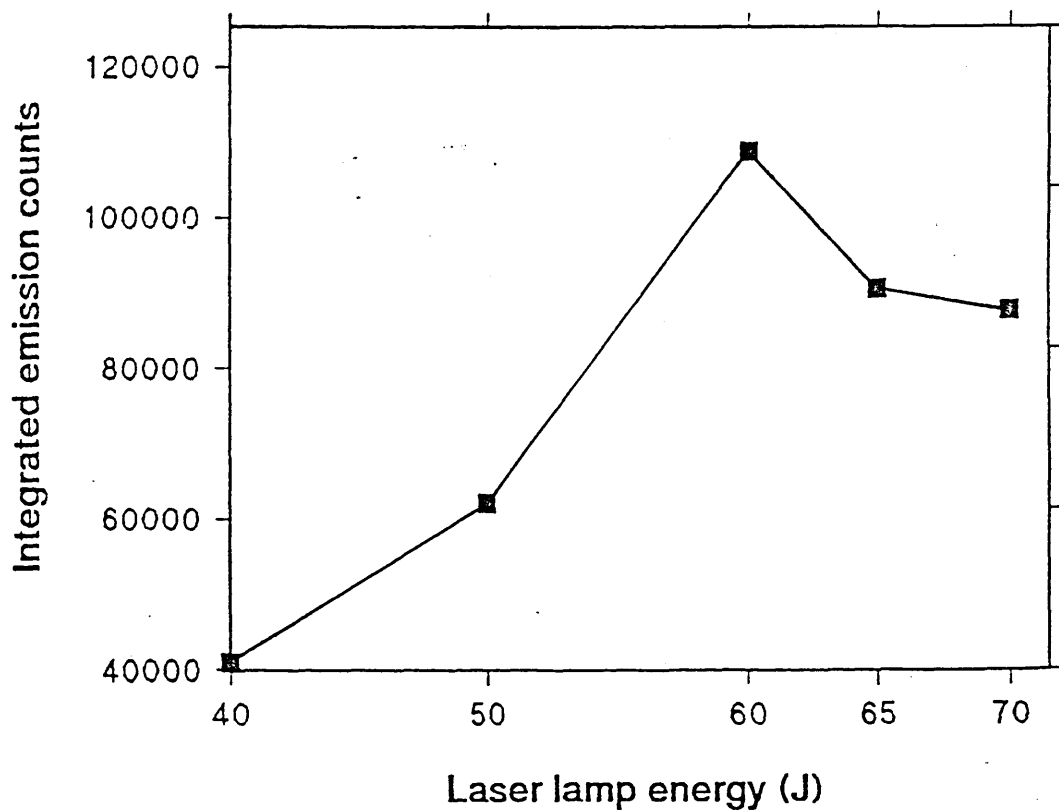


The emission time profiles for each of the elements for 40, 50 and 60 J laser lamp energies produced transient peaks. It was observed that increasing the laser lamp energy from 40 to 60 J, resulted in a decrease in base peak width from about 30 to 20 s, and a corresponding increase in the peak height for laser lamp energies of up to 60 J, suggesting that the liquid was ablated at a

ablation rate at higher laser energies. The increase in the ablation rate for higher laser energies was as a direct results of increased heating of the carbon cup resulting in a increased rate of sample vaporisation into the plasma. However, a decrease in the emission height was seen for a laser lamp energy of 70 J, due to a marked increase in sample spattering, which means that less of the sample was actually ablated. A visual check of the contents of the carbon cup showed that not all the sample had been ablated for laser energies of 40 and 50 J.

Figure 4.6 shows a graph of the raw counts based on the integration of the transient signal as a function of the laser lamp energy. As the results obtained for each of these elements are similar, only that of titanium is presented here. Each point represents the mean of the results from 5 samples.

Fig 4.6 Graphs showing the raw counts based on integration of the transient signal as a function of laser lamp energy: 40 to 70 J for laser ablation of an aqueous multielement solution containing $100 \mu\text{g g}^{-1}$ Ti, Zn, Na and B (20 μl was ablated using a Q switched laser for 5 s). Results are shown for titanium



The graphs for each of the elements studied show a linear increase in the integrated signal up to a maximum laser lamp energy of 60 J corresponding to a laser irradiance of $1.45 \times 10^{11} \text{ W cm}^{-2}$. These results indicate a direct correlation between laser lamp energy and the amount of analyte entering the plasma. For lamp energies of 65 and 70 J the signal was seen to decrease presumably to an increase in spattering and of liquid onto the ablation chamber this set an upper limit to the laser lamp energy which could be used. Laser ablation studies of glasses seen in **Section 3.5** showed a similar trend with a maximum signal seen for a laser lamp energy of 60 J. Again a similar correlation was found by Booth and McLeod (67) whereby increasing the laser lamp energy increased the signal height. However, no upper limit was seen, which may be due to the increased viscosity of liquid paint compared to an aqueous solution. Reduced of sample spattering is to be expected at high viscosities.

The marked increase in sample spattering at laser energies above 60 J may be as results of an increased generation of high pressure acoustic shock waves produced at higher laser energies which will results in the ejection of liquid from the container. This increase in spattering will reduce the amount of sample that can be vaporised and hence result in a smaller signal. Cremers and Radziemski (105) found that a laser incident on a liquid has a characteristically strong electric field which induces dielectric breakdown of the sample. This not only causes ablation of the liquid but generates high pressure acoustic waves, which results in spattering. Dielectric breakdown of pure water occurs with focussed laser powers of around 10^{10} to $10^{11} \text{ W cm}^{-2}$. However, this breakdown threshold is thought to be influenced by the presence of particles or dissolved material. From this information it is very probable that an increase in laser power density will increase not only the amount of sample ablated but at very high energies above 60 J will result in a marked increase in the production of high pressure acoustic shock waves causing a marked increase in sample spattering. Overall this experiment showed that the problem of sample spattering, set an upper limit on the laser energy that could be used.

The precision was calculated for each of the laser lamp energies used and the results produced as a table for the elements studied (Table 4.4). The use of lamp energies of greater than 60 J showed a marked decrease in sampling precision due to excessive sample spattering. For Ti the precision at was 5.8% RSD at 60 J, which increased to 21% RSD at 70 J. For Zn the precision increased from 7.2% RSD to 28% RSD.

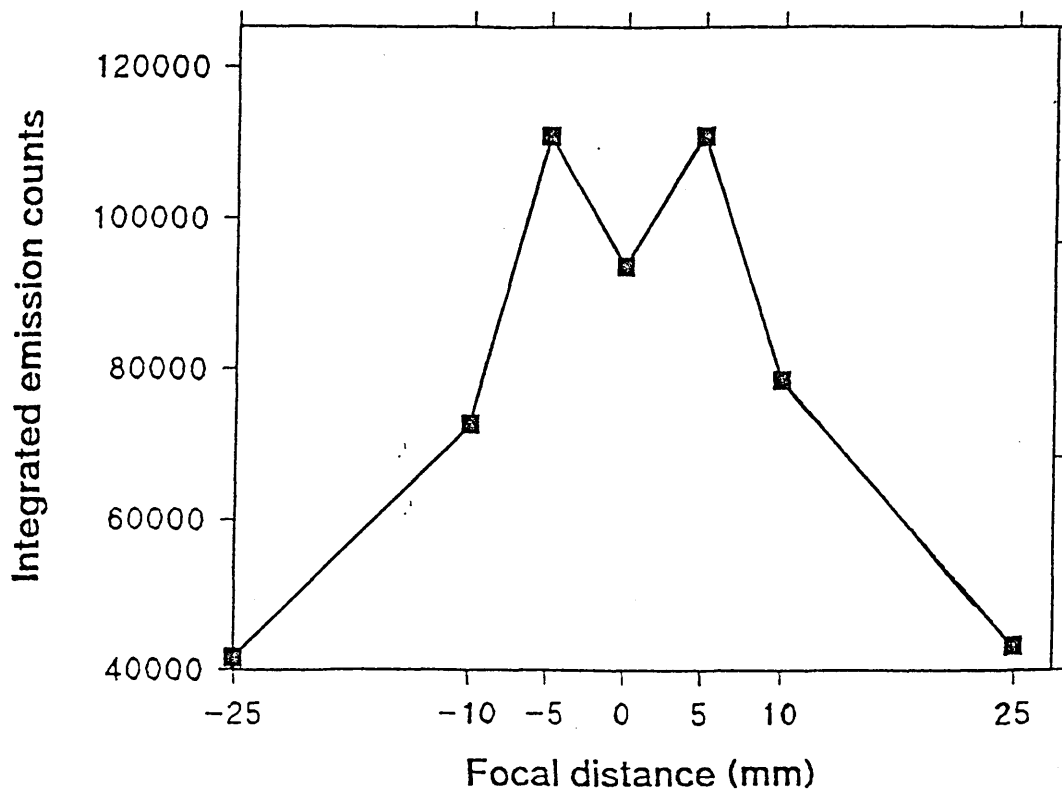
Table 4.4 Showing the level of precision (as the %RSD, n=5) as a function of the laser lamp energy (40 to 70 J) for the elements Ti, B, Zn and Na

| Element | Laser lamp energy / J | | | | |
|---------|-----------------------|-----|-----|------|------|
| | 40 | 50 | 60 | 65 | 70 |
| Ti | 6.0 | 6.1 | 5.8 | 12.5 | 21.0 |
| B | 7.2 | 5.9 | 5.8 | 10.9 | 20.0 |
| Zn | 7.0 | 6.9 | 7.2 | 9.0 | 19.7 |
| Na | 6.8 | 7.9 | 6.3 | 13.0 | 25.6 |

4.6 Effect of laser focusing

As well as altering the laser lamp energy, the incident laser energy on the sample can be altered by changing the laser focus. Changing the laser focus will alter the laser spot size on the sample surface and this in turn will alter the laser irradiance. Defocusing the laser increases the laser spot size incident on the sample and which decreases the irradiance. The analytical signal was studied as a function of laser focusing. This was achieved by moving the sample in the vertical direction between 25 mm above and below the focal point of the laser. This corresponded to a laser spot size of between $8.82 \times 10^{-5} \text{ cm}^2$ when the laser is focussed 25 mm above or below the focal point and $1.38 \times 10^{-3} \text{ cm}^2$ at the laser beam focal point. This gave a laser irradiance of between $2.36 \times 10^{10} \text{ W cm}^{-2}$ and $3.70 \times 10^{11} \text{ W cm}^{-2}$. A laser lamp energy of 60 J was used for a 5 s ablation period. The results are presented graphically in Figure 4.7.

Fig 4.7 Graph showing the raw counts based on the integration of the transient signal as a function of the laser focussing distance (25 mm above and below the sample surface for a 5 s ablation period using a laser lamp energy of 60 J). The results shown are for titanium



The results showed an increase in the emission signal from 25 mm above the sample surface to a maximum signal at 5.0 mm above the sample surface. A second maximum was seen at 5.0 mm below the sample surface. This increase in the signal is as a result of the increasing irradiation by the laser which results in increased heating of the carbon cup leading to more sample vaporisation. A direct correlation between the incident laser energy and the amount of analyte entering the plasma is observed.

The lowering of the signal at the focal point is as a result of the increase in the amount of sample spattering at higher sample irradiance. This increase in the degree of spattering was also seen as a lowering in the sampling precision. Table 4.5 shows the level of precision for different focussing distances of the laser beam. The results show a very poor level of precision at the focal point of the laser of over 19 %RSD for each element, which is also seen to improve dramatically when the laser is defocused. Defocusing the laser may help to improve sampling sensitivity and improve

precision by providing a wider beam profile, resulting in smoother heating of the sample, thereby reducing sample spattering and increasing the amount of analyte entering the plasma. Defocusing of the laser by 5 mm also increased sensitivity for laser ablation of glass samples seen in Section 3.4.

Table 4.5 Table showing the level of precision (as the %RSD, n=5) obtained as a function of the laser focussing distance (25 mm above and below the sample surface) for Ti, B, Zn and Na

| Element | Laser beam focussing distance / mm | | | | | | |
|---------|------------------------------------|-----|-----|----|-----|-----|-----|
| | -25 | -10 | -5 | 0 | 5 | 10 | 25 |
| Ti | 6.8 | 7.2 | 6.4 | 19 | 6.5 | 7.0 | 6.5 |
| B | 5.9 | 6.0 | 5.9 | 20 | 5.3 | 6.0 | 4.9 |
| Zn | 5.0 | 7.9 | 7.4 | 23 | 5.9 | 7.2 | 6.8 |
| Na | 6.7 | 7.1 | 6.3 | 28 | 6.1 | 6.3 | 7.0 |

These results show that for a 5 s ablation period a laser lamp energy of 60 J was required to ablate all the sample with the laser focussed 5.0 mm above the sample surface. As has been seen there is a direct correlation between the ablation time, laser lamp energy, degree of laser focus and the amount of analyte entering the plasma. Therefore, a change in the laser lamp energy and/or a change in laser focus would change the ablation time needed to ablate all of the 20 µl sample. However, laser lamp energies greater than 60 J result in excessive sample spattering. Increased sample spattering is also observed for by a focussed beam. Therefore, it is concluded that the optimum conditions for a 20 µl aqueous sample are a laser lamp energy of 60 J for an ablation period of 5 s with the laser focussed 5.0 mm above the sample surface. This corresponds to an irradiance of $1.45 \times 10^{11} \text{ W cm}^{-2}$ for a 5 s ablation period.

4.7 Effect of sample volume

The effect of sample volume on the reproducibility of the analytical signal was investigated. Three different sample volumes 1 ml, 40 μ l, and 20 μ l were used. The sample was held in one of two carbon cups. One had a maximum liquid volume of 1 ml and the other a maximum volume of 40 μ l. Both cups were manufactured for use in atomic absorption spectrometry, and so are made from highly pure pyrolytic carbon so as to avoid contamination. Four consecutive single shots were used for each of the sample volumes. The laser was fired every 20 s over a 100 s time period using a laser lamp energy of 60 J. The emission-time profiles for titanium are shown in **Figure 4.8** for each of the sample volumes.

From the emission-time studies for each of the sample volumes it is seen that the analytical signal is greatly reduced for the 1 ml volume compared to 20 and 40 μ l volumes. This may be due to the fact that vaporisation of the sample is through a thermal heating process where by the laser heats the carbon cup. For smaller volumes there will be sufficient heat available to vaporise the liquid. However, with larger volumes of liquid there will be insufficient heat from the heated carbon cup to vaporise the same amount of liquid.

A similar study was performed using a blank carbon cup in order to obtain information of the degree of element contamination found in the carbon after a 20 μ l aqueous solution had been previously ablated. This would show the degree of sample migration into the pores of the carbon and hence any memory effects that may result between samples. Emission time profiles produced showing 4 single laser shots of the carbon cups for titanium, are illustrated in **Figure 4.9** after a 20 μ l aqueous standard had been ablated for 5 s. The signals show that after the first shot the emission signal falls markedly. Hence memory effects due to contamination from migration of solution into the pores of the carbon can be reduced simply by ablating the carbon cup for 5 s between sampling. Laser cleaning was routinely performed between samples to prevent any such contamination.

Fig 4.8 Emission-time profiles showing four consecutive single shot laser shots for titanium, using three sample volumes 1 ml, 40 μ l, and 20 μ l of an aqueous multielement solution, containing: 100 μ g ml⁻¹ Ti, Zn, Na and B. A laser lamp energy of 60 J was used and the laser beam was defocused 5 mm above the sample surface

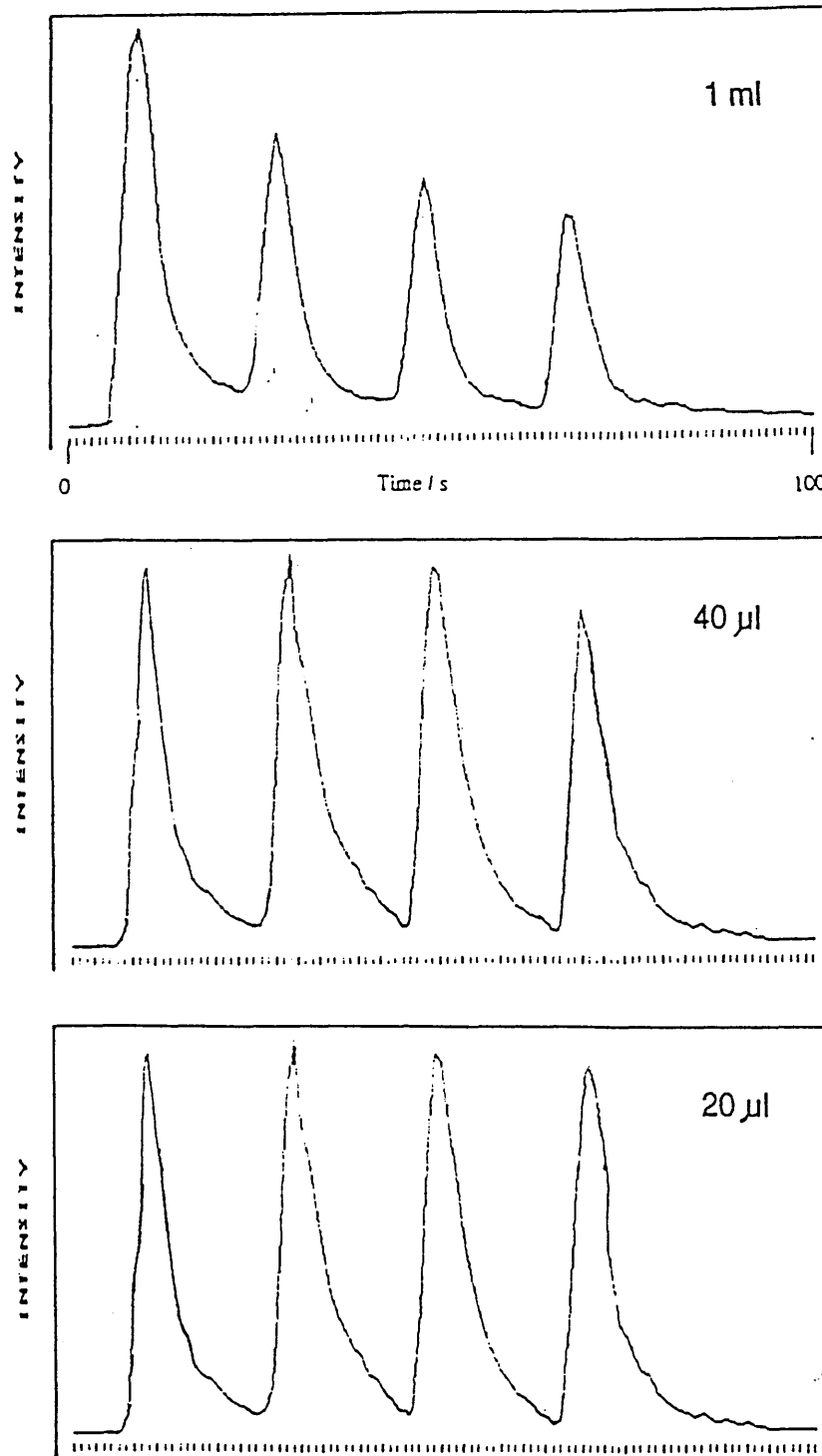
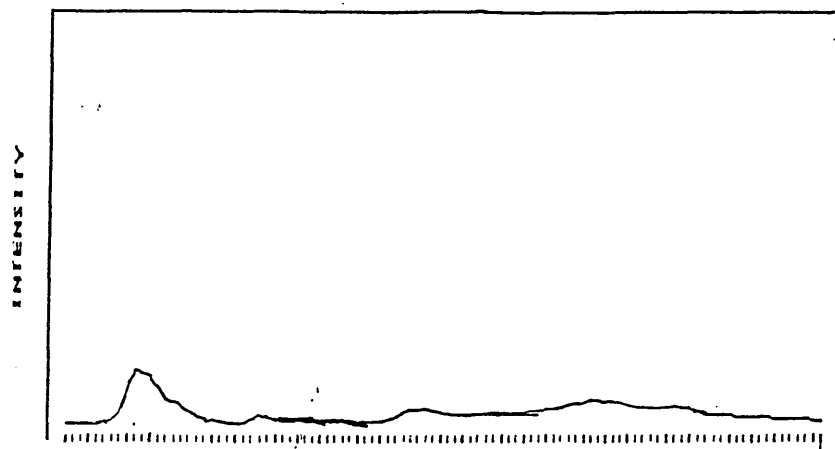


Fig 4.9 Emission time profiles for titanium showing four consecutive single shot laser shots for a carbon cup after a 20 μ l solution had been ablated for 5 s. A laser lamp energy of 60 J was used

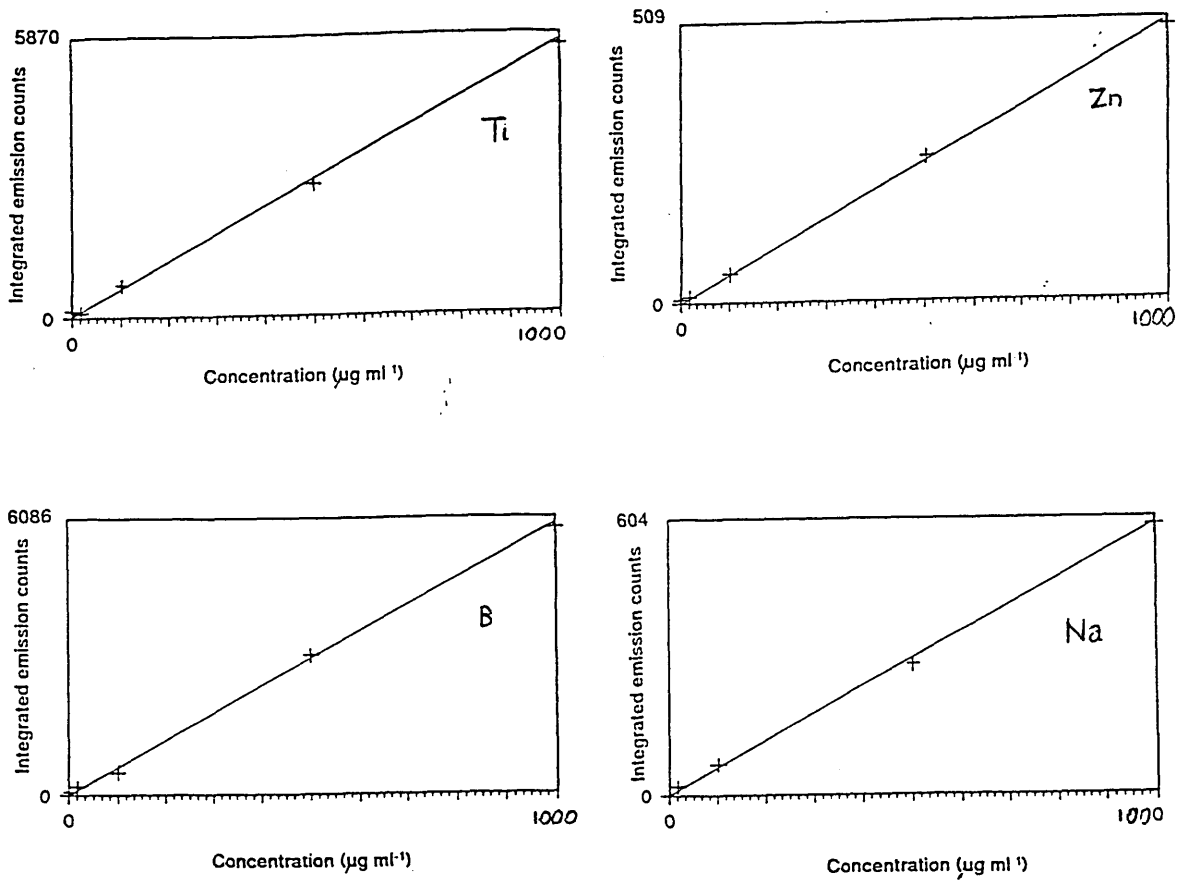


4.8 Calibration

Calibration curves were constructed in order to demonstrate analytical potential of microsampling aqueous solutions by laser ablation. Data was obtained for limits of detection, and the linear dynamic range. Multielement standard solutions were used containing the following elements Ti, B, Zn, Na and Co. The solutions used were made up by dilution of a 1000 $\mu\text{g ml}^{-1}$ multielement standard at the following concentrations 1000, 500, 100, 10, and 1.0 $\mu\text{g ml}^{-1}$. 20 μl samples were ablated for an ablation period of 5 s, using a laser lamp energy of 60 J. The laser was focussed 5.0 mm above the surface of the sample.

Raw counts based on the integration of the transient signal were obtained. For each sample a mean of 5 ablations were obtained. After calibration five blank aliquots containing distilled water were ablated to determine the limits of detection. The results are shown graphically in Figure 4.10 for the elements Ti, B, Zn and Na. The straight line is the least squares fitted line. The calibration curves are plots of concentration versus mean minus blank intensities. Analytical performance is given in Table 4.6.

Fig 4.10 Calibration graphs for Ti, Zn, B and Na over the concentration range 1.0-1000 $\mu\text{g ml}^{-1}$. 20 μl samples of aqueous standards were ablated using a laser lamp energy of 60 J for an ablation time of 5 s



The graphs produced show that for the elements Ti, B, and Zn linearity was exhibited up to $1000 \mu\text{g ml}^{-1}$. For the four elements studied the limits of detection (calculated as the concentration corresponding to three standard deviations of the blank ie 20 μl of Milli Q water) varied between 0.3 and $7.3 \mu\text{g ml}^{-1}$.

Table 4.6 Table of analytical performance for laser ablation of aqueous multielement solutions.

| Element | Equation of line | Limit of detection $/\mu\text{g g}^{-1}$ | Dynamic range $/\mu\text{g ml}^{-1}$ |
|---------|------------------|------------------------------------------|--------------------------------------|
| Ti | $y=582.5x+0$ | 0.3 | 1 to 1000 |
| B | $y=53.9x+0$ | 2 | 1 to 1000 |
| Zn | $y=500.9x+0$ | 0.5 | 1 to 1000 |
| Na | $y=30.0x+0$ | 7.3 | 1 to 1000 |

The limits of detection obtained are two to three orders of magnitude worse than those that can be obtained for pneumatic nebulisation and for ETV. Limits of detection reported by Gunn et al (4) for electrothermal vaporisation are at the sub ppb level.

4.9 Precision

The preliminary studies showed that relatively poor precision was obtained for laser sampling of aqueous multielement standards. The %RSD values were seen to average 9 % for the elements studied. As has previously been mentioned the relatively poor precision is most likely to be due to differences in the ablation yield due to sample spattering. A simple method for correcting these sampling fluctuation may be to use an internal standard, and in this case Co was used.

This experiment utilised a multielement solution containing Ti, B, Zn, Na, and Co at $100 \mu\text{g ml}^{-1}$. A 20 μl was placed into a carbon cup and ablated for 5 s, using a Q-switched mode pulsed laser beam with 60 J laser lamp energy. The emission time signal was integrated and results were produced as the raw counts based on the integration of the transient signal. The procedure was

repeated 10 times. The intensity data is presented in Table 4.7, with the resultant mean, standard deviation and %RSD values.

Table 4.7 Precision study data for laser ablation of aqueous solutions

| | Raw counts based on the integration of the transient signals | | | | |
|------|--------------------------------------------------------------|-----|-----|-----|-----|
| | Counts x 1000 | | | | |
| | Ti | B | Zn | Na | Co |
| 1 | 115 | 11 | 116 | 11 | 114 |
| 2 | 109 | 11 | 110 | 9 | 108 |
| 3 | 132 | 14 | 129 | 13 | 126 |
| 4 | 141 | 14 | 129 | 14 | 131 |
| 5 | 128 | 13 | 125 | 12 | 125 |
| 6 | 117 | 12 | 116 | 12 | 115 |
| 7 | 110 | 10 | 111 | 10 | 109 |
| 8 | 112 | 11 | 111 | 10 | 109 |
| 9 | 115 | 11 | 116 | 12 | 115 |
| 10 | 117 | 12 | 119 | 12 | 118 |
| Mean | 120 | 12 | 118 | 11 | 118 |
| SD | 11 | 1.3 | 7.2 | 1.1 | 7.8 |
| %RSD | 8.9 | 11 | 6.9 | 12 | 6.6 |

The precision compares favourably with that found by ETV for the microanalysis of aqueous samples. Gunn and Millard (23) described a graphite rod ETV used to assess the analytical performance of standard multielement solutions. The precision of the technique was based on measurement of Ag ($0.4 \mu\text{g ml}^{-1}$) and was found to be approximately 6 %RSD. Similar values were observed for other elements. However, the level of precision is higher than compared to pneumatic nebulisation where precisions of less than 1 % RSD are often obtained. High blank uncertainties also contributed to reduced limits of detection. It may be possible and desirable to choose a better blank method.

The precision data presented in **Table 4.7** gives a clear indication that the trends for each element are very similar. The implication is that the use of an internal standard may help to improve precision. Precision data were recalculated using the element to Co signal ratios (**shown in Table 4.8**). This showed substantial improvement in precision for all elements. For Ti the precision improved from 8.9 to 2.4 %RSD, for B from 10.6 to 4.1 %RSD, for Zn from 6.9 to 1.0 %RSD and for Na from 12.2 to 4.0 %RSD. This significant improvement for elements of different thermochemical properties supports the conclusion that precision is affected by variations in the amount of aqueous solution which is vaporised due to spattering of the sample.

Table 4.8 Precision study using Co as an internal standard

| | Raw counts based on the integration of the transient signal for each element divided by the raw counts based on the integration of the Co signal | | | |
|------|--------------------------------------------------------------------------------------------------------------------------------------------------|-------|------|-------|
| | Ti | B | Zn | Na |
| Mean | 1.02 | 0.103 | 1.01 | 0.105 |
| SD | 0.02 | 0.004 | 0.01 | 0.006 |
| %RSD | 2.4 | 4.1 | 1.0 | 4.0 |

5.1 Introduction

The spectrometric analysis of lubricating oils includes the determination of wear metals, contaminant and additive elements. Engine wear patterns are monitored by wear metal analysis which involves analysing large numbers of samples. Used oil contamination originating from dirt and leaks can be traced by contaminant element determination. Additive packages for lubricating oils consist of among other things anti-wear agents, antioxidants, dispersants, detergents and viscosity index improvers. Some of these additives include organometallic components. In industry oils are routinely analysed for Fe as wear metals, Ni and V as contaminants which are present in the oil from the original rock formations, and Ca, Na, Mg and Zn used as additives (133).

Inductively coupled plasma emission spectrometry offers a quick and highly sensitive determination of elements in oil samples and is used in the Kuwait analysis system (134). In many circumstances large numbers of samples have to be analysed in a short space of time, and Granchi et al (135) have described a system of analysis using robotics in conjunction with inductively coupled plasma emission spectrometry to meet this requirement.

The viscosity of oil is usually too high for direct conventional nebulisation, and dilution with kerosine is widely used. Other solvents used include metholated spirits and xylene. Kerosine proves to be the most practical solvent because of it's good solvent properties, low volatility and toxicity. Sample dilution is typically in the range $\times 5$ to $\times 10$.

Different oil samples may exhibit different viscosities which will result in differences in the sample uptake rate between the calibrant and the test oils, and internal standardisation with cobalt is usually employed.

Sample treatment includes acid digestion and dry ashing but the associated problems may include the loss of analytes. These methods are also time consuming and need skilled technicians.

Another problem is encountered in the use of pneumatic nebulisation when the analysis of wear metal particulates is required. Jansen et al (136) found that the average Fe particle size was less than 2.0 μm , with some as large as 25 μm . They report that ICP nebulisers generally accept particles up to 10 μm before blockages occur. Larger particles, therefore, were filtered prior to analysis, resulting in an overall loss of Fe.

In the work reported in this chapter all oils were of 20 μl volume and sampled using laser ablation. This leads to a number of possible advantages: (i) doing away with extensive sample pretreatment; (ii) reduction in sample volume; (iii) reduction in plasma instability seen for certain organic compounds when sampling by pneumatic nebulisation; (iv) elimination for the need to dilute the sample; (v) analysis that reflects the total element content (response independent of particle size); (vi) simplified calibration through the use of aqueous multielement standards; (vii) elimination of matrix effects associated with sample viscosity; (viii) the improvement in transport efficiency approaching that of electrothermal vaporisation and (ix) overcoming the problems associated with sampling of refractory compounds and volatile elements seen in ETV.

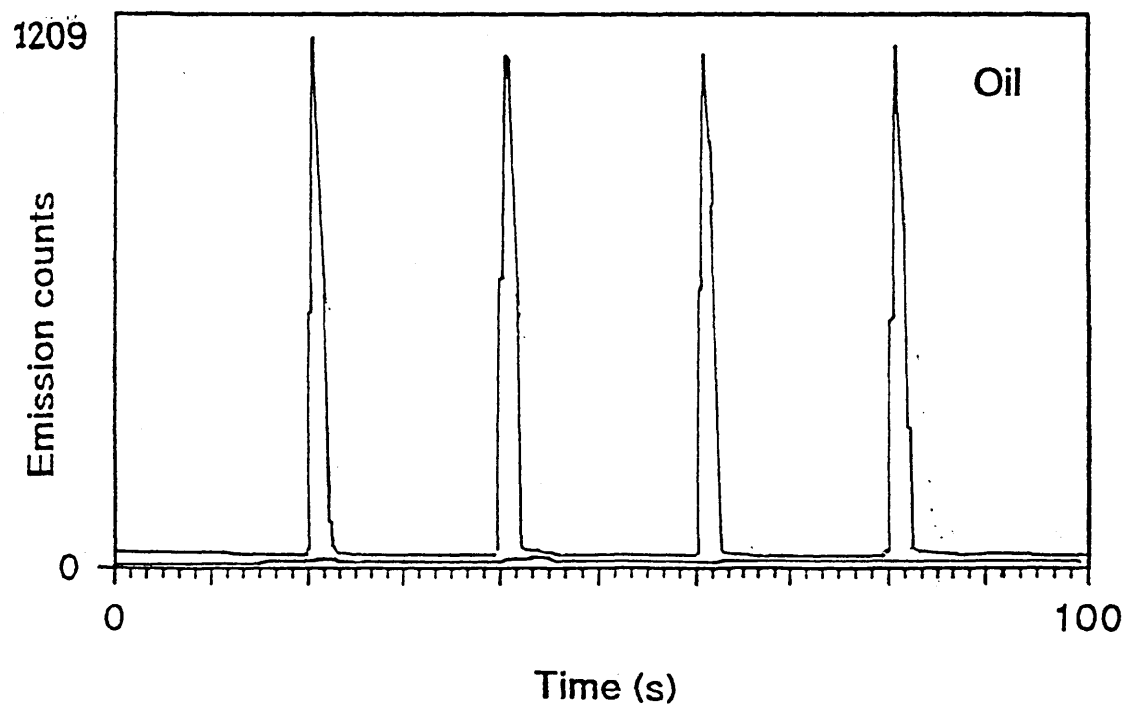
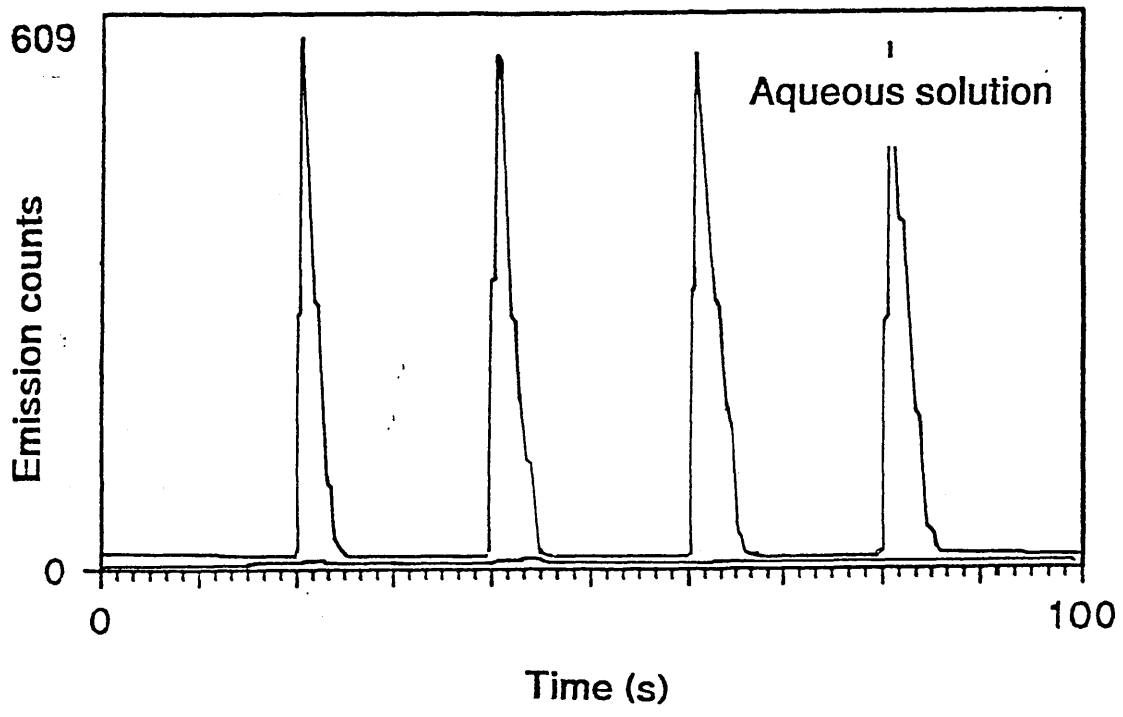
5.2 Preliminary experiments

Preliminary studies were performed to ascertain inductively coupled plasma optical emission for laser ablation of oils compared to laser ablation of synthetic aqueous multielement solutions. Two standards were used an aqueous multielement solution containing Zn, Fe, Mg and Ca at 100 $\mu\text{g ml}^{-1}$ and a multielement oil standard (Conostan S 21 100 $\mu\text{g g}^{-1}$). The procedure was as follows: 20 μl of sample were contained in a carbon cup with a maximum volume of 40 μl . A pulsed laser beam operating at 10 Hz was focused 5 mm above the surface of the liquid and fired using a laser lamp energy of 60 J, for each of four consecutive single shots. Emission time profiles are shown in Figure 5.1 for zinc for the aqueous multielement standard and the oil standard.

The results show that transient signals are obtained for each of the four laser shots for both the oil and aqueous solutions. The transient signals for oil have a base line width which is half that for the aqueous standards (3 s for oil and 6 s for the aqueous solution) and a signal height approximately twice as great. Similar trends were seen for the other elements studied. The difference in the transient signals between oils and aqueous standards may be attributed to an increased ablation rate of oils compared to aqueous solutions which may be accounted for by a lower boiling point, lower heat capacity and heat of vaporisation of oils, compared to aqueous solutions.

A visual check made on the oil sample after laser ablation showed that some liquid still remained after 4 single shots. In order to improve sensitivity (as seen in **Chapter 4**) an increased ablation period is needed to remove all the oil. As with laser ablation of aqueous solutions sample spattering on the ablation chamber walls was observed. However, it was noted that the degree of spattering was less than that for aqueous ablation, which accounted for improved precision for laser ablation of oils compared to aqueous solutions (typically 5.5 %RSD for oils compared to 9.8 %RSD for the aqueous solution for Zn). The reduction in spattering may be due to greater viscosity of the oil compared to aqueous solutions.

Fig 3.1 Emission time profiles for laser ablation of an aqueous multielement solution ($100 \mu\text{g ml}^{-1}$: Zn, Fe, Mg and Ca) and a multielement oil standard (Conostan S 21 $100 \mu\text{g g}^{-1}$). 20 μl samples were subjected to 4 single laser shots using a Q switched laser at 60 J laser lamp energy. The results shown are for zinc



As has been stated in **Chapter 4** the main mechanism by which analytes in aqueous solutions are ablated is by thermal vaporisation due to laser heating of the carbon cup with little interaction of laser radiation with the aqueous solution. However, it is likely that there is more direct interaction of laser radiation with oil resulting in increased heating and vaporisation. Some atomisation of the sample may occur due to interaction with the laser induced plasma in the region above the liquid surface.

5.3 Effect of laser ablation time

The laser was operated for time periods of between 1 and 5 s. 20 μl samples of the multielement oil standard were ablated using a laser lamp energy of 60 J. Emission time profiles for 1, 3, and 5 s ablation times were overlayed. The results produced for zinc are shown in **Figure 5.2**. Results were similar for Fe, Mg and Ca.

The emission time profiles for each of the elements for 1, 3 and 5 s ablation periods produced transient signals, similar to those produced for laser ablated aqueous solutions. It is seen that increasing the ablation time from 1 to 3 s resulted in an increase in the base peak width from about 10 to 20 s. This is due to an increase in the total quantity of sample ablated for longer ablation times and is similar to what happened with ablated aqueous sample. For ablation times over 3 s no further increase in the peak width is observed, suggesting that all the oil had been ablated (this compares with a 5 s ablation period which was needed for the aqueous samples for 20 μl of sample).

Graphs of the raw counts based on the integration of the transient signal as a function of ablation time, are shown in **Figure 5.3**. The integration period was started at the time of laser firing. The total integration time was 20 s and each data point used for the graph is a mean of 5 samples. The levels of precision are given in **Table 5.1**. As the results obtained with each of these elements are similar, only those of Zn are presented here.

Fig 5.2 Emission time profiles for laser ablation of a mineral oil standard (Conostan S 21 $100 \mu\text{g ml}^{-1}$) showing the emission intensity as a function of laser ablation time 1, 3 and 5 s ($20 \mu\text{l}$ was ablated, using a Q switched laser at 60 J laser lamp energy). Results are shown for zinc

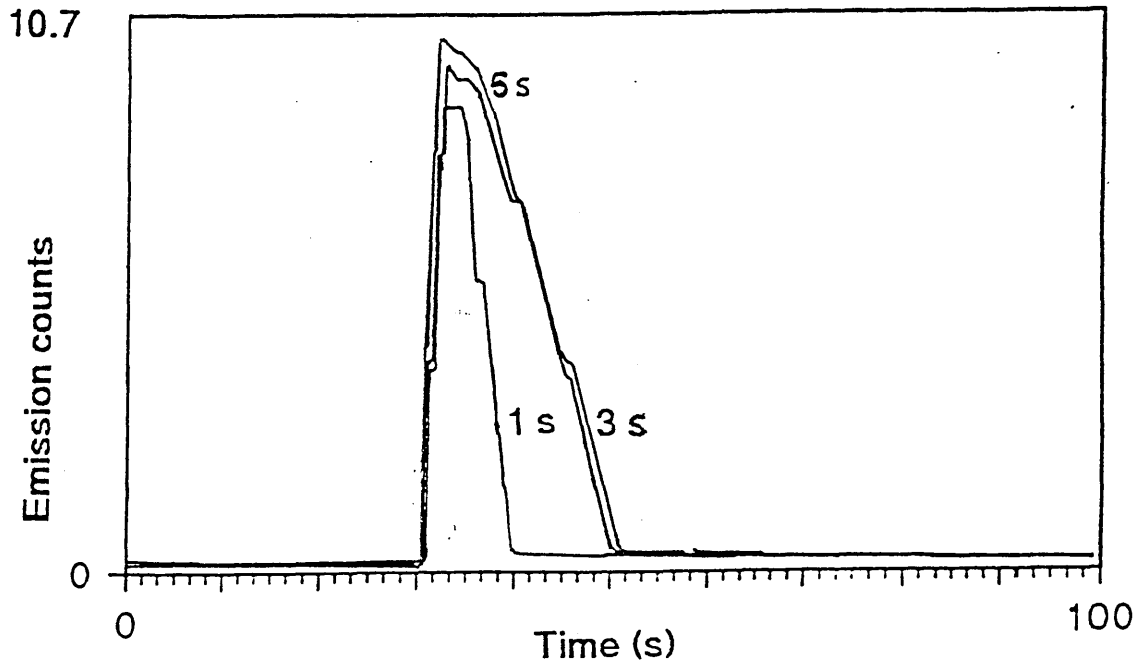


Fig 5.3 Graphs showing the raw counts based on integration of the transient signal as a function of ablation time: 1 to 5 s for laser ablation of a mineral oil standard (Conostan S 21 $100 \mu\text{g ml}^{-1}$). $20 \mu\text{l}$ was ablated using a Q switched laser operating at 60 J. Results are shown for zinc

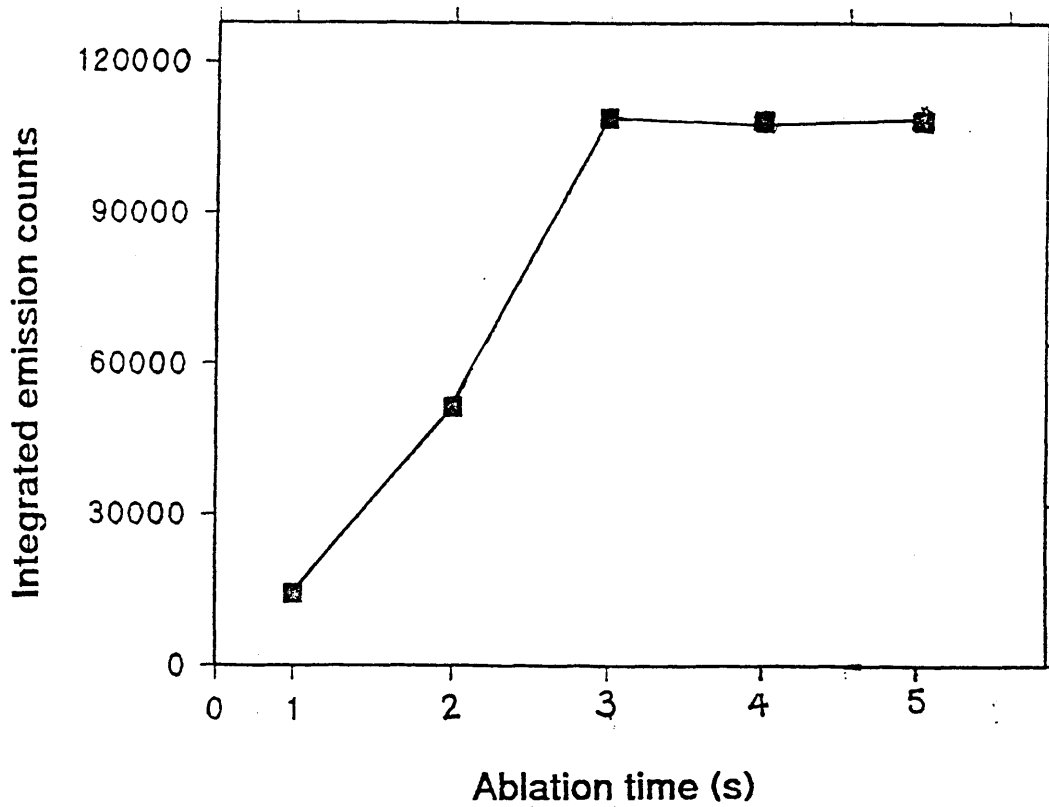


Table 5.1 Table showing the level of precision (as the %RSD n=5) for raw counts based on the integration of the transient signals obtained as a function of the laser ablation time (1 to 5 s) for Zn, Fe, Mg and Ca

| Element | Ablation time / s | | | | |
|---------|-------------------|-----|-----|-----|-----|
| | 1 | 2 | 3 | 4 | 5 |
| Zn | 7.3 | 5.9 | 3.5 | 3.6 | 3.4 |
| Fe | 6.9 | 6.2 | 3.8 | 3.3 | 3.8 |
| Mg | 6.0 | 6.4 | 3.6 | 3.2 | 3.5 |
| Ca | 6.5 | 6.5 | 3.0 | 2.9 | 3.0 |

The graphical data shown in **Figure 5.3** indicates a direct correlation between duration of laser operation and the amount of analyte entering the plasma up to a maximum duration of 3 s with no further increase beyond 3 s. For ablation times of 1 and 2 s an average precision of about 6.5 %RSD is seen. For an ablation time of 3 s and beyond the average precision is about 3.4 %RSD. A similar trend emerged for ablated aqueous samples where a dramatic improvement in precision occurred for ablation times of 5 s and beyond. This improvement in precision is due to all the oil being ablated for ablation times of 3 s and beyond.

From these results it is concluded that for a 20 μl oil sample ablated with a laser lamp energy of 60 J, a 3 s ablation period gave maximum sensitivity and precision.

5.4 Calibration

Calibration curves were constructed for laser ablation of oil standard (conostan S-21). Fe, Zn, Mg, and Ca were studied at the following concentrations; 1.0, 10, 50, and 100 $\mu\text{g ml}^{-1}$, with xylene used as the diluent and the blank. 20 μl of sample was ablated for an ablation period of 5 s using a laser lamp energy of 60 J. The laser was focussed 5.0 mm above the surface of the sample.

Raw counts based on the integration of the transient signals were obtained. For each concentration a mean of 5 ablations was obtained. The calibration curves are shown in

Figure 5.4 for Fe, Zn, Mg and Ca. The straight lines are the least squares fits. The calibration curves are plots of concentration versus the mean minus the blank intensities. The calibration graphs show that for Fe, Zn, Mg and Ca linearity up to $100 \mu\text{g g}^{-1}$ is obtained.

The limits of detection are calculated for four elements and are given in Table 5.2. For comparison corresponding data reported by Anderson et al (137) for conventional inductively coupled plasma emission spectrometry, is also given.

Fig 5.4 Calibration graphs for Fe, Zn, Mg and Ca over the concentration range 1.0 to $100 \mu\text{g g}^{-1}$, by laser ablation of oil, 20 μl samples were ablated using a laser lamp energy of 60 J for an ablation time of 5 s

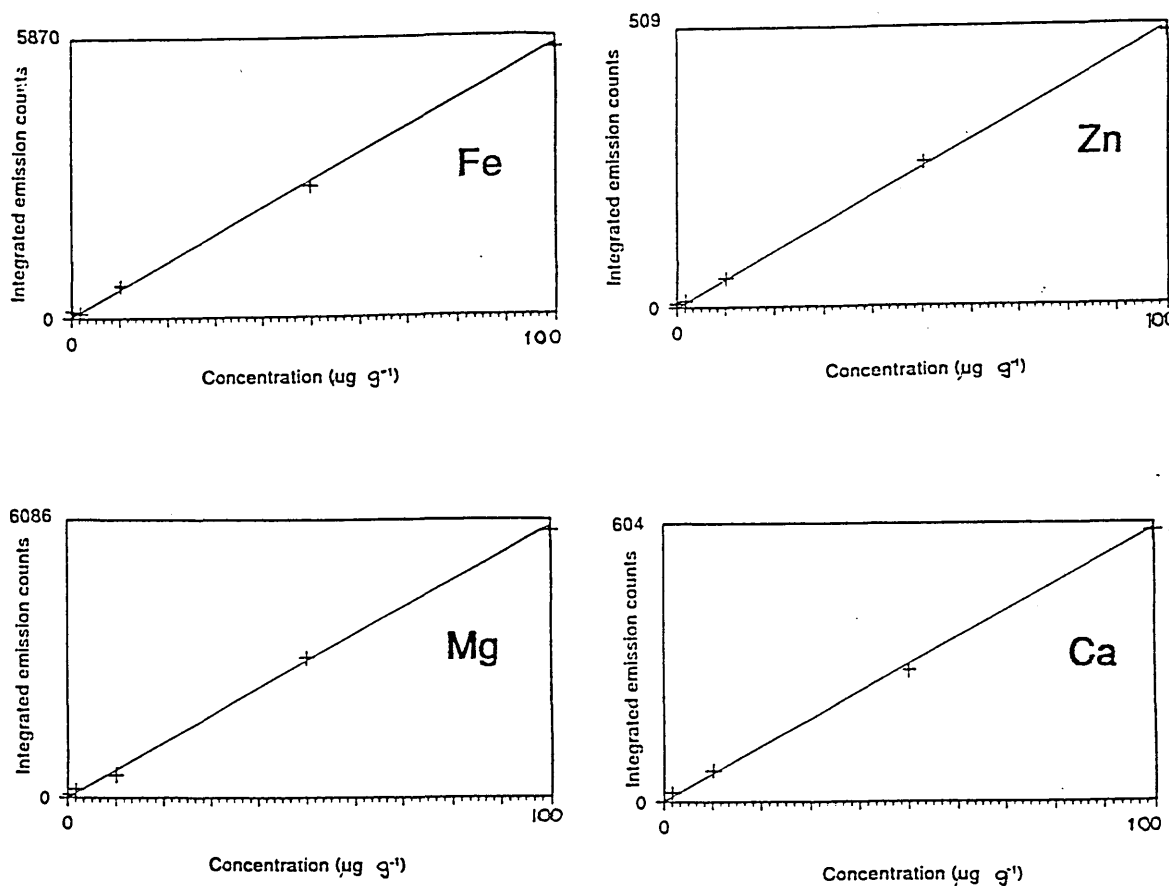


Table 5.2 Table of analytical performance for laser ablation of oils

| Element | Equation of line | Limit of detection / $\mu\text{g ml}^{-1}$ by LA | Limits of detection / $\mu\text{g ml}^{-1}$ by ICP (undiluted sample) for oils (150) |
|---------|------------------|--------------------------------------------------|--------------------------------------------------------------------------------------|
| Fe | $y=1199.2x + 0$ | 0.1 | 0.004 |
| Zn | $y=1281.5x + 0$ | 0.3 | 0.004 |
| Mg | $y=426.1x + 0$ | 0.3 | 0.0002 |
| Ca | $y=624.8x + 0$ | 0.05 | 0.0002 |

The data show that limits of detection range between 0.05 and 0.4 $\mu\text{g g}^{-1}$, and are far inferior to those obtained by conventional ICP analysis.

5.5 Precision

The precision was determined using a multielement oil standard (Conostan S 21) at a concentration of $100 \mu\text{g ml}^{-1}$. $20 \mu\text{l}$ was placed into a carbon cup and ablated for 5 s using a Q switched laser operating at 60 J. The resulting transient signals were integrated and the results produced as raw counts based on the integration of the transient signals. The procedure was repeated 10 times, and the data together with the calculated mean standard deviation and %RSD is presented in **Table 5.3**.

Table 5.3 Precision data for laser ablation of an oil standard (Conostan S 21)

| | Raw counts based on the integration of the transient signals Counts X 1000 | | | | |
|------|-------------------------------------------------------------------------------|-----|-----|-----|-----|
| | Zn | Fe | Mg | Ca | Co |
| 1 | 114 | 346 | 123 | 113 | 114 |
| 2 | 118 | 372 | 132 | 118 | 118 |
| 3 | 108 | 356 | 122 | 112 | 117 |
| 4 | 112 | 362 | 119 | 115 | 109 |
| 5 | 114 | 372 | 123 | 122 | 107 |
| 6 | 115 | 389 | 134 | 114 | 109 |
| 7 | 117 | 365 | 128 | 109 | 112 |
| 8 | 103 | 380 | 123 | 117 | 116 |
| 9 | 106 | 364 | 119 | 118 | 109 |
| 10 | 119 | 368 | 128 | 113 | 111 |
| Mean | 114 | 367 | 125 | 115 | 112 |
| SD | 3.9 | 12 | 4.6 | 3.7 | 3.9 |
| %RSD | 3.4 | 3.3 | 3.7 | 3.2 | 3.4 |

For all elements the precision compares favourably with that found using conventional pneumatic nebulisation. Jansen et al (136) reported a precision of 5 %RSD for additive elements in fresh oils and a 10 %RSD for wear metals in used oils.

Cobalt was used as an internal standard, at a concentration of $10 \mu\text{g g}^{-1}$. The results are shown in Table 5.4. However, unlike the results obtained for aqueous solutions there is little or no improvement in precision using the internal standardisation method for oils. This is not surprising since aqueous solutions exhibit a greater degree of spattering compared to oils.

Table 5.4 Precision study data using cobalt as an internal standard

| | Raw counts based on the integration of the transient signal for each element divided by the raw counts based on the integration of the Co signal | | | |
|------|--------------------------------------------------------------------------------------------------------------------------------------------------|-------|--------|--------|
| | Zn | Fe | Mg | Ca |
| Mean | 1.02 | 3.28 | 1.12 | 1.03 |
| SD | 0.0357 | 0.112 | 0.0392 | 0.0330 |
| %RSD | 3.5 | 3.4 | 3.5 | 3.2 |

5.6 Analysis of oils

Analysis of oils were performed using the Conostan S-21 oil standard for calibration at the following trace metal concentrations 1.0, 10, 50 and 100 $\mu\text{g g}^{-1}$. In order to compensate for differences in oil viscosity between the calibrant and the samples, Co at 10 $\mu\text{g g}^{-1}$ was added to the calibrant as well as the samples. Results were obtained for two fresh certified lubricating oils and an oil containing wear metal particulates ranging from 1 to 20 μm . 20 μl samples were ablated using a laser lamp energy of 60 J for 5 s ablation time and the integrated emission intensities were related to the calibration data for the Conostan S 21 oil standard by the linear equations for the calibration curves in **Section 5.4**.

The commercial lubricating oils were also analysed by ICP spectrometry using pneumatic nebulisation. This was achieved by dilution of the sample (1 in 10) with xylene and aspiration of the sample into the plasma. In this case the Conostan S-21 oil at 100 $\mu\text{g g}^{-1}$ was used as a calibrant. Cobalt at 10 $\mu\text{g g}^{-1}$ was also used as an internal standard. Results for analysis for laser ablation and ICP spectrometry using pneumatic nebulisation are given in **Table 5.5**.

Table 5.5 Analysis of certified lubricating oil

Oil sample No 1

| Element | Certified concentration $/\mu\text{g g}^{-1}$ | Found concentration by conventional ICP analysis $/\mu\text{g g}^{-1}$ | Found concentration by laser ablation $/\mu\text{g g}^{-1}$ |
|---------|--------------------------------------------------|---------------------------------------------------------------------------------|-------------------------------------------------------------------|
| Zn | 131 | 105 (-20 %) | 121 (-8 %) |
| Fe | 82 | 56 (-32 %) | 77 (-6 %) |
| Mg | 106 | 85 (-20 %) | 104 (-2 %) |
| Ca | (3.5 %w/w) | ---- | ---- |
| Ni | 142 | 116 (-18 %) | 148 (+4 %) |
| V | 52 | 36 (-30 %) | 53 (+2 %) |
| Na | 326 | 261 (-20 %) | 336 (+3 %) |

Figures in parenthesis are the % agreement between certified and found values

Table 5.5 Analysis of certified lubricating oil - continued

Oil sample No 2

| Element | Certified concentration $\mu\text{g g}^{-1}$ | Found concentration by conventional ICP analysis $\mu\text{g g}^{-1}$ | Found concentration by laser ablation $\mu\text{g g}^{-1}$ |
|---------|-------------------------------------------------|--------------------------------------------------------------------------|---------------------------------------------------------------|
| Zn | 32 | 24 (-25 %) | 33 (+2 %) |
| Fe | 151 | 121 (-20 %) | 139 (-8 %) |
| Mg | 89 | 73 (-18 %) | 84 (-6 %) |
| Ca | (3.4 % w/w) | ---- | ---- |
| Ni | 223 | 174 (-22 %) | 236 (+6 %) |
| V | 45 | 34 (-25 %) | 41 (-5 %) |
| Na | 208 | 141 (-32 %) | 216 (+4 %) |

Wear particulates in oil

| Element | Certified concentration $\mu\text{g g}^{-1}$ | Found concentration by conventional ICP analysis $\mu\text{g g}^{-1}$ | Found concentration by laser ablation $\mu\text{g g}^{-1}$ |
|---------|-------------------------------------------------|--------------------------------------------------------------------------|---------------------------------------------------------------|
| Fe | 250 | 100 (-60 %) | 260 (+4 %) |
| Ag | 3.50 | 1.58 (-55 %) | 3.22 (-8 %) |
| Al | 1.61 | 0.67 (-58 %) | 1.55 (-4 %) |
| Cu | 271 | 124 (-54 %) | 250 (-8 %) |
| Mg | 25.3 | 11.1 (-56 %) | 26.1 (+3 %) |

Figures in parenthesis are the % agreement between certified and found values

The results of the analysis of certified lubricating oil samples the results were close to the certified values and are typically within the range +6% and -8%. Overall there is better agreement for laser ablation than for conventional ICP analysis where results are typically within the range -18% and -32 %. Inaccuracies in the analysis of oil by conventional aspiration of relatively large amounts of liquid will be due to differences in the viscosity between the sample and the calibrant. Even with a five fold dilution aspiration of oil by pneumatic nebulisation proved difficult as blockages occurred in the nebuliser tip and carbon deposits formed on the torch sample injection tube. Such blockages on the sample injection tube are not seen when laser ablation is used, due to the small volume of oil sampled (20 μl). Other reasons for lack of accuracy by pneumatic nebulisation when

aspirating large amounts of sample (approximately 5 ml for a single analysis) may be due to interferences such as background shift and spectral overlap. Most samples of oil contain large amounts of Ca, (up to 3.5 % m/m) which could not be measured in this case without further dilution of the samples.

With laser ablation it was also possible to successfully carry out analysis on wear metal particles in oil samples, results which are difficult to obtain with aspiration as blockages in the nebuliser tip would readily occur. Poor accuracies are obtained for pneumatic nebulisation of such samples (typically between -60 and -54% of the certified value)). Results for laser ablation, however, show good accuracies typically between +4% and -8% of the certified value. This shows that ablation and successful transfer into the plasma of all the particulate matter is occurring

6.1 Introduction

Coatings are widely used in industry to give corrosion resistance and resistance to wear for metals. For example, metallic coatings such as Zr, Cr, and Ni are applied to steel to provide corrosion resistance for various products such as car bodies, tools, and containers. Titanium nitride and Zirconium nitride coatings produced by various sputtering techniques such as arc bond sputtering (ABS) (138, 139), are applied frequently to drill bits, knife blades, scissors and other tools, in order to improve wear resistance. Coatings such as gold are also frequently used in jewellery and electronic components for aesthetic purposes and to improve electrical conductivity. Metallic coatings are also applied to glass surfaces in order to exchange their optical properties. For example tin oxide is applied to glass as a heat reflecting material for double glazed windows.

Numerous instrumental techniques have been utilised to determine the composition of these coatings. The technique used is dependent on the quality of the information required. Techniques such as ESCA, SIMS, Auger and X-ray photoelectron spectrometry are capable of providing information on the atomic scale (140, 141). Thicker coatings such as those described above are usually determined by X-ray spectroscopy (142), mechanically by ball etching techniques (143), and by glow discharge optical emission (144, 145) and mass spectroscopy (146, 147).

This study considers the feasibility of using the laser ablation inductively coupled plasma emission spectroscopy technique for the analytical determination of various metallic coatings on steel and glass substrates. Probing the sample using a laser provides a route for the determination of lateral and depth distributions of elements in a solid sample. Depth gradients can be profiled by comparing the surface and bulk constituents. Sampling depth resolution is on the order of 1 to 10 μm (148) per laser pulse, although laser ablation ICP emission spectrometry cannot provide the depth resolution that can be routinely achieved by other surface analysis techniques such as ESCA, secondary ion mass spectrometry (SIMS), and Auger spectroscopy (149, 150). Most depth gradients are in the micrometer region and can be easily determined using laser ablation inductively coupled plasma emission spectrometry. A major advantage of laser ablation over the

other surface analysis techniques is the speed of analysis as no sample preparation is needed. Because the sample is held under atmospheric pressure no vacuum is needed which reduces sample turnover time. Another advantage is that the technique uses photons rather than electrons or charged particles, which means that non conducting samples can be analysed. Potential advantages relative to glow discharge techniques include small crater size (typically 10-500 μm using a laser compared to 5 mm for glow discharge) and a more rapid analysis time (approximately 180 s compared to 15 minutes).

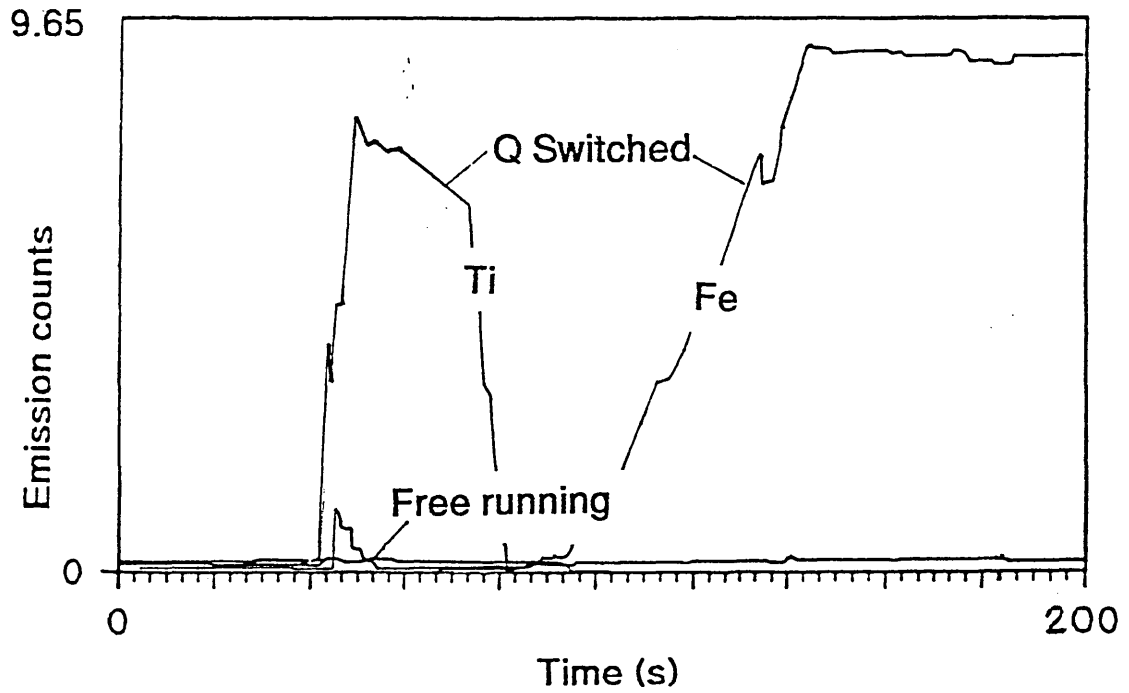
In this work laser ablation was applied as a tool for depth profiling of Ti, Zr, Sn, an ultra thin Cr coating on a steel substrate and also a tin oxide coating on a glass substrate. Parameters such as the magnitude of laser energy and the pulse repetition rate markedly influence the depth resolution for the analysis of multilayered materials. Therefore, systematic experiments were used to investigate and optimise key laser operating parameters such as laser energy and the pulse repetition rate for each sample type. Results were produced as emission time profiles for each of the coated samples for each laser operating parameter (laser pulse repetition rates of 1, 2, 5, and 10 Hz were studied for each of the following laser lamp energies; 45, 50, 60, and 70 J). It was assumed that the a transient signal would be produced by laser ablation of the coating material and that the shape of the peak would vary according to not only the type and depth of the coating material but also to the laser operating parameters used. Once optimised laser operating parameters were found it was proposed to investigate whether the width at half the maximum peak height of the transient signal was proportional to the coating depth using the same laser operating conditions. In this way it was proposed to perform quantitative depth analysis for multiple layers. Such data will be presented here.

6.2 Preliminary experiments

Preliminary experiments with laser ablation of titanium nitride coated steel samples show that distinct signals for the coating material and the Fe substrate were obtained when using the Q switched mode of laser operation. Results for the free running mode of operation yielded

smaller signal intensities and there was no distinction between the signal produced for the coating and the substrate materials. The Q-switched mode of operation was chosen for all subsequent experiments. Figure 6.1 shows an emission time profile for a 3 μm TiN coated sample, for both modes of laser operation (using a 10 Hz laser at 60 J) for Ti and Fe.

Fig 6.1 Emission time profiles for laser ablation of a TiN (3 μm) coated steel sample showing the signals for Ti and Fe as a function of the two modes of laser operation (Q-switched and free running). The laser was operated at 10 Hz repetition rate using a laser lamp energy of 60 J. For a single site



The two pulse modes offered by the NdYAG laser can lead to significantly different analytical outcomes. The physical characteristics of the sample crater of Q-switched and free running modes of laser operation are significantly different. Consequently, the two modes can be used to achieve different sampling objectives. Both modes can be executed as a single pulse or a series of pulses. A single pulse will produce a transient signal. On the other hand, multiple pulsing can be used to produce a steady state signal analogous to that obtained by solution aspiration. The pulse mode and the repetition rate both effect not only the intensity and duration of the analytical signal, but also the size and shape of the sample crater. Q switched laser pulses produce wide shallow craters, whereas free running pulses produce narrow deep craters. The production of deep narrow craters produced by free running laser action may account for the lack of sampling resolution for depth analysis of these samples.

Results for bulk sampling of glasses show that the analytical signal produced for Q-switched mode of operation is more intense than that for free running. This may be due to the fact that sample material ablated by Q-switching is more amenable to transport in a gaseous stream than that produced by free running. The dominant process during ablation in the free running mode is melting. Relatively large amounts of sample are ejected from the area of laser sample interaction but little of this material is transported to the plasma. Deep craters are produced but this results in relatively small emission signals. Q switching on the other hand vaporises the sample, and relatively small amounts are removed. However, a greater portion of the ablated particles are carried into the plasma, resulting in relatively large emission signals. This would account for the reduction in the emission signal shown for the free running mode of laser operation compared to that seen for Q switching. The results show that Q switching is more relevant to layer by layer removal for depth profiling.

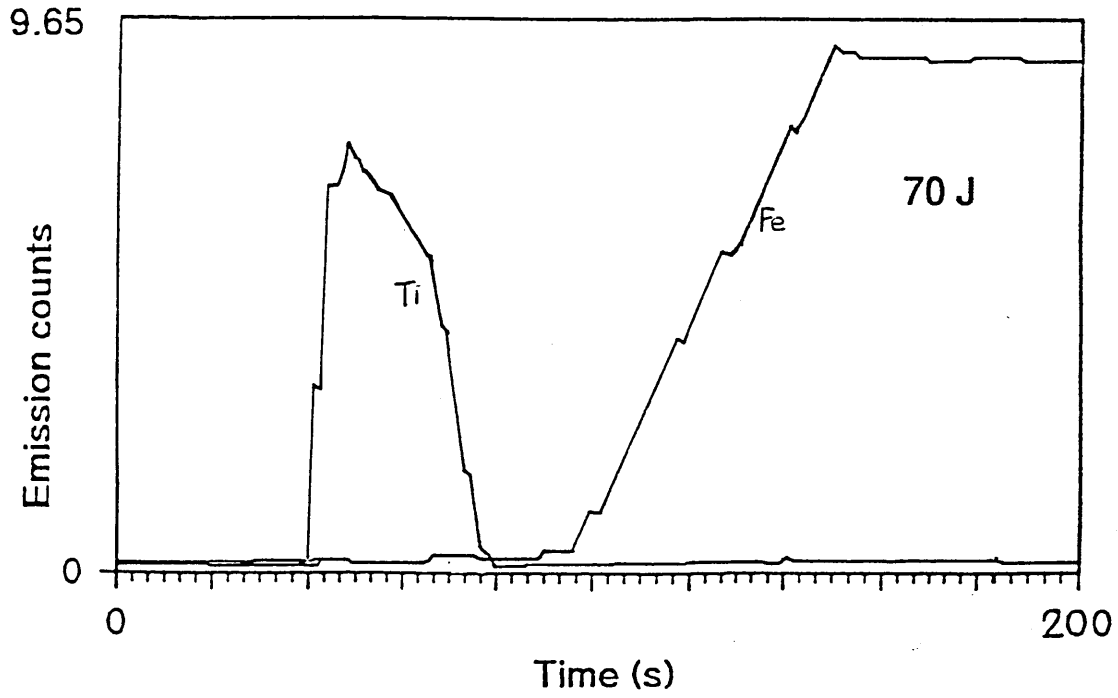
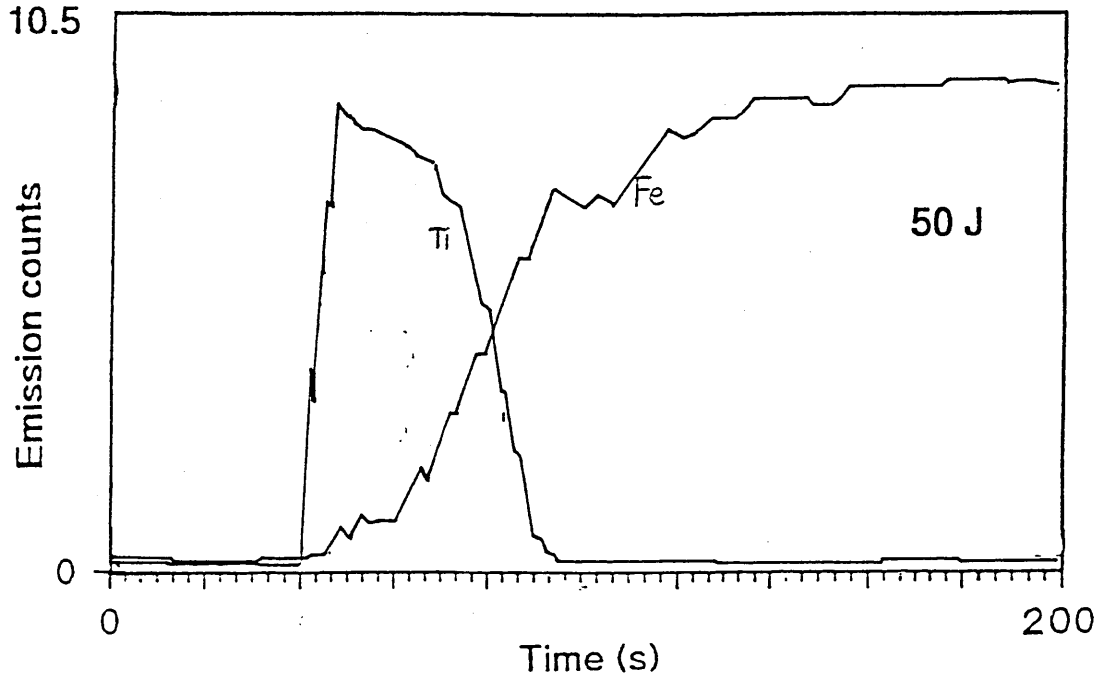
These initial emission time studies produced two distinct signals, the first being a transient signal resulting from ablation of the coating material in this case Ti, followed by a continuous steady state signal due to ablation of the Fe substrate material. The absence of Fe during the initial stages of ablation indicates that the surface of the coating did not contain Fe, either as a

contaminant of the TiN coating or from diffusion of Fe from the substrate, and that the laser did not penetrate through the coating into the steel substrate in the first 40 s of ablation. The second steady state signal for Fe showed that ablation of the steel substrate was achieved. In addition, no signal for Ti was seen during the ablation of the substrate which indicates that the coating had been removed.

Systematic studies were undertaken to investigate the effect of different laser operating conditions in order to give insight into the ablation processes and to obtain operating conditions most suitable for depth profile measurements. Results for the titanium nitride steel coated sample (3 μm) were produced as emission time profiles using different laser operating conditions at 50 and 70 J laser lamp energy for a pulse repetition rate of 10 Hz are illustrated in **Figure 6.2**. Incidentally no signals were seen for laser energies of 45 J. The signal for the coating element are shown overlaid with the signal for the Fe substrate.

Signal characteristics vary with laser energy. The emission signal intensity increased slightly from 9,500 at 50 J to 11,000 at 70 J for titanium, and the emission intensity also increased correspondingly for Fe, from 14,550 to 16,780. The transition between the two signals was also seen to be more distinct at higher laser energies. The most interesting thing to note is that the width of the transient peak due to titanium decreases from 46 to 32 s as the laser lamp energy is increased. The separation of the Ti transient peak and the continuous state Fe signal also decreases as the energy increases. The craters produced by the two laser energies were examined by scanning electron microscopy and are illustrated in **Figure 6.3**. The crater produced using 50 J shows a central hole which is approximately 100 μm in diameter, and the ablated crater being approximately 1.5 mm in diameter. The crater produced using 70 J shows no central hole and has a larger diameter of 1.7 mm. The crater also appears to be more circular and flat.

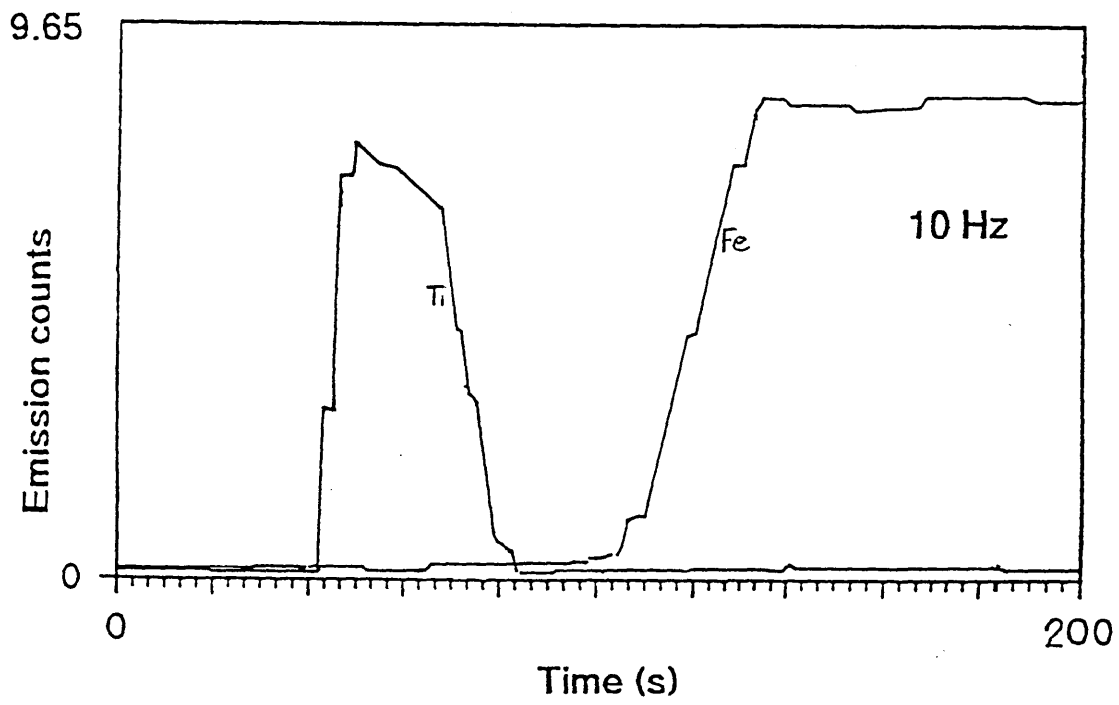
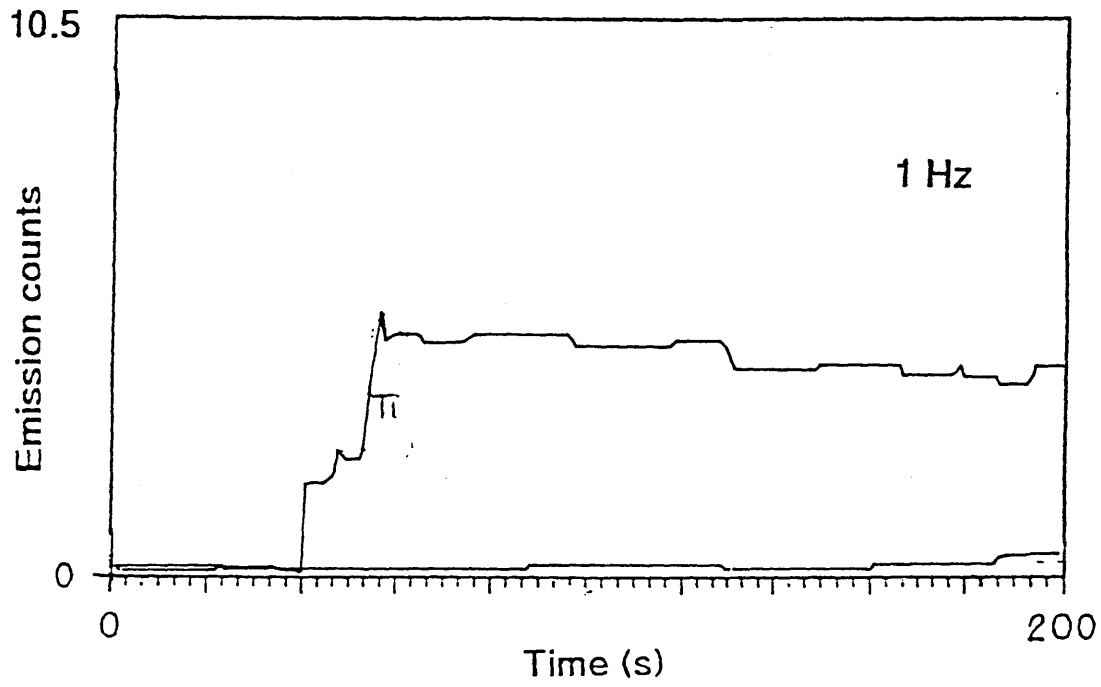
Fig 6.2 Emission time profiles for laser ablation of a TiN (3 μ m) coated steel sample showing the signals for Ti and Fe as a function of different laser lamp energies (50 and 70 J), at a 10 Hz pulse repetition rate



At higher laser lamp energies, the predominant ablation process is due to interaction of the laser induced plasma with the sample surface. No central hole is seen due to no direct interaction of the laser beam with the sample surface. This results in a more uniform ablation of the sample surface which produces emission peaks with a more distinct transition. The increase in the ablation crater size also lead to an increase in the emission signal. The reduction in the peak widths at higher laser energies is also due to a higher ablation rate.

The effect of the pulse repetition rate on the emission time profiles shows that by increasing the repetition rate of the laser the width of the peaks at half their maximum heights reduces. This reduction was accompanied by an increase in the emission intensities, due to a higher ablation rate at higher pulse repetition rates. It is also observed that the separation of the two peaks due to ablation of the Ti coating and the Fe substrate are reduced. **Figure 6.4** shows emission time profiles for pulse repetition rates of 1 and 10 Hz at 70 J laser lamp energy.

Fig 9.4 Emission time profiles for laser ablation of a TiN (3 μ m) coated steel samples showing the signals for Ti and Fe as a function of different pulse repetition rates (1 and 10 Hz), at a laser lamp energy of 70 J



6.3 Depth profiling calibration

The signal for the coating element was seen as a transient peak whose width varied not only with differences in laser operating conditions but with the thickness of the coating material. Studies investigating whether the emission signal characteristics would be proportional to the coating thickness were carried out. Titanium nitride coated steel samples with coating thicknesses varying between 1 and 10 μm were ablated using different laser lamp energies (45, 50, 60, and 70 J) for different pulse repetition rates (1, 2, 5, and 10 Hz). The peak width of each transient peak at half the maximum height was calculated and the results are tabulated in Table 6.1 using 10 different sampling points. The optimum laser operating conditions were seen to vary with the coating thickness and possibly with the degree of laser coupling with the surface which may vary with the the mature of the coating ie colour and reflectivity.

Table 6.1 Full width at half the maximum heights (FWHM) produced for the peak signals produced for TiN coated steel samples as a function of different laser pulse repetition rates (1, 2, 5, and 10 Hz) at different laser lamp energies (45, 50, 60, and 70 J)

Titanium nitride on a steel substrate (10 μm)

| Laser energy / J | Pulse repetition rate / Hz | | | |
|------------------|----------------------------|------|-----------|-----------|
| | 1 | 2 | 5 | 10 |
| 45 | ---- | ---- | ---- | ---- |
| 50 | ---- | ---- | 168 (4.5) | 130 (2.0) |
| 60 | >180 | >180 | 118 (4.5) | 104 (2.0) |
| 70 | >180 | >180 | 110 (5.0) | 100 (4.0) |

Titanium nitride on a steel substrate (7 μm)

| Laser energy / J | Pulse repetition rate / Hz | | | |
|------------------|----------------------------|------|-----------|-----------|
| | 1 | 2 | 5 | 10 |
| 45 | ---- | ---- | ---- | ---- |
| 50 | ---- | ---- | 120 (3.5) | 105 (2.0) |
| 60 | >180 | >180 | 90 (3.0) | 77 (3.0) |
| 70 | >180 | >180 | 85 (3.5) | 75 (3.5) |

Table 6.1 Full width at half the maximum heights (FWHM) produced for the peak signals produced for TiN coated steel samples as a function of different laser pulse repetition rates (1, 2, 5, and 10 Hz) at different laser lamp energies (45, 50, 60, and 70 J)

Titanium nitride on a steel substrate (5 μm)

| Laser energy / J | Pulse repetition rate / Hz | | | |
|------------------|----------------------------|------|----------|----------|
| | 1 | 2 | 5 | 10 |
| 45 | ---- | ---- | ---- | ---- |
| 50 | ---- | ---- | 89 (2.5) | 65 (2.0) |
| 60 | >180 | >180 | 62 (3.0) | 51 (2.0) |
| 70 | >180 | >180 | 60 (3.0) | 52(2.5) |

Titanium nitride on a steel substrate (3 μm)

| Laser energy / J | Pulse repetition rate / Hz | | | |
|------------------|----------------------------|-----------|----------|----------|
| | 1 | 2 | 5 | 10 |
| 45 | ---- | ---- | ---- | ---- |
| 50 | ---- | ---- | 70 (3.5) | 46 (3.5) |
| 60 | >180 | 120 (4.0) | 38 (3.5) | 33 (4.0) |
| 70 | >180 | 124 (5.5) | 36 (4.5) | 32 (5.0) |

Titanium nitride on a steel substrate (1 μm)

| Laser energy / J | Pulse repetition rate / Hz | | | |
|------------------|----------------------------|----------|----------|----------|
| | 1 | 2 | 5 | 10 |
| 45 | ---- | ---- | ---- | ---- |
| 50 | ---- | ---- | 32 (5.0) | 19 (4.0) |
| 60 | 35 (3.0) | 16 (4.0) | 10 (3.0) | 9 (3.5) |
| 70 | 34 (4.0) | 15 (3.0) | 8 (5.0) | 8 (4.5) |

Figures in parenthesis represent the %RSD (n=10)

Generally, as the pulse repetition rate is increased the transient peak (which corresponded to ablation of the coating material) width decreases. This is clearly seen for higher laser lamp energies of 60 and 70 J. The reduction in the peak width at higher repetition rates and laser lamp energies corresponds to a faster ablation process. For each of the samples no transient signal is seen for low laser energies of 45 J over the range of pulse repetition rates used (1 to 10 Hz). At 50 J no transient signal is seen at lower repetition rates (1 to 5 Hz), the peak width being larger for 50 J than for 60 J and above. The peak widths are similar for 60 and 70 J.

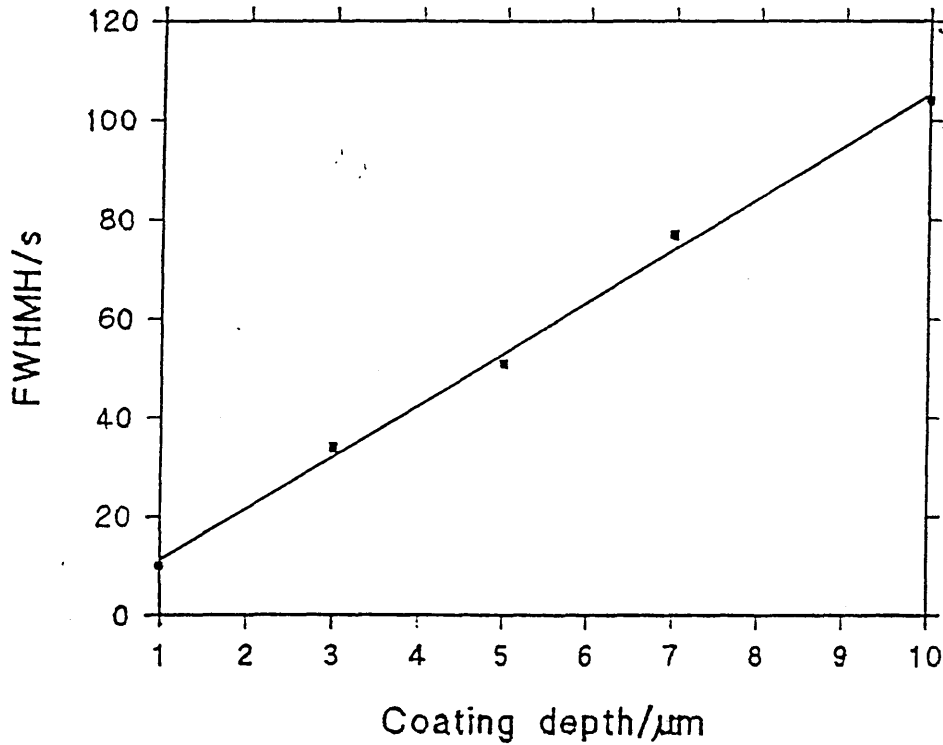
The results also show that the separation between the transient signal (corresponding to ablation of the coating material, in this case Ti), and the steady state signal (corresponding to ablation of the steel substrate, in this case Fe) is reduced as the pulse repetition rate and the laser energy are decreased. This is due to a slower ablation process and reduces mixing and diffusion of the ablated vapour produced by both the coating element and the Fe substrate.

For coating thicknesses above 1 μm , a 1 Hz pulsed laser produced signals of greater widths than the total integration time of the analysis (i.e. greater than 180 s). In order to analyse coating thicknesses of 3 μm and over it is concluded, therefore, that a greater acquisition time or a higher repetition rate was needed. Because there is little change in the peak width at 5 and 10 Hz and between 60 and 70 J laser lamp energy (and that the laser is optimised at 10 Hz) it was concluded that the optimum laser operating conditions for the analysis of such coatings are a laser pulse repetition rate of 10 Hz and a laser lamp energy of 60 J. The results also show that the degree of precision also improves as the repetition rate increases, with the best precision seen for a repetition rate of 10 Hz. Precision also improved for a laser lamp energy of 60 J.

A graph of the signal peak widths as a function of the titanium nitride coating thickness (for the optimised laser operating conditions) for the 1, 3, 5, 7, and 10 μm thick coatings is given in **Figure 6.5**. The graph shows that the width of the peak at half the maximum height is proportional to the coating thickness. It is suggested, therefore, that this technique may be useful in quantitative

depth determination. Further experiments were performed on other coating materials to evaluate whether the same laser operating parameters would prove successful.

Fig 6.5 Graph of the width at half the maximum height of the transient peak signal as a function of the coating thickness for TiN coated samples (1, 3, 5, 7 and 10 μm), using a laser pulse repetition rate of 10 Hz and a laser lamp energy of 60 J



Two titanium nitride coated knife blades (with dimensions of 25 cm length and 4 cm width) were ablated using the above laser operating conditions, with a coating thickness of $3.0 \pm 0.1 \mu\text{m}$. Results were obtained as emission time profiles and the peak width at half the maximum height of the signal was measured. A mean of 5 ablations gave a coating thickness of $3.1 \mu\text{m}$. Depth profiling by laser ablation proved to give fast accurate results for various geometries of sample.

6.4 Zirconium nitride and titanium/zirconium nitride coated steels

The same experiment was repeated for samples of a steel coated with zirconium nitride (3 μm), and a coating made up of a mixture of zirconium and titanium nitride on a steel substrate. The samples were subjected to the same range of laser lamp energies and pulse repetition rates, and the results obtained as emission time profiles. The full width at half the maximum heights were calculated for each operating parameter. The results are given in Table 6.2.

The results for the 3 μm zirconium nitride are very similar to the 3 μm TiN coating, which shows that each given laser operating parameter the signal is proportional to the coating thickness and not to the chemical composition of the coating. This was confirmed by investigating a sample coated with a mixture of titanium and zirconium nitride (1 μm). The signal peak widths at each laser operating conditions were the same, and also very similar to those obtained for the TiN 1 μm coated steel

Table 6.2 Full width at half the maximum heights (FWHM) produced for the peak signals produced for ZrN, and Ti/ZrN coated steel samples as a function of different laser pulse repetition rates (1, 2, 5, and 10 Hz) at different laser lamp energies (45, 50, 60, and 70 J)

Zirconium nitride on a steel substrate (3 μm)

| Laser energy / J | Pulse repetition rate / Hz | | | |
|------------------|----------------------------|-----------|----------|----------|
| | 1 | 2 | 5 | 10 |
| 45 | ---- | ---- | ---- | ---- |
| 50 | ---- | ---- | 70 (4.0) | 48 (3.0) |
| 60 | >180 | 110 (4.0) | 38 (3.0) | 34 (2.0) |
| 70 | >180 | 112 (5.0) | 37 (4.0) | 34 (3.0) |

Table 6.2 Full width at half the maximum heights (FWHM) produced for the peak signals produced for ZrN, and Ti/ZrN coated steel samples as a function of different laser pulse repetition rates (1, 2, 5, and 10 Hz) at different laser lamp energies (45, 50, 60, and 70 J) - continued
Titanium/Zirconium nitride on a steel substrate (1 μm) results for Zirconium - continued

| Laser energy / J | Pulse repetition rate / Hz | | | |
|------------------|----------------------------|----------|----------|----------|
| | 1 | 2 | 5 | 10 |
| 45 | ---- | ---- | ---- | ---- |
| 50 | ---- | ---- | 16 (5.0) | 10 (4.0) |
| 60 | 35 (2.0) | 15 (3.0) | 10 (2.0) | 9 (3.0) |
| 70 | 32 (3.0) | 14 (2.5) | 9 (2.0) | 7 (3.0) |

Titanium/Zirconium nitride on a steel substrate (1 μm) results for titanium

| Laser energy / J | Pulse repetition rate / Hz | | | |
|------------------|----------------------------|----------|----------|----------|
| | 1 | 2 | 5 | 10 |
| 45 | ---- | ---- | ---- | ---- |
| 50 | ---- | ---- | 17 (4.5) | 10 (4.0) |
| 60 | 35 (3.0) | 15 (3.5) | 10 (4.0) | 9 (3.5) |
| 70 | 33 (2.0) | 14 (3.5) | 10 (4.0) | 7 (3.0) |

Figures in parenthesis represent the %RSD (n=10)

6.5 Multilayered steels

Experiments were carried out in order to investigate the ablation of more than one coating on the same substrate. In this case a titanium nitride coating was sputtered over a zirconium nitride coating, and each coating was calculated to be 3 μm in thickness. Experiments were then carried out investigating the effect of the laser repetition rate and the laser lamp energy. Results were obtained as emission time profiles. **Figure 6.6** illustrates the emission time profiles as overlays for Ti and Zr using a laser lamp energy of 60 J with a pulse repetition rate of 1 and 10 Hz.

Both spectra show two transient signals, the first due to Ti, the second due to Zr. Finally a steady state signal due to ablation of the steel substrate was seen. As the pulse repetition rate increased

the separation of the two transient signals decreased, at 10 Hz the peaks were slightly overlapped, and at 1 Hz pulse repetition rate the two transient peaks are well separated, due to a decreased ablation rate.

The full width at half the maximum height was also determined for each laser operating parameter used, and the results are tabulated below in Table 6.3. The results for the full width at half the maximum height for the elements Ti and Zr are similar to those obtained for the single coatings of Ti and Zr of 3 μm thickness.

Table 6.3 Full width at half the maximum heights (FWHM) produced for peak signals produced for a multilayered steel sample of titanium nitride (3 μm) on Zirconium nitride (3 μm) on a steel substrate as a function of different laser pulse repetition rates (1, 2, 5 and 10 Hz) at different laser lamp energies (45, 50, 60 and 70 J)

Results for titanium

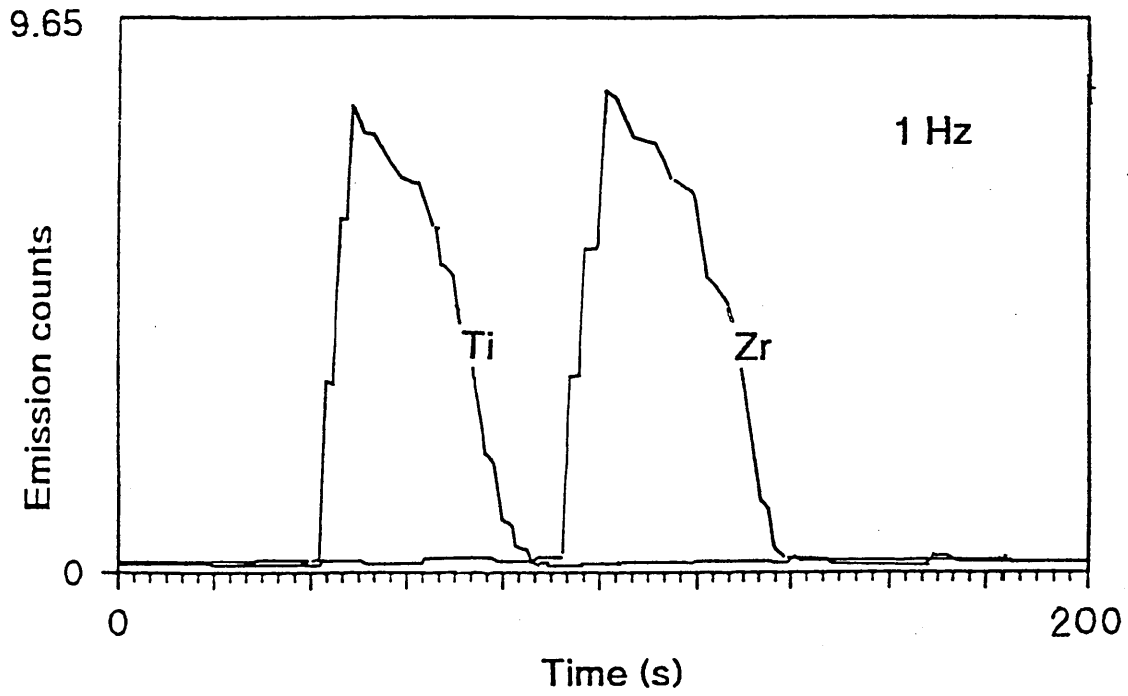
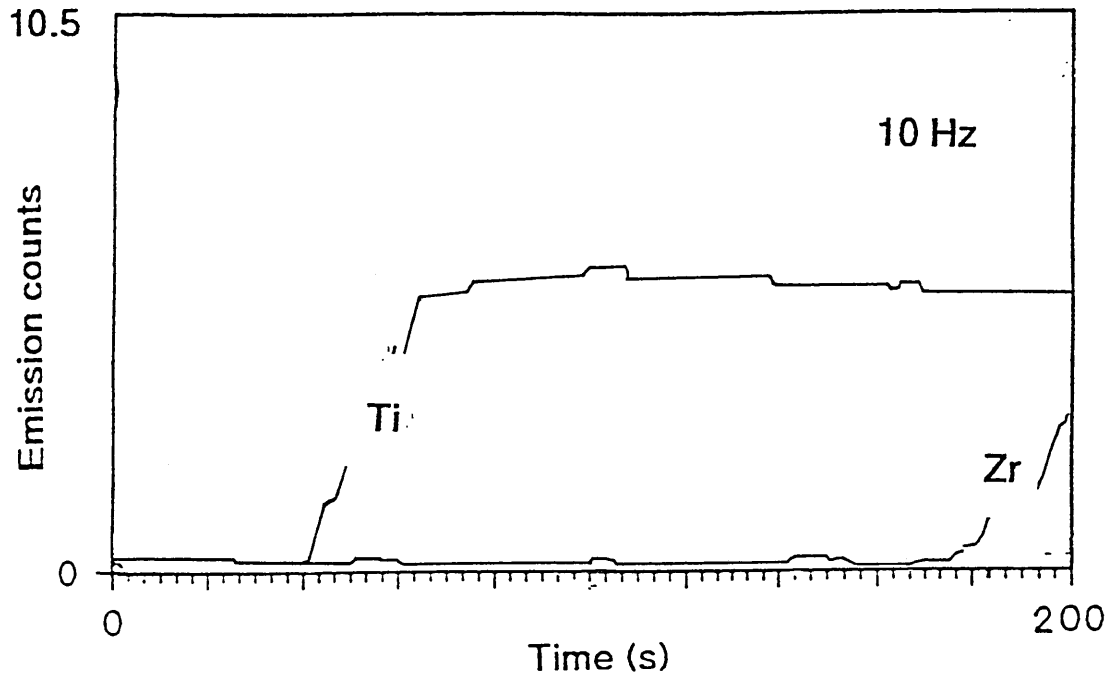
| Laser energy / J | Pulse repetition rate / Hz | | | |
|------------------|----------------------------|-----------|----------|----------|
| | 1 | 2 | 5 | 10 |
| 45 | ---- | ---- | ---- | ---- |
| 50 | ---- | ---- | 68 (4.0) | 50 (3.5) |
| 60 | >180 | 109 (4.0) | 37 (3.0) | 33 (2.0) |
| 70 | >180 | 114 (4.5) | 39 (4.0) | 34 (3.0) |

Results for zirconium

| Laser energy / J | Pulse repetition rate / Hz | | | |
|------------------|----------------------------|-----------|----------|----------|
| | 1 | 2 | 5 | 10 |
| 45 | ---- | ---- | ---- | ---- |
| 50 | ---- | ---- | 70 (4.0) | 48 (3.0) |
| 60 | >180 | 110 (4.0) | 38 (3.0) | 34 (2.0) |
| 70 | >180 | 112 (5.0) | 37 (4.0) | 34 (3.0) |

Figures in parenthesis represent the %RSD (n=10)

Fig 6.6 Emission time profiles for laser ablation of a TiN on ZrN (3 μm) coated steel sample showing the signals for Ti, Zr as a function of different laser pulse repetition rates (1, 2, 5, and 10 Hz) using a laser lamp energy of 60 J



6.6 Ultrathin coated steels

The results obtained for materials with coatings with a thickness in the μm range show that it is possible to obtain a separate signal for the coating material at depth resolutions of about $1\ \mu\text{m}$. It may be possible, however, to obtain information on coatings in the sub micron range using this technique. Results were produced for the Sn and Cr coated steel coated samples. Again the results were produced as emission time profiles the signal for the coating element was seen as a transient signal overlaid with the signal for the Fe substrate. The emission time profiles show a transient signal corresponding to the coating material followed by a steady state signal due to ablation of the substrate. **Figure 6.7** shows the emission time profiles for the Sn and the Cr coated steel materials (using a laser lamp energy of 60 J at 10 Hz). The full width at half the maximum heights were also calculated and are tabulated in **Table 6.4**.

These coatings are much thinner than the Ti and ZrN coatings, being in the sub micron range, and the results showed that the peak widths at half the maximum heights are correspondingly smaller in **Table 6.4**. Again no signals were seen at 45 J laser lamp energy and at 50 J signals are only seen at repetition rates of 5 and 10 Hz. For the Sn coated material the peak width decreases as the pulse repetition rate of the laser is increased.

The results for the Cr coated material showed little or no change in the peak shape over the range of laser operating parameters used. So although it is possible to detect the sample coating on very thin coatings we have not yet carried out quantitative depth analysis of coatings in the nm range.

Fig 6.7 Emission time profiles for laser ablation of a Cr and a Sn coated steel sample showing the signals for both Cr, Sn and Fe, using a laser lamp energy of 60 J and a pulse repetition rate of 10 Hz.

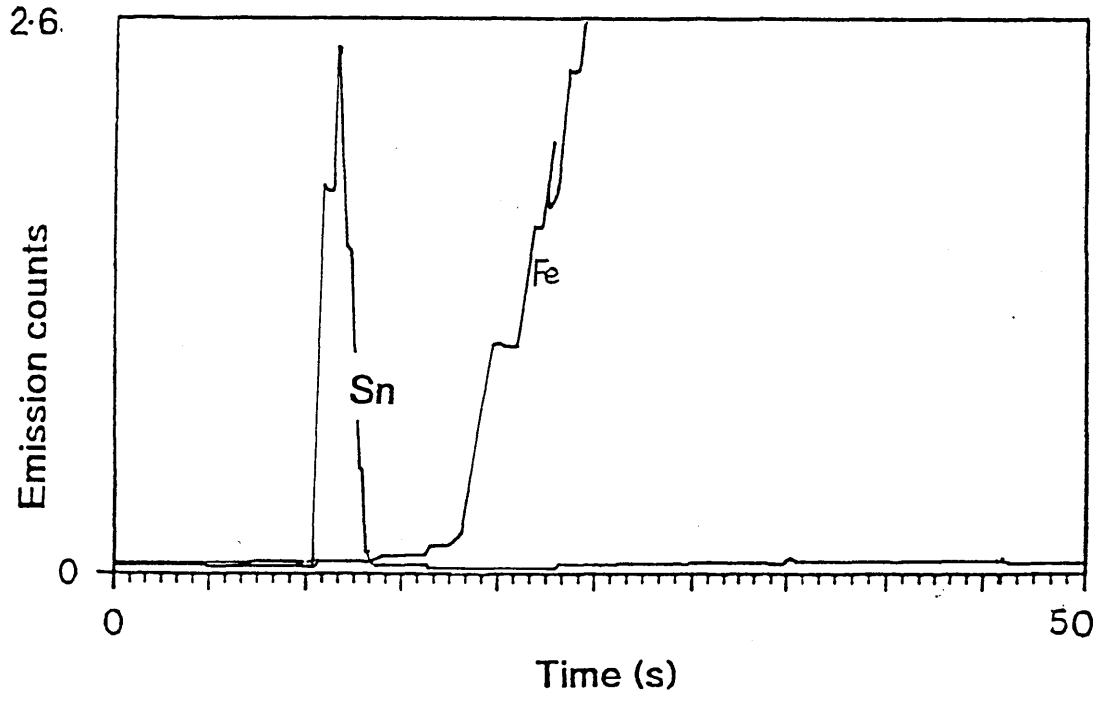
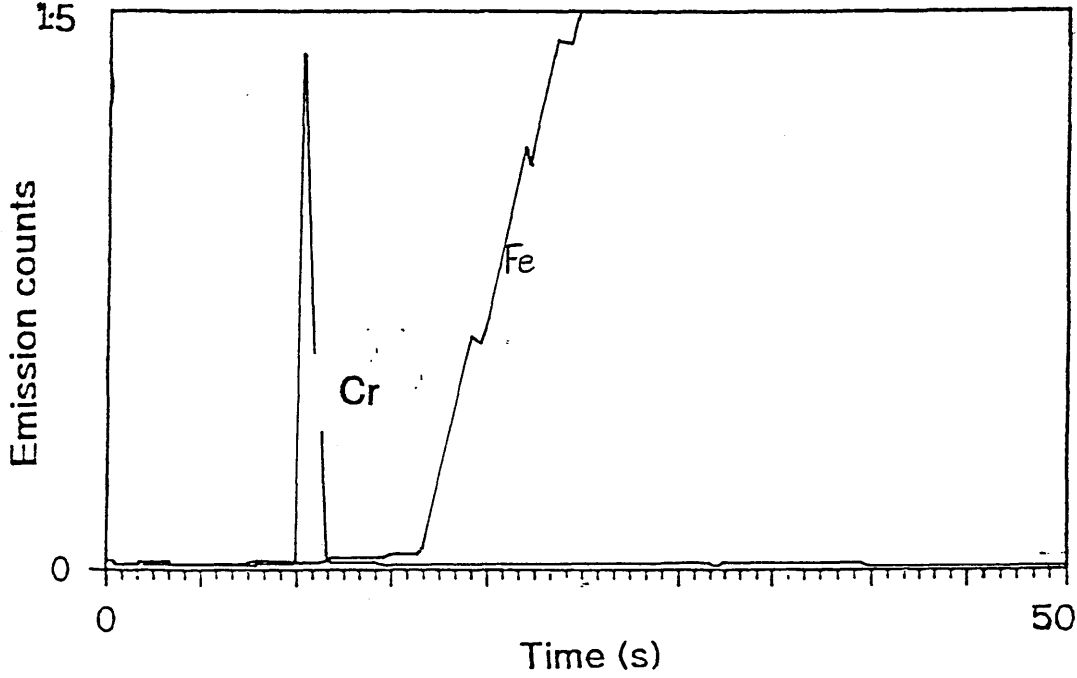


Table 6.4 Full width at half the maximum heights (FWHM) produced for the peak signals for tin and chromium coated steel samples as a function of different laser pulse repetition rates (1, 2, 5 and 10 Hz) at different laser lamp energies (45, 50, 60 and 70 J)

Tin on a steel substrate

| Laser energy / J | Pulse repetition rate / Hz | | | |
|------------------|----------------------------|---------|----------|----------|
| | 1 | 2 | 5 | 10 |
| 45 | ---- | ---- | ---- | ---- |
| 50 | ---- | ---- | 7 (8.0) | 4 (7.0) |
| 60 | 9 (6.0) | 4 (4.0) | 2 (10.0) | 2 (10.0) |
| 70 | 8 (5.0) | 4 (5.0) | 2 (10.0) | 1 (12.0) |

Chromium on a steel substrate

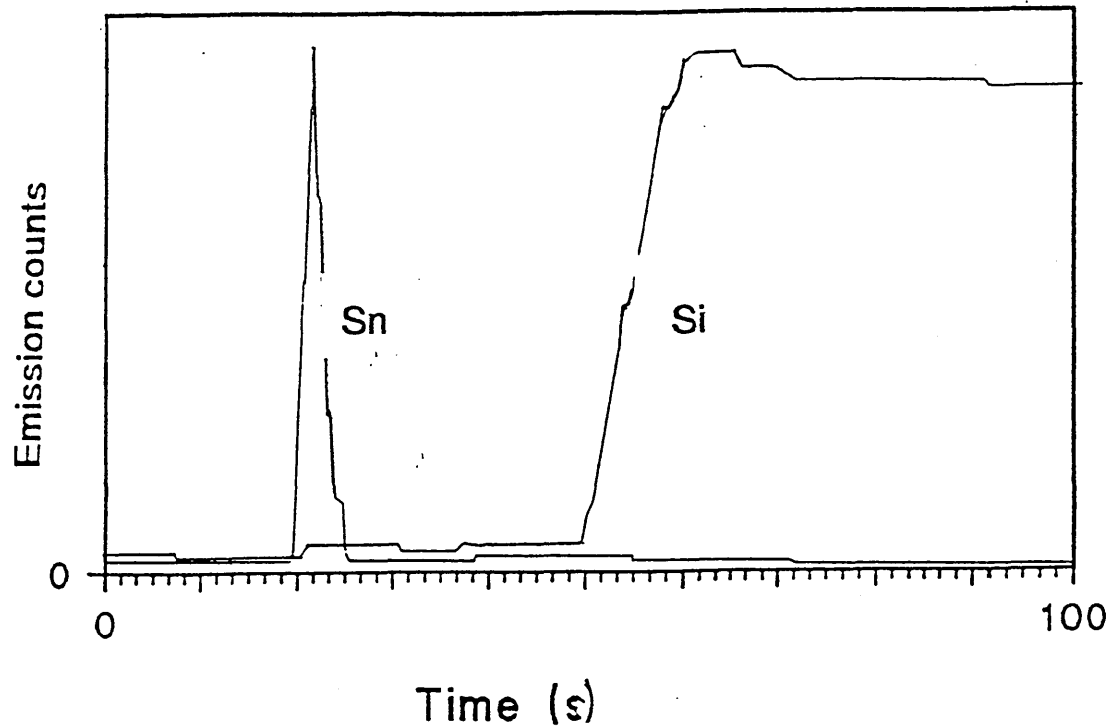
| Laser energy / J | Pulse repetition rate / Hz | | | |
|------------------|----------------------------|------|------|------|
| | 1 | 2 | 5 | 10 |
| 45 | ---- | ---- | ---- | ---- |
| 50 | ---- | 1 | 2 | 2 |
| 60 | 2 | 1 | 1 | 1 |
| 70 | 2 | 2 | 1 | 1 |

Figures in parenthesis represent the %RSD (n=10)

6.7 Tin oxide coated glass

So far the materials studied have been metal coatings on a steel substrate. Investigations were then turned to the use of this technique for non metal substrates. Depth profiling was undertaken for a glass substrate. For this example a tin oxide coated glass (which was used as low emissivity glass) was ablated and the laser operating parameters were studied in the same way as before. The results were produced as emission time profiles. **Figure 6.8** shows the emission time profiles for the tin oxide coated glass using a laser lamp energy of 10 Hz at 70 J laser lamp energy. The full width at half the maximum heights were also calculated and are tabulated in **Table 6.5**.

Fig 6.8 Emission time profiles for laser ablation of a tin oxide coated glass sample showing the signals the signals for Sn and Si using a laser lamp energy of 70 J, for a 10 Hz pulsed laser.



The results show that for the Sn coated glass sample no signals are seen at 45 and 50 J laser lamp energy, for any given pulse repetition rate. At 60 and 70 J lamp energy signals are only seen at higher pulse repetition rates of 5 Hz and above, where a single transient signal due to tin is seen. Generally the peak shapes remain unchanged at laser energies of 60 J and above and repetition rates of 5 Hz and above. No signal is seen for the glass substrate until a laser lamp energy of 70 J and a pulse repetition rate of 10 Hz was used. In this case substantial damage was seen on the surface of the material and a deep crater had formed. It was obvious that because of the transparent nature of the glass and low coupling of the laser the ablation rate of the surface was less than that for the metal samples.

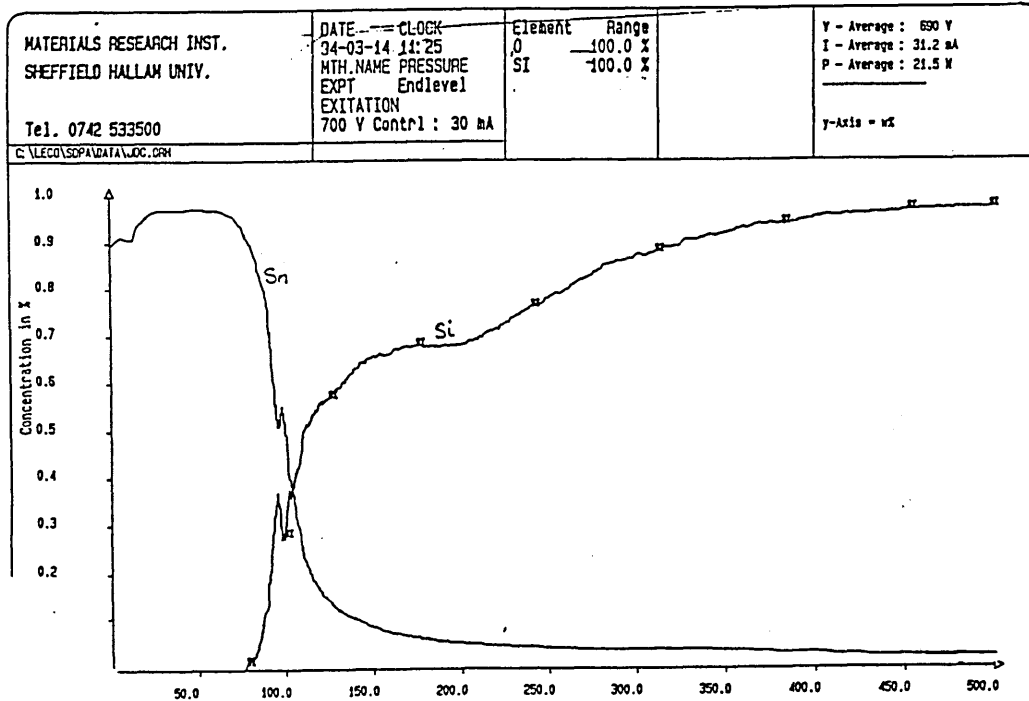
Table 6.5 Full width at half the maximum heights (FWHM) produced for the peak signals produced for Sn coated glass samples as a function of different laser pulse repetition rates (1, 2, 5, and 10 Hz) at different laser lamp energies (45, 50, 60, and 70 J)

| Laser energy / J | Pulse repetition rate / Hz | | | |
|------------------|----------------------------|------|----------|----------|
| | 1 | 2 | 5 | 10 |
| 45 | ---- | ---- | ---- | ---- |
| 50 | ---- | ---- | ---- | ---- |
| 60 | ---- | ---- | 12 (8.0) | 10 (5.0) |
| 70 | ---- | ---- | 9 (8.0) | 10 (5.0) |

Figures in parenthesis represent the %RSD (n=10)

The coating thickness was determined by glow discharge spectrometry, using a GDS-750 QDP Glow discharge spectrometer. The depth concentration profile for the glass sample by glow discharge is given in Figure 6.9. The tin oxide coating thickness was found to be approximately 100 nm.

Figure 6.9 Depth concentration profile of a tin oxide coated glass sample by glow discharge spectrometry



7.1 Introduction

Trace element analysis of biological materials is currently undertaken using a number of instrumental techniques, principally atomic absorption spectrometry (151), neutron activation analysis (152), X-ray fluorescence (153), and inductively coupled emission spectroscopy (154, 155). The potential sources of error in determination of trace element levels using these techniques are primarily related to pre-analysis sample dissolution of solid materials; high analyte blank uncertainties from reagents and numerous sources of contamination such as flasks and pipettes.

Direct sampling of solid materials can greatly shorten the analysis time compared with procedures requiring a tedious dissolution stage. Such dissolutions can be enormously time consuming and occupy qualified people for long periods of time. Beauchimin et al (155) reported a nitric acid-hydrogen peroxide digestion procedure for marine biological reference materials for trace metals (DOLT-1 Dogfish liver and DORM-1 Dogfish muscle) that required at least a full days work.

So far relatively little has been reported on laser ablation inductively coupled plasma mass spectrometry as a direct solid sampling technique for biological samples. The potential advantages for such sampling lie in the fact that this technique requires little or no sample preparation, which leads to the reduction in sample contamination; the ability to sample any matrix; and the ability to achieve spatially resolved as well as bulk analysis.

The potential advantages of laser ablation are tempered by the difficulties of calibration, which in turn depend on the use of standard reference materials for which elements are well certified. These are expensive and relatively few are available. In this work laser ablation inductively coupled plasma mass spectrometry was used to benefit from the following advantages over emission spectrometry; improved sensitivity, and the ability to utilise a computer controlled translation stage and remote imaging of the sample which lead to easier and more precise control

of positioning the sample for laser ablation (especially useful when very small sections of microtome tissue are to be ablated).

Preliminary experiments into the feasibility of using a new approach of providing quantitative information without the need of standard reference materials was tested for laser ablation inductively coupled plasma mass spectrometry. This was achieved by using multielement gels as a novel calibration source. In this work agarose gels containing known amounts of aqueous multielement standards were dispensed onto glass microscope slides, producing a thin film which was allowed to dry. Experiments were performed to optimise the sampling parameters (laser lamp energy), and to investigate whether reproducible signals could be obtained, and calibration studies in order to calculate the linear range and limit of detection.

7.2 Gel multielement standards

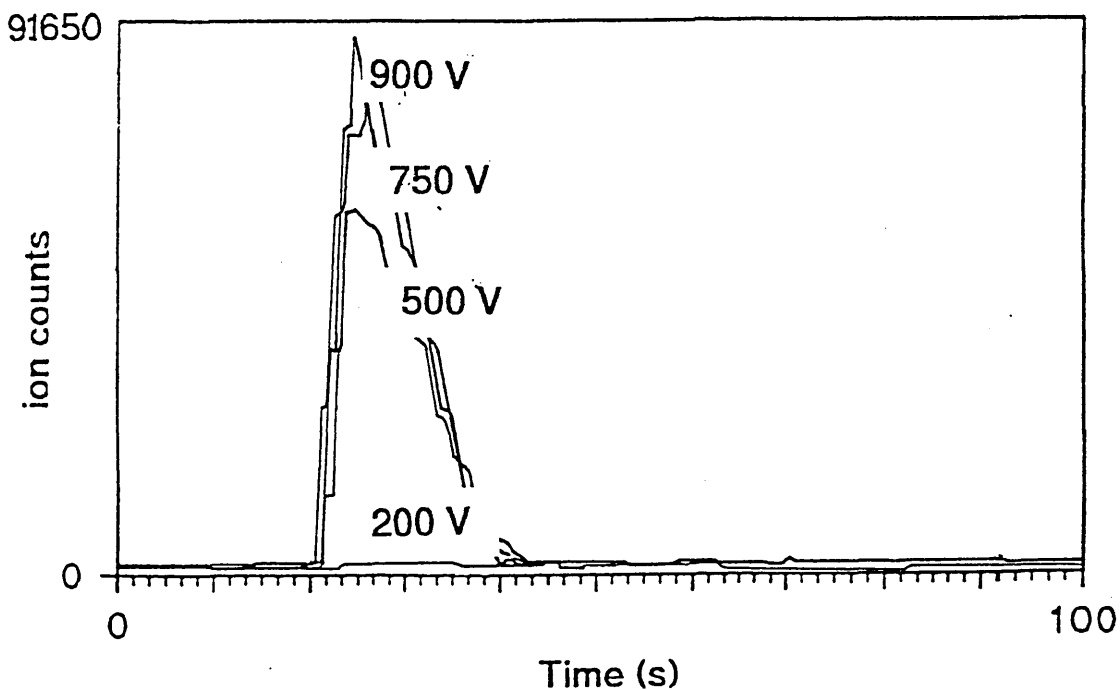
The effect of laser operating parameters was investigated using a $100 \mu\text{g g}^{-1}$ multielement gel standard. Studies included investigating the effect laser focusing and laser lamp energy for single laser shot laser firing (laser lamp energies of 200, 500, 750, and 900 V). Results were produced as emission time profiles. **Figure 7.1** shows the emission time profiles for nickel as overlays using laser lamp energies of 200, 500, 750 and 900 V for single Q switched laser shots.

Defocusing the laser approximately 5 mm above the surface of the sample resulted in a substantial improvement in the signal compared to a laser beam focused on the surface. This is due to an increased laser spot size and hence a larger area sampled.

A narrow transient signal was observed for each of the elements studied. The peak height increases as the laser lamp energy increases from 500 to 900 V (no signal is seen for a laser lamp energy of 200 V). No damage to the glass slide was apparent for single shots.

From the results it is concluded that a minimum laser lamp energy of 500 V is needed to obtain any ablation of the gel surface and that by increasing the laser energy this would also increase the sampling sensitivity. However, contamination due to ablation of the glass substrate must also be considered and, therefore, a laser lamp energy of 750 V was judged sufficiently high.

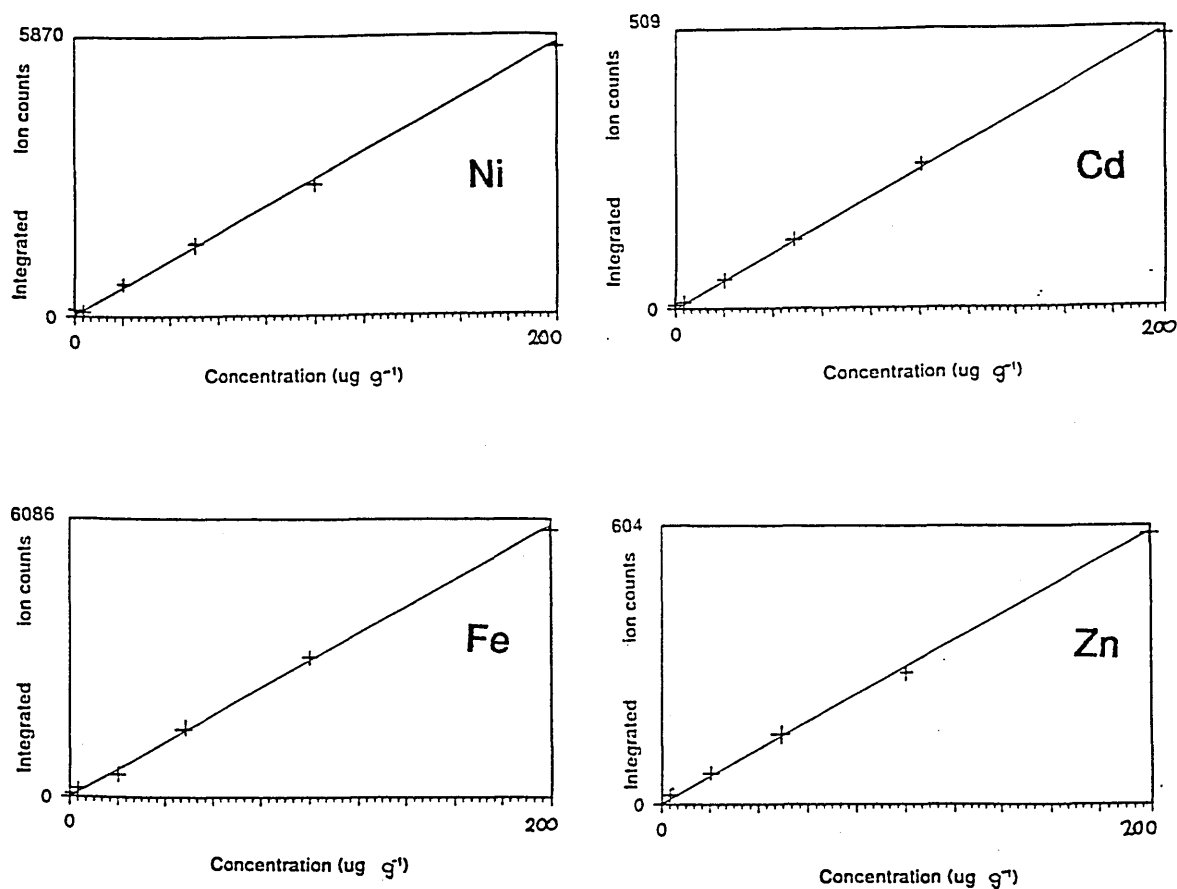
Fig 7.1 Emission time profiles for laser ablation of a $100\mu\text{g g}^{-1}$ multielement gel standard for single shot laser operation of 200, 500, 750 and 900 V. Results are shown for nickel



7.3 Calibration

In order to investigate the potential of using multielement gel standards as a method of calibration for laser ablation calibration curves were constructed. Each of the gel standards (5, 25, 50, 100 and 200 $\mu\text{g g}^{-1}$), were ablated using a laser lamp energy of 750 V for single shot laser operation. Each slide was ablated 5 times using a fresh sampling point. A pure gel was employed as the blank. Each duplicate slide was ablated so that 10 sampling points were obtained for each calibration point. Results were obtained as raw counts based on the integration of the transient signal. Figure 7.2 shows the raw intensity values plotted against the concentration minus the blank for Ni, Cd, Fe and Zn. The straight line is the least squares fitted line. The integration was started at the time of laser firing 20 s after the start of analysis and the peak was integrated for 10 s.

Fig 7.2 Plots of the integrated emission signal against the concentration for Ni, Cd, Fe, and Zn over the concentration range 0 to 200 $\mu\text{g g}^{-1}$. Each point is the mean of 10 sampling points



The results of the calibration studies showed linearity over the concentration range 5 to 200 $\mu\text{g g}^{-1}$. It was not possible, however, to check whether linearity extended further than 200 $\mu\text{g g}^{-1}$ as a gel could not be produced that would set at higher element concentrations. The laser ablation ICP mass spectrometer proved to be very sensitive with single laser shots giving relatively high signals. The calibration data is given in Table 7.1. Limits of detection at sub $\mu\text{g g}^{-1}$ level were obtained.

Table 7.1 Table of analytical performance for laser ablation of gel multielement standards

| Element | Equation of line | Limit of detection $\mu\text{g g}^{-1}$ | Dynamic range $\mu\text{g g}^{-1}$ |
|---------|------------------|-----------------------------------------|------------------------------------|
| Ni | $y=324x + 0$ | 0.9 | 5 to 200 |
| Cd | $y=105x + 0$ | 0.02 | 5 to 200 |
| Fe | $y=150x + 0$ | 0.2 | 5 to 200 |
| Zn | $y= 98x + 0$ | 0.7 | 5 to 200 |

7.4 Analysis of microtome tissue samples

In order to test whether quantitative microanalysis of tissue sections was possible using the new calibration procedure, a frozen microtome section (approximately 5 μm thickness) of rat liver tissue was prepared on a microscope slide. For calibration purposes a 100 $\mu\text{g g}^{-1}$ multielement gel standard was used.

The tissue was ablated using the same laser operating conditions as the gel multielement calibration standard (Q switched single shot ablation using a laser lamp energy of 750 V). The tissue and the multielement gel standard were ablated one after the other. For the analysis the sample was ablated 5 times at different points on the sample surface. Results obtained as the raw counts based on the integration of the transient signals are shown for the Fe distribution for the different sampling points. Quantitative analytical data was performed by comparing the analytical signal of the standard with that obtained for the sample. The results are given in Table 7.3.

Table 7.3 Distribution of Fe found in rat liver tissue by laser ablation. Five sampling points were used over the surface of the sample

| | Integrated signals for liver tissue counts x 1000 | Integrated Signals for gel standard (100 $\mu\text{g g}^{-1}$) counts x 1000 | Found concentration $\mu\text{g g}^{-1}$ |
|------|------------------------------------------------------------------|------------------------------------------------------------------------------------------------------------|--------------------------------------------------------------------|
| | 1345 | 347 | 388 |
| | 1200 | 356 | 336 |
| | 890 | 376 | 236 |
| | 1168 | 356 | 328 |
| | 723 | 324 | 222 |
| Mean | 1065 | 352 | 302 |
| SD | 252 | 18 | 70 |
| %RSD | 24 | 5 | 23 |

The results show that iron concentration varies across the surface of the rat liver tissue sample due to the heterogeneous distribution of Fe in the tissue. Precision for laser ablation of the tissue is poor owing primarily to inhomogeneity of the sample. This preliminary study has shown that it may be possible to obtain microanalysis data on the distribution of elements found within thin film biological tissue sections. Precision for the gel multielement standard, was better than that for the tissue sample.

7.5 Determination of nickel distribution in skin tissue samples

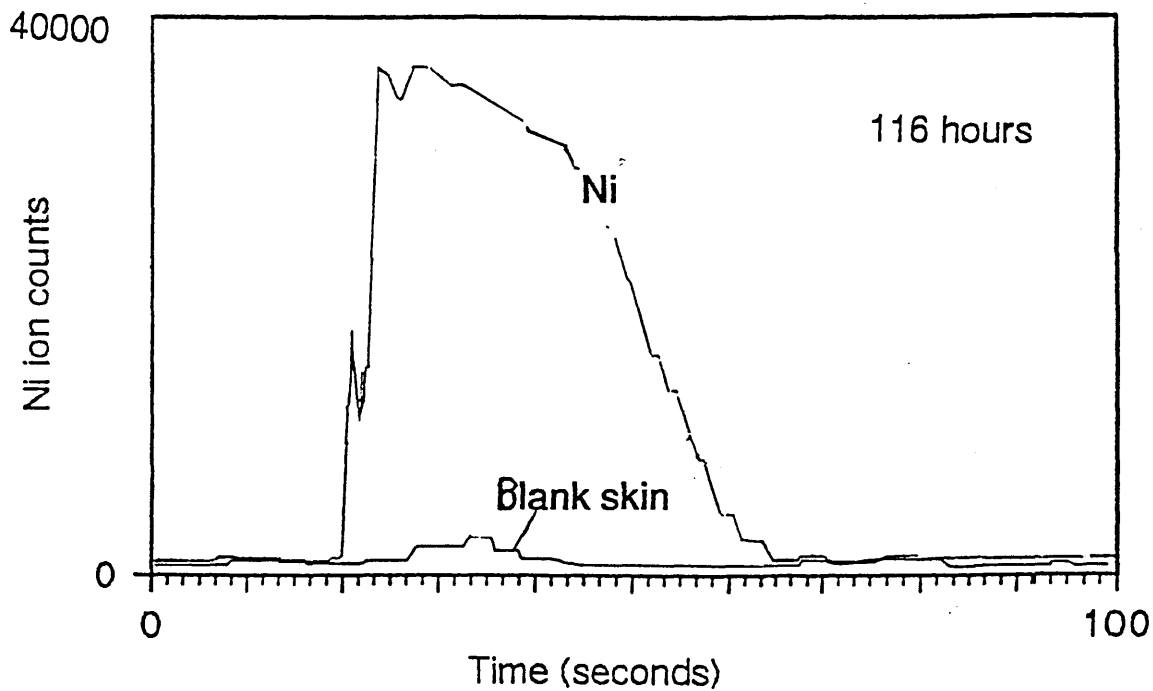
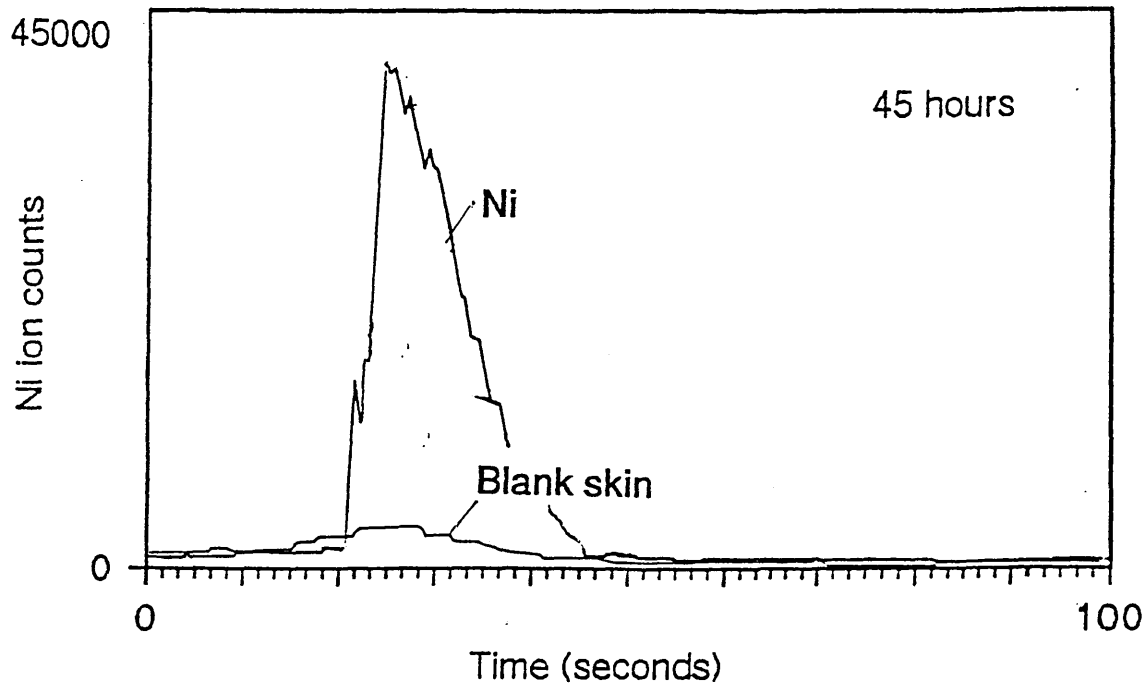
A study was undertaken to determine the depth distribution of nickel in human skin. Nickel compounds are known to be toxic and may give rise to such conditions as nickel dermatitis. Persons who are regularly exposed to such compounds must, therefore, take precautions to minimise their skin exposure. However, in order to evaluate the risks involved the rate of which nickel will travel across human skin is determined. Various methods are currently employed to determine the distribution of Ni in skin samples after exposure to Ni for a set amount of time. The methods employed are based upon acid dissolution techniques and are laborious and time consuming. It was considered that the use of laser ablation mass spectrometry as a microanalysis depth profiling technique would prove useful for such determinations.

Preliminary studies into the feasibility of using laser ablation inductively coupled plasma mass spectrometry as a microanalysis technique for determination of Ni distribution in skin tissue samples were undertaken. Two skin tissue samples were immersed in a solution of NiCl (0.5 ml, at $50 \mu\text{g g}^{-1}$) for different lengths of time (45 and 116 hours).

The two skin samples were each subjected to a low repetition rate pulsed laser of 1 Hz using a laser energy of 700 V and ablated until the laser had penetrated each sample. A skin tissue sample that had not been subjected to Ni solution was also ablated and used as a blank. Results were obtained as transient signals (Ni ion count versus time over 100 s) illustrated in **Figure 7.4**.

The width of each peak at half the maximum peak height was proportional to the degree that the skin sample had been subjected to Ni (this trend is similar to depth profiling of coated materials as seen in **Chapter 6**). The transient signal for the skin which had been immersed in the nickel solution for 116 hours shows a much broader peak (base line width of 40 s) suggesting that the Ni had penetrated the sample to a greater extent than the skin immersed for 45 hours (base line width of 25 s). The blank skin tissue sample gave only a very small peak due to very small amounts of Ni which is naturally present in skin. The results show that this method of sampling is successful at determining different Ni concentrations in skin tissue samples.

Fig 7.4 Emission time profiles showing the depth distribution of Ni in two skin tissue samples which were exposed to a solution of Ni chloride for 45 and 116 hours respectively both sets of results are overlaid with a blank tissue sample. A 1 Hz laser was used with a laser energy of 750 V



8.1 Conclusions and future work

Overall conclusions and future work

The use of laser ablation has provided a quick and reliable means of microsampling of a diverse range of samples: glasses, aqueous solutions, oils, coated steels and glasses and biological samples. Results have shown acceptable accuracy for glass analysis with respect to conventional acid dissolution procedures (which needs skilled technicians as well as being a very much more lengthy procedure compared to laser ablation). Laser microsampling of liquids has shown to be a useful alternative to conventional pneumatic nebulisation, especially for liquids such as oils when blockages in the nebuliser may occur. The use of aqueous multielement solutions also proves useful as an alternative calibration strategy for analysis of liquids. Depth analysis for coated steel and glasses by laser ablation has shown that very quick and reliable results could be obtained down to the sub micrometer level. Finally it is possible to obtain trace element analysis of microtome biological samples and with the use of a novel calibration technique i.e. gel multielement standards it may be possible to obtain fully quantitative microanalysis of tissue sections using laser ablation.

Laser ablation signals, however, are very dependant on the laser operating parameters used and optimisation is needed for different sample types. Variable ablation yields and element enrichment/suppression for different sample matrices is observed, therefore, closely matched calibration standards are needed for accurate quantitation.

The experimental facilities may be improved, by providing computer control of laser operating parameters and sample manipulation. These are presently set manually which takes time as well as resulting in a possible reduction in precision. The positioning of the sample could be achieved by mounting the ablation chamber on a computer controlled motorised XYZ translation stage. Automated sample manipulation would enable the sample to be quickly positioned, providing versatile laser sampling of materials, such as allowing a fresh area of sample to be

ablated by each laser shot, or a large area of sample to be examined by ablating a grid pattern. The provision of a miniature CCD video camera to monitor the sample position would provide precise ablation of different regions of the sample. This was especially important for small samples such as microtome sections (Chapter 7) where the laser ablation ICP mass spectrometer was used.

More importantly the use of UV laser ablation using both frequency quadrupled Nd YAG, excimer and frequency doubled lasers (92-95) in recent years have proved to give superior sampling compared to infra red lasers in every analytical aspect and therefore the use of UV lasers have now superseded infra red lasers. So it is clear that potentially the use of a UV laser may improve all analytical aspects such as accuracy, precision and limits of detection for analysis of glasses, liquids, thin coated materials and biological samples. Similar experiments to those undertaken in this thesis should therefore be undertaken using a UV laser. The use of UV lasers has also shown to decrease matrix effects and therefore, it may be possible to do away with matrix matched calibration standards.

Glasses

This work has for the first time shown the effects of laser operating parameters on the analytical signal for the matrix elements of glass. Pre-ablation of the glass surface results in increased sensitivity compared to a non pre ablated sample. This confirms sensitivity gains obtained for pre ablation of metal surfaces reported in the literature (126, 127), where the ablation yield was seen to increase after the reflective surface of a metal was roughened using a laser beam.

Increasing the laser energy as well as increasing the ablation time also results in sensitivity gains, however, a limit for sensitivity gains is also observed. A maximum sensitivity is observed for an ablation time of 5 s. Further increases in ablation time resulted in melting of the sample, which reduced the amount of ablated material. Similarly increasing the laser lamp energy over 60 J result in the sample being shattered.

Experiments also show the dependence of laser focus on the sample surface on the sensitivity. The maximum sensitivity is seen when the laser was defocused by 5 mm from the sample surface. This was due to a reduction in sample melting for the defocused laser beam.

Overall the results show that the analytical signal is very dependant on the experimental parameters used, and it is, therefore, necessary to optimise laser operating parameters for each type of sample

Limits of detection are found to be in the sub $\mu\text{g g}^{-1}$ range, varying between 0.015 and 0.11 $\mu\text{g g}^{-1}$, and are similar to those obtained by sample digestion and solution nebulisation into a plasma emission spectrometer where limits of detection are typically in the $\mu\text{g g}^{-1}$ range (130-132). They are also at least a factor of 10 better than those found by graphite furnace atomic absorption spectrometry. Headridge et al (124) obtained limits of detection of around 5 $\mu\text{g g}^{-1}$, using graphite furnace atomic absorption spectrometry. Pre ablation of the surface resulted in an analytical signal proportional to element concentration, regardless of its matrix.

As with other solid microsampling techniques the precision is relatively poor when compared to solution nebulisation. This is probably due to shot to shot variation in the ablated mass and also the heterogeneity of the sample and non reproducible losses of volatile analytes. Precision varied between 7.3 and 23.6 %RSD, with poorer precision observed for volatile elements such as Ag and Pb with values of 23.6 and 18.6 %RSD respectively. Precision compared favourably with that seen by Franks et al (125), using laser ablation inductively coupled plasma emission spectrometry where precision was found to be around 10 %, but was also seen to be as high as 28 % for more volatile elements. This may be accounted by irreproducible losses of material due to condensation of these elements on the ablation chamber walls and the sample transfer tubing. The use of internal standardisation improved precision with precision for boron improving from 8.6 to 4.8 %RSD using cobalt as the internal standard. However, these improvements are dependant on similarities in thermochemical properties between the chosen internal standard

and the element. Internal standardisation is most effective when the thermochemical properties for the internal standard are similar to the element.

Good agreement was obtained between the found and the certified values for a range of glass types. Results are given for a wide range of elements, for major, minor and trace elements, which has not previously been undertaken in a single study. Overall the laser ablation technique proved to be a quick and effective analytical technique for analysis of glasses, it provides an attractive alternative to conventional glass analysis techniques.

So far experiments have been performed on solid glasses, however, ablation of molten glasses may also be investigated. This may prove of benefit to the glass making industry as a technique used for on line element monitoring of molten glasses. Electrothermal heating and melting of glasses prior to ablation may be used to investigate laser ablation of molten glasses. Although this is unsuitable for volatile elements precision for non volatile elements may be improved as a consequence of the fluidity of molten materials.

Diamond impregnated plastic discs have been used for the analysis of metal samples (66) and there is clear potential to use this technique for analysis of glasses. The technique involves, gently abrading the surface of the sample with a flexible polymer disc impregnated on one side with 15 μm diamond particles. The discs are sampled by laser ablation. The technique is essentially non destructive, the sample can be virtually any shape or size, sampling can be performed in situ and then the disc can be sent back to the laboratory. Applications of this technique may include the analysis of valuable works of art where it is important to minimise damage done to the sample.

Aqueous solutions

This work has shown the potential of microsampling aqueous solutions by laser ablation. The mechanism by which the analytes were mobilised is likely to be by a thermal process in which the laser energy heats the base of the carbon cup, thereby transferring thermal energy to the liquid so that a portion of it is vaporised. The vaporised material will also interact with the laser induced plasma which exists at or over the surface of the liquid at high laser energies (typically $1 \times 10^8 \text{ W cm}^{-2}$) this interaction will cause further atomisation of the vapour. The mechanism by which the sample is mobilised has been shown to have a dramatic influence on sensitivity and precision.

Approximately 30 % of the analyte reaches the plasma compared to <1 % for pneumatic nebulisation. There is no differential loss of elements by laser ablation which may occur with ETV, because of the formation of refractory compounds or losses of volatile elements when using high filament temperatures.

As seen for laser ablation studies of glass samples sampling sensitivity is greatly influenced by changing laser operating parameters, particularly ablation time and laser energy. Maximum sensitivity is reached for a 5 s ablation time, which corresponded to ablation of the whole 20 μl sample. This also helped to improve precision which decreases from an average of 12 %RSD for ablation times of 1 to 3 s to an average of 6 %RSD for times of 5 s and above. An increase in the signal is seen for increased laser energy up to a maximum of 60 J. Higher energies result in increased spattering of the sample and a decrease in vaporised material which results in poorer precision at high laser energies. Typically 6 %RSD for laser energies of 60 J and below to an average of 12 %RSD at higher energies.

Limits of detection are worse by 3 orders of magnitude than for ETV and pneumatic nebulisation where limits of detection are typically at the sub $\mu\text{g ml}^{-1}$ level. Values of between 0.3 and $7 \mu\text{g ml}^{-1}$ were obtained for laser ablation. Laser ablation produced linear calibration data for four

elements of different thermochemical properties (Na and Zn were relatively volatile and Ti and B non volatile, Ti and B readily form refractory compounds) over a range of 0.1 to 1000 $\mu\text{g ml}^{-1}$.

Precision is poor (average value of 9 %RSD) compared with pneumatic nebulisation which typically gives a precision of < 1% RSD. However, precision was comparable with ETV. Poor precision results from irreproducible levels of spattering of the sample particularly at high laser energies. Spattering results from the production of acoustic pressure waves caused by dielectric breakdown of the sample. The poor precision also gave rise to relatively poor limits of detection. Trends in the signals for each element were very similar, and the use of an internal standard improved precision. The element to Co signal ratios showed a dramatic improvement in precision from 6.9 %RSD to 1.0 %RSD for Zn. Similar improvements were seen for the other three elements.

Clearly, laser ablation of aqueous solutions is a viable option for calibration purposes. With the success seen in these studies it would be desirable to expand the applications of this technique for sampling of other liquid types which are at present difficult to sample by conventional pneumatic nebulisation. For example liquids with a high viscosity and high solids content. In cases where samples need to be diluted or require tedious sample preparation techniques laser ablation is very attractive. Such samples may include biological samples such as blood and plasma and organic samples such as paints or oils.

Oils

The rate of ablation is greater for oils than for aqueous solutions. 20 µl of oil is ablated after 3 s compared to 5 s for 20 µl of aqueous solution. This is due to the lower boiling point and heat capacity of oils. As with aqueous solutions, an improvement in precision is seen when ablation times are increased to 3 s and over, typically from 6.5 to 3.4 %RSD. Spattering is also less for oils compared to aqueous solutions, which results in an improvement in precision 3.4 %RSD for oils compared to 9.1 %RSD for aqueous solutions. Reduced spattering is due to a higher viscosity for oils compared to aqueous solutions.

Limits of detection varied between 0.05 and 0.4 µg g⁻¹ for Fe, Zn, Mg and Ca and are inferior to those typically obtained by pneumatic nebulisation. Anderson et al (137) reported limits of detection between 0.0002 and 0.004 µg g⁻¹ for the same elements using pneumatic nebulisation.

Precision is similar to pneumatic nebulisation and is found to be less than 4 %RSD. These values compare well with precisions of about 5 %RSD reported by Jansen et al (136). The use of internal standardisation does not help to improve precision significantly. This contrasts with significant improvement when using internal standardisation for laser ablation of aqueous solutions which exhibits significant spattering. Spattering is not seen to be such a problem for ablation of oils.

Analysis of certified lubricating oils by laser ablation shows good agreement, typically between -8 and +6 % of the certified concentrations. Laser ablation produces better agreement than pneumatic nebulisation where values are typically between -18 and -32 % of the certified concentration. The poor results by pneumatic nebulisation are due to a constant problem with blockages caused by the build up of carbon deposits on the tip of the sample injection tube. Lubricating oils contain some elements at very high concentrations, for example calcium which is present at concentrations > 3.5 % w/w could not be determined without dilution.

Excellent results were obtained for total metal concentration in the oils containing wear metal particulates, values are typically between +4 and -8 % of the certified concentration. Whereas with pneumatic nebulisation results are considerably poorer (typically between -54 and 60 % of the certified concentrations). This is due to blockages of the nebuliser by large particulate matter. It is in this type of analysis that laser ablation would prove very effective where true concentrations of wear particulates need to be obtained without the need for the sample to be filtered or digested prior to analysis.

Precision of the laser ablation process for the analysis of aqueous solutions needs further improvement. Internal standardisation provides some significant improvement. However, the main lack of precision is due to irreproducible losses of solution due to spattering (spattering for oils is much reduced due to greater viscosity compared to aqueous solutions). The use of a more viscous medium such as glycerol to help overcome the effects of acoustic pressure waves, warrants investigation. Also sample cups of different geometries may be used. For example cups with high walls may reduce losses due to spattering.

Also the use of different solid supports such as filter papers may offer advantages over carbon cups. Various inert materials such as porous carbon filters may offer the advantage of a reduction in sample spattering compared to carbon cups and hence improve precision.

Further investigations into the use of aqueous standards for calibration purposes would need to be studied for qualitative oil analysis. Standard addition experiments should be performed to investigate the presence of matrix effects which may prevent the analysis of samples such as oils using this calibration technique. Spiked recovery experiment would support this.

Thin coated materials

This thesis reports the first experiment to fully utilise laser ablation as a routine method for quantitative determination of coating depth. It is found that transient signals are obtained for ablation of the coating and that the peak width at half the signal height is proportional to the coating thickness. Calibration of coating depth as a function of the peak width at half the signal height is linear over a range of 1 to 10 μm . With optimised laser ablation conditions (with respect to laser energy and pulse repetition rate) a depth resolution of around 0.1 μm or less (a depth resolution of 20 nm is seen for the chromium coated steel sample). This is at least a factor of 10 better than that typically quoted for depth profiling resolution of laser ablation, with values of between 1 and 10 μm (78). Although the depth resolution obtained is not as good as glow discharge spectrometry, which has a depth resolution range of down to 0.005 μm (144), laser ablation has the advantage of sampling a smaller surface area (glow discharge samples an area of at least 5 mm, compared to an area of less than 2 mm for laser ablation).

Optimised conditions of a repetition rate of 10 Hz, with a laser lamp energy of 60 J are the same irrespective of the coating material. Which is similar to bulk sampling where a high repetition rate of 10 Hz would be used to obtain a transient signal as seen for bulk sampling of glasses in **Chapter 3**. No signal is seen for pulse repetition rate of below 5 Hz.

This work confirmed observations of Anderson et al (50) for laser microprobe depth profiling studies of coated steel samples, that a very high laser lamp energy of 70 J would cause a reduction in the ablation yield giving rise to a reduction in the analytical signal due to a greater absorption of laser radiation with the optically dense laser plasma plume formed at higher laser energies. However, it is also seen that lower laser lamp energies of 50 J and less caused the formation of a central hole to appear in the middle of the crater, which gave rise to ablation of the substrate which lead to the formation of a less distinct transition between the signal for the coating and the substrate. The formation of this central hole is due to the fact that the laser induced plasma is more optically thin at lower energies hence allowing the incident laser beam to

pass through and ablate the sample directly. With this in mind a laser lamp energy of 60 J is recommended.

Overall, laser ablation inductively coupled plasma emission spectrometry proved to be a quick and simple technique for depth profiling of metal and glass samples (calibration and analysis taking just a few minutes) with a good accuracy (3.0 μm c.f. 3.1 μm for titanium nitride coated steel samples, and good precision with values typically less than 4 %RSD. This technique is also suitable for depth profiling of multilayered coatings and finally it is just as easy to determine coating composition for glass materials. However, for full quantitation suitable glass calibration standards would be necessary. Improved resolution for depth profiling may be obtained by using an aperture between the laser beam and the sample, this may provide a flatter beam profile which would in theory create sampling craters with a flatter bottom and squarer edges.

Biological samples

Results for laser ablation of gel multielement standards demonstrate that signal intensity is proportional to element concentration for the gel multielement standards over a range of between 5 and 200 $\mu\text{g g}^{-1}$. Limits of detection are found to be in the sub $\mu\text{g g}^{-1}$ level and a precision of <5 %RSD is typical.

The great potential for the use laser ablation as a microanalysis sampling technique for microtome tissue and skin samples has been demonstrated. Results for the analysis of liver tissue show that microanalysis is possible, even though precision is poor owing to sample inhomogeneity.

The technique could differentiate between two skin tissue samples with different nickel concentrations, simply by comparing the different base line peak widths of the transient signals for the two samples.

Preliminary studies into laser ablation of microtome biological samples proved successful and further work would be warranted. The use of laser ablation inductively coupled plasma mass spectrometry has shown that good sensitivity can be achieved. However, the use of a laser beam which is focused by microscope optics with a very very small spot size would provide a great degree of lateral spatial resolution so that areas on a microscopic scale can be analysed.

The use of gel multielement standards should be further investigated for its use as a standard for a greater comprehensive range of tissue types. The accuracy would require determining, but this would require the availability of appropriate reference materials.

References

- 1 Tolg, I., and Lorenz, I., *Fortschr. Chem. Forsch.*, 1969, **11**, 507.
- 2 Tolg, G., *Analyst*, 1968, **94**, 705.
- 3 Yoe, J. H., and Koch, H. J. Jr., *Trace. Analysis.*, 1957, 645.
- 4 Minczewski, J., *Chim. Anal.*, **47**, 1965, 401.
- 5 West, P. W., and West, F. K., *Anal. Chem.*, 1968, **40**, 138.
- 6 Specker, H., *Z. Anal. Chem.*, 1966, **221**, 33.
- 7 Cali, J. P., *Trace Analysis of semiconductor Materials*, Pergamon, Oxford, 1964.
- 8 Babat, G. I., *J. Inst. Elect. Eng.*, 1947, **94**, 27.
- 9 Reed, T. B., *J. Appl. Phys.*, 1961, **32**, 821.
- 10 Greenfield, S., et al, *Analyst*, 1964, **89**, 713.
- 11 Greenfield, S., et al, *Anal. Chim. Acta.*, 1975, **74**, 225.
- 12 Fassel, V. A., et al, *Spectrochim. Acta.*, 1962, **18**, 1127.
- 13 Dickinson, G. W., and Fassel, V. A., *Anal. Chem.*, 1969, **41**, 1021.
- 14 Boumans, P. W. J. M., and De Boer, F. J., *Spectrochim. Acta.*, 1972, **27B**, 391.
- 15 Fassel, V. A., and Niseley, R. N., *Anal. Chem.*, 1974, **46**, 1110A.
- 16 Boumans, P. W. J. M., and De Boer, F. J., *Spectrochim. Acta.*, 1978, **30B**, 309.
- 17 Scot, R. H., et al, *Anal. Chem.*, 1974, **46**, 75.
- 18 Web, J. P., *Anal. Chem.*, 1972, **44**, 30A.
- 19 Fassel, V. A., *Science.*, 1978, **202**, 185.
- 20 Thompson, M., and Walsh, J. N., *A handbook of Inductively Coupled Plasma Spectrometry, 1983, 176, Blackie, Glasgow.*
- 21 Ng, K. N., and Caruso, J. A., *Appl. Spectrosc.*, 1985, **39**, 719.
- 22 Matusiewicz, H., *J. Anal. At. Spectrom.*, 1986, **1**, 176.
- 23 Gunn, A. M., and Millard, D. L., *Analyst*, 1978, **103**, 1066.
- 24 Park, C. J., *Anal. At. Spectrom.*, 1987, **2**, 473.
- 25 Gray, A. L., *Spectrochim. Acta.*, 1986, **41 B**, 151.
- 26 Clarke, P. A., McLeod, C. W., and Mowthorpe, D. J., *Anal Proc.*, 1986, **23**, 15.
- 27 Darke, S. A., Pickford, C. J., and Tyson, J. F., *Analytical. Proceedings.*, 1989, **26**, 379.
- 28 Salin, E. D., Horlic, G. and Sing, R. L. A., *Anal. Chem.*, 1984, **56**, 2596.
- 29 Boomer, D. W., Powell, M., Sing, R. L. A., and Salin, E. D., *Anal Chem.*, 1986, **58**, 975.
- 30 Hall, G. E. M., et al, *J. Anal. At. Spectrom.*, 1988, **3**, 791.
- 31 Jiang, S. J., and Houk, R. S., *Anal. Chem.*, 1986, **58**, 1739.
- 32 Williams, J. G., et al, *J. Anal. At. Spectrom.*, 1987, **2**, 469.
- 33 Wilkinson, J. R., Ebdon, L., and Jackson, K. W., *Anal Proc.*, 1982, **19**, 305.
- 34 Ebdon, L., and Wilkinson, J. R., *J. Anal. At. Spectrom.*, 1987, **2**, 39.
- 35 Morales, A., and Pomares, F., *J. Anal. At. Spectrom.*, 1989, **4**, 329.

- 36 Darke, S. A., Long, S. E., Pickford, C. J., and Tyson, J. F., *Fresenius. J. Anal. Chem.*, 1990, **337**, 284.
- 37 Maiman, T. H., *Nature*, 1960, **187**, 493.
- 38 Moenke-Blankenburg, L., *Laser Micro Analysis, 1989*, Wiley, New York.
- 39 Mossoti, V. G., Laqua, K., and Hagenah, W. D., *Spectrochim. Acta.*, 1967, **23**, 197.
- 40 Brech, F., and Cross, L., *Appl. Spectrosc.*, 1962, **16**, 59.
- 41 Brech, F., and Cross, L., *Appl. Spectrosc.*, 1963, **22**, 107.
- 42 Niemax, K., Leis, F., Sdorra, W., and Ko, J. B., *Mikrochim. Acta.*, 1989, **2**, 185.
- 43 Iida, Y., *Anal. Sci.*, 1991, **7**, 61.
- 44 Niemax, K., and Sdorra, W., *Mikrochim. Acta.*, 1992, **108**, 1.
- 45 Kagawu, K., et al, *Bunko. Kenkyu.*, 1988, **37**, 360.
- 46 Kagawu, K., et al, *J. Anal. At. Spectrom.*, 1988, **3**, 415.
- 47 Leis, F., Sdorra, W., and Ko, J. B., *Microchim. Acta.*, 1989, **II**, 185.
- 48 Grant, K. J., Paul, G. L., and O'Neill, J. A., *Appl. Spectrosc.*, 1991, **45**, 701.
- 49 Anderson, D. R., and McLeod, C. W., *J. Anal. At. Spectrom.*, 1994, **9**, 67.
- 50 Anderson, D. R., and McLeod, C. W., *J. Anal. At. Spectrom.*, 1995, **4**, 43.
- 51 Abercrombie, F. N., et al, *Applications of ICP to Emission Spectrometry*, 1978, 121, Franklin Institute Press, Philadelphia.
- 52 Barringer, A. R., *US. Pat.*, 4220414, 1980.
- 53 Thompson, M., and Goulter, J. E., *Analyst*, 1981, **106**, 32.
- 54 Thompson, M., Cherney, S., and Brett, L., *J. Anal. At. Spectrom.*, 1989, **4**, 11.
- 55 Darke, S. A., and Long, S. E., *Anal. Proc.*, 1989, **26**, 159.
- 56 Lin, S. J., and Su, G., *J. Anal. At. Spectrom.*, 1988, **3**, 841.
- 57 Lin, S. J., and Peng, C. J., *J. Anal. At. Spectrom.*, 1990, **5**, 509.
- 58 Thompson, M., and Hale, M., *Prospect. Areas. Glaciated. terrain.*, 1984, 211.
- 59 Thompson, M., and Goulter, J. E., *Jena. Rev.*, 1981, **26**, 202.
- 60 Chan, W. T., and Russo, R. E., *Spectrochim. Acta. Part B.*, 1991, **46**, 1471.
- 61 Ramsey, M. H., et al, *J. Anal. At. Spectrom.*, 1992, **7**, 587.
- 62 Marshall, J., and Franks, J., *J. Anal. At. Spectrom.*, 1991, **6**, 145.
- 63 Watling, R. J., et al, *J. Anal. At. Spectrom.*, 1997, **12**, 195.
- 64 Moenke-Blankenburg, L., Schumann, T., and Gunther, D., *J. Anal. At. Spectrom.*, 1992, **7**, 251.
- 65 Ward, N. I., et al, *J. At. Spectrom.*, 1992, **7**, 1139.
- 66 Raith, A., Hutton, R. C., and Abell, D., *J. Anal. At. Spectrom.*, 1995, **10**, 591.
- 67 Booth, P. K., and McLeod, C. W., *Microchimica. Acta. (Wien).*, 1989, **III**, 283.
- 68 Darke, S. A., et al, *J. Anal. At. Spectrom.*, 1989, **4**, 715.
- 69 Williams, J. G., and Jarvis, K. E., *J. Anal. At. Spectrom.*, 1993, **8**, 25.
- 70 Wilkinson, J. J., et al, *Geochimica. et. Cosmochimica. Acta.*, 1995, **58**, No3, 1133.

- 71 Crain, J. S., and Gallimore, D. L., *J. Anal. At. Spectrom.*, 1996, 7, 605.
- 72 Cherney, S., and Cook, J. M., *J. Anal. At. Spectrom.*, 1995, 8, 299.
- 73 Moissette, A., *J. Anal. At. Spectrom.*, 1996, 11, 177.
- 74 Goodall, P. S., and Johnson, S. G., *J. Anal. At. Spectrom.*, 1996, 11, 57.
- 75 Kenneth, K. K., and Chan, W. T., *J. Anal. At. Spectrom.*, 1997, 12, 7.
- 76 Denoyer, E. R., The Perkin Elmer Coporation. *Unpublished Work*.
- 77 Pearce, J. G., Perkins, W. T., and Fuge, R., *J. Anal. At. Spectrom.*, 1992, 7, 595.
- 78 Arrowsmith, P., and Hughes, S. K., *Appl. Spectrosc.*, 1988, 42, 1231.
- 79 Archibold, E., Harper, D. W., and Hughes, T. P., *J. Appl. Phys.*, 1964, 15, 1321.
- 80 Lee, Y. I., Sawan, S. P., and Sneddon, J., *J. Appl. Spectrosc.*, 1992, 46, 436.
- 81 Sneddon, J., et al, *Spectrochim. Acta. Part B.*, 1992, 46, 436.
- 82 Dienstbier, M., Benes, R., and Rejfir, P., *Appl. Phys. B.*, 1990, 51, 137.
- 83 Pang, H., Wiederin, D. R., Houk, R. S., and Yeung, E. S., *Anal. Chem.*, 1991, 63, 390.
- 84 Daido, H., et al, *Jpn. J. Appl. Phys. Part 2.*, 1983, 22, 248.
- 85 Liu, J. M., Yen, R., Kurz, H., and Bloemberg, N., *Appl. Phys. Lett.*, 1981, 39, 755.
- 86 Friichtennicht, J. F., *Rev. Sci. Instrum.*, 1974, 45, 51.
- 87 Huie, C. W., and Yeung, E. S., *Anal. Chem.*, 1986, 58, 1989.
- 88 Thompson, M., Cherney, S., and Brett, L., *J. Anal. At. Spectrom.*, 1990, 5, 49.
- 89 Vogel, K., and Backlund, P., *Appl. Phys.*, 1965, 36, 3697.
- 90 Klocke, H., *Spectrochim. Acta. Part B.*, 1969, 24, 263.
- 91 Eyett, M., and Bauerle, D., *Appl. Phys.*, 1987, 51, 2054.
- 92 Geertsen, C., et al, *J. Anal. At. Spectrosc.*, 1994, 9, 17.
- 93 Gagean, M., and Mermet, J. M., *J. Anal. At. Spectrosc.*, 1997, 12, 189.
- 94 Gunther, D., et al, *J. Anal. At. Spectrosc.*, 1997, 12, 939.
- 95 Gunther, D., et al, *J. Anal. At. Spectrosc.*, 1997, 12, 165.
- 96 Sneddon, J., and Mitchell, P. G., *Int. Lab.*, 1987, April, 18.
- 97 Ready, J. F., *Effects of High-Power Laser Radiation*, 1971, Acedemic Press, New York.
- 98 Lee Smith, W., Liu, P., and Bloembergen, N., *Phys. Rev.*, 1977, A15, 2396.
- 99 Smith, D. C., *J. Appl. Phys.*, 1977, 48, 2217.
- 100 Sacchi, C. A., *J. Opt. Soc. Am.*, 1991, B8, 337.
- 101 Telle, H. R., and Laubereau, A., *Opt. Commun.*, 1980, 34, 287.
- 102 Radziemski, L. J., and Cremers, D. A., *Spectrochemical Analysis Using Laser Plasma Excitation*, 1989, *Laser Induced Plasmas and Applications*, Marcel Dekker, New York.
- 103 Majidi, V., and Joseph, M. R., *Crit. Reviews. Anal. Chem.*, 1992, 23, 143.
- 104 Thiem, T. L., Lee, Y. I., and Sneddon, J., *Microchem. J.*, 1992, 45, 1.
- 105 Cremers, D. A., and Radziemski, L. J., *Applied. Spectroscopy.*, 1984, 38, 721.
- 106 Cheung, N., and Yeung, E. S., *Applied. Spectrosc.*, 1993, 47, 882.

- 107 Locke, J., *Anal. Chim. Acta.*, 1980, **113**, 3.
- 108 Hickman, D. A., *Anal. Chim. Acta.*, 1984, **56**, 844A.
- 109 Hickman, D. A., *Forensic. Sci. Int.*, 1981, **17**, 265.
- 110 Hickman, D. A., *Forensic. Sci. Int.*, 1983, **23**, 189.
- 111 Hickman, D. A., *Forensic. Sci. Int.*, 1983, **23**, 213.
- 112 Hickman, D. A., *Forensic. Sci. Int.*, 1987, **33**, 23.
- 113 Koons, R. D., Fiedler, C., and Rawalt, R. C., *Forensic. Sci.*, 1988, **33**, 49.
- 114 Mariciello, L., Jarrell Ash Plasma Newsletter, 1981, Waltham, MA.
- 115 Goode, G. C., Wood, G., and Coleman, R. F., *A. W. R. E. Rep.*, No. 024/71, 1971.
- 116 Sayre, E. V., and Smith, R. W., *Recent Advances in Science and Technology of Materials, Volume 3, Ed. Bishey, A., 1974, 47, Plenum Press, New York.*
- 117 Hoare, H. C., and Mostyn, R. A., *Anal. Chem.*, 1967, **39**, 1153.
- 118 Dagnall, R. M., et al, *Anal. Chim. Acta.*, 1971, **54**, 397.
- 119 Lorbar, A., and Goldbar, Z., *Analyst*, 1985, **110**, 155.
- 120 Grimm, W., *Spectrochim. Acta.*, 1968, **23B**, 443.
- 121 Gough, D. S., *Anal. Chem.*, 1978, **48**, 1926.
- 122 Kwong, H. S., and Measures, R. M., *Anal. Chem.*, 1979, **51**, 428.
- 123 Catterick, T., and Hickman, D. A., *Analyst*, 1979, **104**, 516.
- 124 Headridge, J. B., et al, *Analyst*, 1982, **107**, 1200.
- 125 Franks, L. S., et al, *Anal. Chim. Acta.*, 1990, **40**, 103.
- 126 Kantor, T., et al, *Talanta*, 1976, **23**, 585.
- 127 Kantor, T., et al, *Spectrochim. Acta.*, 1979, **34B**, 341.
- 128 Mitchel, P. G., et al, *Anal. Lett.*, 1985, **18**, 1723.
- 129 Helmer, D. J. C., and Walters, J. P., *Appl. Spectros.*, 1984, **38**, 392.
- 130 Van Heuzen, A. A., *Spectrochim. Acta. Part B.*, 1991, **46**, 1803.
- 131 Jarvis, K. E., *J., Anal. At. Spectrom.*, 1989, **4**, 563.
- 132 Gray, A. L., *Analyst*, 1985, **110**, 551.
- 133 Brown, R. J., *Spectrochim. Acta. Part B.*, 1983, **38**, 283.
- 134 Botto, R. I., *Spectrochim. Acta. Part B.*, 1987, **42**, 181.
- 135 Granchi, M. P., Biggerstaff, J. A., Hillard, L. J., and Grey, P., *Spectrochim. Acta. Part B.*, 1987, **42**, 169.
- 136 Jansen, B. M., et al, *J. Anal. At. Spectrom.*, 1992, **7**, 127.
- 137 Anderson, D. P., et al, *Spectro Inc.*, Fitchburg, MA, USA.
- 138 Munz, W. D., Schulze, D., and Hauzer, F. J. M., *Surface and Coatings Technology*, 1992, **50**, 169.
- 139 Sproul, W. D., Rudnik, P. J., and Legg, K. O., *Surface and Coatings Technology*, 1993, **56**, 179.

- 140 Munz, W. D., Hauzer, F. J. M., and Schulze. D., *Surface Coatings and Technology*, 1991, **49**, 161.
- 141 Bengaston, A., and Danielson, D., *Thin. Solid. Films.*, 1985, **124**, 231.
- 142 Hall, D. J., and Sanderson, N. E., *Surface. Interface. Anal.*, 1988, **11**, 40.
- 143 Raith, A., Hutton, R. C., and Huneke, J. C., *J. Anal. At. Spectrom.*, 1993, **8**, 867.
- 144 Wachter, J. R., and Cremers, D. A., *Appl. Spectrosc.*, 1987, **41**, 1042.
- 145 Geersten, C., Briand, A., and Chartier, J. L., *J. Anal. At. Spectrom.*, 1994, **9**, 17.
- 146 Iida, Y., Morikawa, H., and Tsuge, A., *Anal. Sci.*, 1991, **7**, 61.
- 147 Grant, K. J., Paul, G. L., and O'Neill, J. A., *Appl. Spectrosc.*, 1991, **45**, 701.
- 148 Talimi, Y., Moenke-Blankenburg, L. J., and Sieper, H. P., *Anal. Chim. Acta.*, 1981, **127**, 71.
- 149 Darmadasa, I. M., Ives, M., Brooks, J. S., and France, J. H., *Semicond. Sci. Technol.*, 1995, **10**, 369.
- 150 Takayama, R., et al, *J. Appl. Phys.*, 1989, **65**, 1666.
- 151 Ishizuka, T., Uwamino, Y., and Sunahara, H., *Anal. Chem.*, 1977, **49**, 1339.
- 152 Kojima, I., et al, *Anal. Sci.*, 1988, **4**, 211.
- 153 Uchida, T., et al, *Anal. Chim. Acta.*, 1989, **116**, 205.
- 154 Ishizuka, T., Uwamino, Y., *Spectrochim. Acta. Part B.*, 1983, **38**, 519.
- 155 Beauchemin, J., et al, *Analyst*, 1987, **117**, 1563.